To the Graduate Council:

I am submitting herewith a thesis written by John M. Maltry III entitled "The Effect of Flow Parameters on Dilatations in Stenotic Arterial Models." I recommend that it be accepted in partial fulfillment of the requirements for the degree of Master of Science, with a major in Engineering Science.

John H. Forrester, Major Professor

We have read this thesis
and recommend its acceptance:

Accepted for the Council:

Vice Chancellor
Graduate Studies and Research

Thesis
T7
.M3698
Cop. 2

# THE EFFECT OF FLOW PARAMETERS ON DILATATIONS IN STENOTIC ARTERIAL MODELS

A Thesis

Presented for the

Master of Science

Degree

The University of Tennessee, Knoxville

John M. Maltry III

December 1977

1346241

With Gratitude

to My Mother and Father

# ACKNOWLEDGMENTS

This study was one phase of a project funded by the National Science Foundation (Grant Number ENG74-15555) and the National Institutes of Health (Grant Number HL-15564). Dr. John H. Forrester has been the Principal Investigator, working in the Department of Engineering Science and Mechanics at the University of Tennessee, Knoxville. The author was supported from these grants both as an undergraduate and graduate student. This support, as well as that from the Department of Engineering Science and Mechanics, was necessary for the research to be completed. A special thanks is extended to Dr. Forrester not only for his concern for the author's professional growth, but also for his genuine concern for the author as an individual. Without his influence this thesis would not have been completed.

The author wishes to extend his appreciation to E. L. Rosenbalm, Stephen L. Hunley, and the late James Ray Moyer for their instructional sessions. Their interest and eagerness to help has surely made this research project much more informative as well as enjoyable for the author.

Dr. William T. Snyder and Professor John Buchan are gratefully acknowledged for their willingness to serve as committee members.

The author would also like to thank Vicki Butcher for her professional efficiency in typing the manuscript, and Steven B. Cliff for his technical assistance.

# ABSTRACT

A sudden constriction or narrowing of the cross-sectional area of a blood vessel is referred to as a stenosis. These constrictions are usually caused by intravascular lesions. One common adverse effect of a severe stenosis is a weakening and bulging of the vessel wall distal to the stenosis, commonly referred to as poststenotic dilatation. Such a condition may lead to complete structural fatigue of the vessel wall, permitting the vessel to rupture, and, in some cases, causing death.

The purpose of this research project was to conduct a model study of stenotic vessels under various flow conditions, and to determine, *in vitro*, the conditions to produce poststenotic dilatation. The long-range goal is to compare such studies with rigid model studies and *in vivo* dilatation, in hopes of determining a prognostic tool to determine the likelihood of poststenotic dilatation occurrence in patients' stenotic vessels.

Latex models of a stenosed canine femoral artery were fabricated, and their moduli of elasticity evaluated. Utilizing dimensional analysis and similitude, pertinent dimensionless terms were developed which could be reproduced *in vitro*. A series of tests were run using small models (0.6 cm diameter) in a mock circulatory system. Other tests were conducted with larger models (2 cm diameter) in a

different system. Most of the models had an area reduction of 75% at the throat of the stenosis.

Under modeled normal physiological conditions, poststenotic dilatation did not occur in any of the models. Rather, the models developed prestenotic dilatations. Increasing the mean velocity to abnormally high values only accelerated prestenotic dilatation. However, when the modeled pulse rate was increased above its normal value and all other variables were held at normal values, poststenotic dilatation did develop in the larger models. Unlike the larger models which were made entirely of latex rubber, the stenoses in the smaller models were machined from Plexiglas, which may have contributed to the prestenotic dilatations in these models. The only time poststenotic dilatation developed in a small model was when the support for the model distal to the stenosis was partially removed. Pressure variations along the inside wall of the models were obtained by a specially designed pressure catheter. The results indicated no localized high pressure region within the tube.

From the results of these experiments, it is believed that mechanical effects are complemented by biological effects to produce poststenotic dilatation. Furthermore, the significance of pulse rate in their production has been indicated. Other important parameters appear to be the method of support, the material properties of the model, and the degree of constriction. Further studies are needed to

determine more information on this complicated but important problem.

# TABLE OF CONTENTS


| CHAPTER | | PAGE |
|---|---|---|
| I. | INTRODUCTION. . . . . | 1 |
| II. | LITERATURE REVIEW . . . . . | 4 |
| | A. Jet-Stream Lesions. . . . . | 4 |
| | B. Congenital Abnormalities. . . . . | 5 |
| | C. High Lateral Pressure . . . . . | 5 |
| | D. Vortex Formation. . . . . | 9 |
| | E. Cavitation. . . . . | 10 |
| | F. Turbulence. . . . . | 11 |
| | G. Drag Forces . . . . . | 12 |
| III. | DIMENSIONAL ANALYSIS. . . . . | 15 |
| IV. | COMPARISON OF PROTOTYPE AND MODEL VARIABLES . . . . . | 24 |
| | A. Vessel Elasticity . . . . . | 24 |
| | 1. Review of material properties of arteries . . . . . | 24 |
| | 2. Latex as an arterial model. . . . . | 32 |
| | 3. Relationships from thick-walled theory . . . . . | 37 |
| | 4. Relationships from thin-walled theory . . . . . | 43 |
| | B. Radius. . . . . | 47 |
| | C. Wall Thickness. . . . . | 49 |
| | D. Poisson's Ratio . . . . . | 51 |
| | E. Viscosity . . . . . | 51 |
| | F. Wall Density. . . . . | 53 |

CHAPTER PAGE

IV. (Continued)

G. Density of Fluid. . . . . 53

H. Pressure Wave Shape . . . . . 53

I. Mean Velocity Wave Shapes . . . . . 57

J. Geometry of the Stenosis. . . . . 60

K. Dilatation Length Scale . . . . . 64

L. Summary of Values for the Prototype Variables . . . . . 69

V. EXPERIMENTAL APPARATUS. . . . . 70

A. Large Mock Circulatory System . . . . . 70

B. Small Mock Circulatory System . . . . . 77

C. Photoelectric Elasticity Measuring System. . . . . 81

VI. RESULTS AND DISCUSSION. . . . . 84

A. Small Arterial Models . . . . . 84

B. Large Arterial Models . . . . . 100

C. Pressure Inside Large Arterial Models . . . . . 120

VII. CONCLUSIONS AND RECOMMENDATIONS . . . . . 127

A. Conclusions . . . . . 127

B. Recommendations . . . . . 129

LIST OF REFERENCES . . . . . 131

APPENDICES . . . . . 138

APPENDIX A: METHOD OF MAKING ARTERIAL MODELS. . . . . 139

APPENDIX B: CAM PROFILES . . . . . 146

APPENDIX C: DESIGN OF CATHETER . . . . . 149

APPENDICES (Continued) PAGE

APPENDIX D: PROGRAMS AND DATA FOR MATERIAL ANALYSIS. . . . . 152

APPENDIX E: PROGRAM AND DATA FOR FOURIER ANALYSIS OF PRESSURE CURVES. . . . . 178

APPENDIX F: PRESSURE DATA FOR STEADY FLOW . . . . . 186

VITA . . . . . 189

# LIST OF TABLES


| TABLE | | PAGE |
|---|---|---|
| 1. | Variables for Dimensional Analysis | 16 |
| 2. | Pi Terms with Modeling Laws | 22 |
| 3. | Comparison of Internal Pressure and Resulting Radius for the Canine Carotid Artery (Hutchison, 1974) | 27 |
| 4. | Elastic Modulus for the Femoral Artery | 32 |
| 5. | Radii at Mean Pressure | 50 |
| 6. | Harmonic Components for the Femoral Pressure Curve | 55 |
| 7. | Harmonic Components for Mean Velocity Curve | 59 |
| 8. | Experimental Results by Roach (1963) on the Effect of Type of Stenosis and Radius of Dilatation | 65 |
| 9. | Relationship between the Degree of Constriction and the Length of Dilatation on the Femoral Artery, from Roach (1963) | 67 |
| 10. | Values of the Prototype Variables | 69 |
| 11. | Small Model Variable Values | 85 |
| 12. | General Comments for Small Models | 86 |
| 13. | Large Model Variable Values | 103 |
| 14. | General Comments for Large Models | 104 |
| 15. | Dilatation Rate for Model Z-4 | 108 |
| 16. | Dilatation Rate for Model Z-1 | 109 |
| 17. | Dilatation Rate for Model Z-8 | 110 |

TABLE PAGE

18. Pressure Drops at Set Locations for Various Volume Flow Rates. . . . . 187

19. Pressure Drops Along Vessel for Various Reynolds Numbers . . . . . 188

# LIST OF FIGURES


| FIGURE | | PAGE |
|---|---|---|
| 1. | Incremental Modulus ($E_{inc}$) of Two Types of Artery. . . . . | 29 |
| 2. | Incremental Modulus ($E_{inc}$) of Three Types of Latex Tubes . . . . . | 35 |
| 3. | Stresses in the Vessel Wall. . . . . | 37 |
| 4. | Stress-Strain Curve for Carotid Artery Based Upon Thick-Walled Theory . . . . . | 42 |
| 5. | A Thin-Walled Vessel . . . . . | 44 |
| 6. | Pressure Elasticity Curves for Three Different Types of Incremental Modulus . . . . . | 48 |
| 7. | Femoral Artery Pressure Curves and Scale Factors for the Small Models . . . . . | 56 |
| 8. | Theoretical and Actual Pressure Curves for the Small and Large Arterial Model Systems. . . . . | 58 |
| 9. | Comparison of Theoretical and Actual Velocity Curves in Model T-18. . . . . | 61 |
| 10. | Possible Methods by Which the Stenosis Might Develop. . . . . | 62 |
| 11. | Geometry of the Models . . . . . | 63 |
| 12. | Relationship between Degree of Constriction and Size of Dilatation . . . . . | 68 |
| 13. | Experimental Apparatus for the Large System . . . . . | 71 |
| 14. | Experimental Apparatus for the Small System . . . . . | 71 |
| 15. | Large Mock Circulatory System. . . . . | 72 |
| 16. | Small Mock Circulatory System. . . . . | 78 |
| 17. | Photoelasticity Measuring System . . . . . | 82 |

FIGURE PAGE

18. Results for Model T-18 . . . . . 87

19. Results for Model T-19 . . . . . 88

20. Results for Model T-20 . . . . . 89

21. Results for Model T-17 . . . . . 90

22. Results for Model T-21 . . . . . 91

23. Results for Model T-8. . . . . 92

24. Results for Model T-13 . . . . . 93

25. Elastic Properties of Model T-17 Before and After Experiment. . . . . 98

26. Resulting Rupture on Some of the Small and Large Models . . . . . 102

27. Results for Model Z-4. . . . . 105

28. Results for Model Z-1. . . . . 106

29. Results for Model Z-8. . . . . 107

30. Dilatation on Model Z-1 and Z-4. . . . . 111

31. Pressure Curves for Various Constrictions in Model Z-7 . . . . . 117

32. Pressure Curves for Various Frequencies in Model Z-7 at 79% Constriction . . . . . 119

33. Dimensionless Pressure Drops for Steady Flow in a 79% Constricted Model (Z-1). . . . . 122

34. Dimensionless Pressure Drops for Steady Flow in a 93% Constricted Model (Z-2). . . . . 123

35. Pressure Profiles for a 79% Constricted Model (Z-3) Under Pulsatile Flow Conditions. . . . . 125

36. Pressure Profiles for a 93% Constricted Model (Z-2) Under Pulsatile Flow Conditions. . . . . 126

FIGURE PAGE

37. Wax Mandrel Being Sprayed With Latex Solution . . . . . 141

38. From Top to Bottom: Plexiglas Model, Plaster Mold, Mandrel Shell, and Resulting Latex Model. . . . . 142

39. Cam Profiles for Cam Numbers 1, 2, 5 and 11 . . . . . 147

40. Cam Profiles for Cam Numbers 7, 12 and 16 . . . . . 148

41. Dimensions of Pressure Catheter for *in vitro* Model Study . . . . . 150

# LIST OF SYMBOLS

| SYMBOL | DESCRIPTION |
|---|---|
| $A_j$ | - cosine Fourier coefficient |
| $B_j$ | - sine Fourier coefficient |
| $C_n$ | - real exponential numbers |
| e | - longitudinal extension |
| E | - modulus of elasticity in tension |
| $E_{inc_p}$ | - incremental modulus based upon pressure-strain model |
| $E_{inc_{p_2}}$ | - incremental modulus of elasticity at pressure $p_2$ |
| $E_{inc_t}$ | - incremental modulus based upon thin wall theory |
| $E_p$ | - pressure-strain modulus |
| $E_{st}$ | - static modulus of elasticity of wall |
| $E'$ | - dynamic elastic modulus of wall |
| f | - fundamental driving frequency |
| G | - modulus of elasticity in shear |
| h | - wall thickness |
| $K_x$ | - scale factor ratio of the model over the prototype for some given variable x |
| L | - fundamental quantity (length) |
| $L_d$ | - length of poststenotic dilatation region |
| $L_s$ | - length of stenosis |
| $L_{sd}$ | - length from throat of stenosis to start of dilatation region |
| m | - model |
| M | - fundamental quantity (mass) |
| p | - prototype |

| SYMBOL | DESCRIPTION |
|---|---|
| $P$ | - instantaneous pressure |
| $P_i$ | - inside pressure of tube |
| $P_j$ | - modulus of pressure |
| $P_o$ | - time average pressure |
| $Q$ | - volume flow rate |
| $R$ | - some radial point away from the radius |
| $R_d$ | - outside radius of dilatation region |
| $R_i$ | - inside radius of tube |
| $\bar{R}_i$ | - inside radius of tube at mean pressure |
| $R_o$ | - outside radius of tube |
| $\bar{R}_o$ | - outside radius of tube at mean pressure |
| $R_s$ | - inside radius at the throat of the stenosis |
| $t$ | - time |
| $T$ | - fundamental quantity (time) |
| $V$ | - instantaneous mean spacial velocity |
| $V_j$ | - modulus of velocity |
| $V_o$ | - time average mean velocity |
| $Z$ | - axial coordinate measured from the throat of the stenosis |
| $\alpha$ | - parameter of oscillatory flow |
| $\gamma$ | - wall thickness to outside radius ratio ($h/R_o$) |
| $\Delta$ | - "a change in" some variable |
| $\varepsilon_\theta$ | - total strains in the circumferential direction |
| $\eta$ | - coefficient of viscosity |
| $\mu$ | - absolute viscosity of fluid |

| SYMBOL | DESCRIPTION |
|---|---|
| $\nu$ | - Poisson's ratio of wall |
| $\Pi$ | - quantity describing physical phenomena |
| $\pi_n$ | - Pi term |
| $\rho$ | - density of fluid |
| $\rho_w$ | - density of vessel wall |
| $\sigma_r$ | - stress component in the radial direction |
| $\sigma_z$ | - stress component in the longitudinal direction |
| $\sigma_\theta$ | - stress component in the circumferential direction |
| $\phi$ | - phase angle |
| $\omega$ | - angular frequency |

# CHAPTER I

## INTRODUCTION

A stenosis is a sudden constriction or narrowing in the cross-sectional area of an artery or vein. These constrictions may be formed by extravascular or (more commonly) intravascular abnormalities such as intravascular plaques (Forrester and Young, 1970). When such narrowing occurs it could have adverse effects upon the circulatory system. The most obvious effect is partial or complete reduction of circulation caused by the occluded vessel. Death may result if occlusion occurs in one of the vital vessels. However, it has been observed that a stenosis in the aorta does not appreciably reduce circulation until 80% of the vessel has been occluded. Before occlusion becomes so serious there are several other related adverse effects which include:

(1) Modification in the blood properties such as coagulation properties.

(2) Development of a thrombus, an intravascular clot, or a thrombotic embolus when the thrombus is detached from the wall.

(3) Ingrowth of tissue into the vessel.

(4) Weakening and bulging of the vessel wall distal to the stenosis (downstream from the constriction), commonly referred to as poststenotic dilatation.

(5) Rupturing of this poststenotic dilatation.

Intuitively, one would anticipate that if the occluded vessel was going to dilate, it would dilate in the proximal region (upstream from the constriction). However, in both humans and animals, poststenotic dilatation has a high degree of occurrence in sufficiently constricted vessels. This dilemma has aroused considerable interest in the field of hemodynamics and has consequently become the focal point of this study.

In contrast to the large amount of information available on arteries, relatively little attention has been paid to the actual development of poststenotic dilatation. Although many theories have been proposed to explain it, very little *in vitro* experimental work has actually been performed. To further understand the mechanical responses of stenotic vessels and lead to a better understanding of poststenotic dilatation in general, the following five objectives were established for this *in vitro* study.

(1) Identify and determine values of pertinent mechanical variables in poststenotic dilatation.

(2) Using dimensional analysis, design an arterial model as well as a mock circulatory system.

(3) Determine a technique for making the arterial model on a repetitive basis.

(4) Examine the model under various flow conditions and determine if it is possible to develop *in vitro* poststenotic dilatation and if so under what conditions.

(5) Provide sufficient information on flexible model behavior so that future comparisons might be made with rigid models.

Both a small and a large series of models were developed and tested. It was intended to use the small series to test a model which was close to the actual size of a femoral artery. On the other hand the large model series was designed with primary emphasis on photographic resolution as well as on homogeneity between stenosis and vessel wall. The canine femoral artery was chosen as the prototype because of the abundance of published information on this artery under both normal and dilated conditions.

# CHAPTER II

## LITERATURE REVIEW

The first conscientious effort to explain the phenomenon of poststenotic dilatation was conducted by Halsted in 1916. With experiments on banded abdominal aortas in dogs, Halsted concluded that "The abnormal, whirlpool-like play of blood in the relatively dead pocket just below the site of the constriction, and the lower pulse pressure may be the chief factors concerned in producing the dilatation." (Halsted, 1918). Since this time, numerous experiments have been performed both *in vivo* and *in vitro*, resulting in the formulation of several theories of poststenotic dilatation development. These theories, which are briefly summarized below, include jet-stream lesions, congenital abnormalities, high lateral pressure, Von Karmen vortex sheddings, cavitation, turbulence, and drag forces.

### A. Jet-Stream Lesions

Kline, et al. (1962) were able to induce poststenotic dilatation to a considerable degree within four to five months in young pigs. Using control cineangiography, they were able to obtain, *in vivo*, the mean velocity and acceleration of blood as it passed through the stenosis. As expected, the velocity increased as it passed through the throat into the distal region, at which time it developed

the whirlpool-like patterns of turbulence. They postulated that the high velocity jet streams shattering on the vessel wall, distal to the stenosis, was responsible for the dilatation in their experimental animals. De Vries and van den Berg (1958) rejected this theory, stating that lesions created by jet streams would be much more localized than poststenotic dilatations.

B. Congenital Abnormalities

After examining the diameter of the pulmonary arteries in patients with varying degrees of pulmonary stenosis, Van Buchem (1956) concluded that "The dilatation may be absent, both in mild and severe cases of stenosis. In idiopathic dilatation of the pulmonary artery, indistinguishable widening of the same nature existed without pulmonary stenosis." This finding supported earlier concepts of Laubry (1943), who suggested that pulmonary dilatation and vascular stenosis are two independent congenital defects. However, the frequent development of poststenotic dilatation in healthy and ligated vessels tends to refute this theory (Roach, 1963; Holman and Peniston, 1955; Kline, et al., 1962; Aars, 1963).

C. High Lateral Pressure

Minimal experimental work was actually performed on poststenotic dilatation until 1954 when Holman (1954a,b) noted formations in banded dog arteries as well as rubber

tubes. Numerous authors (Roach, 1963; De Vries and van den Berg, 1958; Matunobu and Arakawa, 1974) have credited Holman with being able to create poststenotic dilatations in these rubber tubes. However, close scrutiny of his work reveals that for his models to dilate poststenotically, it was necessary for him to restrict the proximal region by some external means. While it appears questionable that these dilatations have always been properly interpreted, it is believed that general information on dilatation as the result of lumen expansion might be ascertained from these experiments.

Holman (1954a,b) demonstrated the importance of hydraulic forces in the development of dilatation by conducting experiments with an artificial circulatory system. Holman suggested that many factors determine the stress and strain the vessel must undergo before dilatations occur. These include natural resistance to dilatations created by the structural characteristics of the vessel wall, pressure and velocity of the fluid, viscosity of the fluid, the degree and the rate of the constriction, the materials surrounding the vessels, and the elasticity of the vessel. Holman limited his *in vitro* experiment to variations in systolic and diastolic pressures, the velocity of the flow by reducing or increasing the stroke volume of the artificial circulatory system, and the pumping rate. Holman stated, "Evidence suggests that there is a maximal degree

of dilatation for each set of conditions under which it occurs ... that dilatation varies in degree with the pressure and velocity with which blood is ejected from the stenotic channel, and that there is a critical level of pressure and of velocity of flow below which dilatation does not occur." (Holman, 1955).

Later *in vivo* studies by Holman (1955) and his colleagues on the banded thoracic aorta of new-born puppies produced poststenotic dilatations. Different studies were conducted to determine how the rate at which the stenosis constricted the vessel affected the development of dilatations. It was discovered that a low rate of constriction (e.g., long stenosis) produced less percent dilatation than a larger rate (e.g., a shorter stenosis). It was also demonstrated that not all poststenotic dilatations resulted in rupture, but some became stationary after a given period of time.

Holman and Peniston (1955) demonstrated *in vivo* that a dilatation will exist after the hydrodynamic forces that produced it are removed. By partial ligation of the thoracic aorta, a poststenotic dilatation was produced in four months. At this time, the ligation was made complete. Four months later, an angiogram revealed that the poststenotic dilatation still existed, but was reduced in size. Further studies revealed that the dilatation was not solely produced by a weakening of the vessel wall. A portion of

the medial layer of the thoracic aorta was stripped off; some of these stripped vessels were partially ligated while others were not. Angiograms several months later revealed little or no dilatation in the non-ligated stripped aortas, while the ligated stripped aortas showed a 50% dilatation.

Holman (1954a,b; 1955) concluded that the physiology of poststenotic dilatation was not biological, but caused by mechanical effects of hydraulic forces resulting from three factors. He stated that, according to the Bernoulli principle, kinetic energy was converted into high lateral pressure when the high velocity fluid, moving from the throat of the stenosis, clashed with the relatively slow-moving mass of fluid distal to the stenosis. This effect, he said, was amplified by the pulsation from the main flow, resulting in high lateral pressure oscillation against the individual fibers of the wall. The second factor mentioned was turbulent motion and reversed flow, resulting in the fluid striking the elastic wall with alternating low and high pressures. Holman stated that the third factor was that the vessel widened as dilatation occurred, further reducing the velocity of the fluid, and increasing the lateral pressure. "It appears that unless the lumen is reduced by one-third or one-fourth of its original diameter by the stenosis, turbulence of the flow will be minimal as disclosed by only a mild thrill and bruit, and dilatation will be minimal, or long delayed, or completely absent.

Moreover, great dilatations will occur in the unsupported thoracic and abdominal vessels in contrast with a more limited dilatation in the muscular and fibrous surrounded vessels of an extremity." (Holman, 1955).

The main assumption in Holman's theory is the existence of a "localized increase" in the lateral pressure, distal to the stenosis. However, studies conducted on patients suffering from pulmonary stenosis using cardiac catheterization (Rodicsek, et al., 1958) revealed that the distal pressure was remarkably reduced compared with the proximal. This was later confirmed by De Vries and van den Berg (1958) in aortas, rigid tubes, and rubber tubes, and again by Rodbard, et al. (1967) by observing the wall thickness of the vessel, distal and proximal to the stenosis.

D. Vortex Formation

Burns (1959) disclaimed the concept of turbulence as the possible cause of poststenotic dilatation because he felt the turbulence itself consumed so much energy that very little remained to be utilized as acoustical sound. Consequently, any murmurs which developed distal to the stenosis were felt to be the result of another force. Burns stated that periodic pressure fluctuation created by Von Karmen vortex trails were the most likely cause of murmurs. These pressure fluctuations occur when surrounding fluids flow into the space that was occupied by the

vortex just prior to being shed off (Etkin, et al., 1957). Burns concluded that the fluctuations were also strong enough to cause wall vibrations which in time could lead to structural fatigue, thereby creating poststenotic dilatation. Burns, et al. (1959) attempted to reproduce these fluctuating pressures with a vibrating blade inside latex tubes under static pressure, thereby transmitting the energy of the vibrations through the water to the elastic walls. It was discovered that dilatations would develop near the end of the blade where vibrations were maximal. It was also noted that both the fixation of the end of the tube to the solid surface as well as high static pressure contributed to dilatation. Roach (1972) repudiated this theory, citing that Von Karmen vortex trails are very rare in occurrence.

## E. Cavitation

Vapor bubbles will form when a liquid flows into a region where the static pressure is equal to, or slightly lower than the vapor pressure of the liquid. These bubbles will be carried along with the liquid, and will collapse when some higher pressure region is reached. This phenomenon is referred to as cavitation. "If the vapor bubbles are near to a solid boundary when they collapse, the force exerted by the liquid rushing into the cavities creates very high, localized pressure" that will erode and vibrate the solid surface (Streeter, 1971).

Rodicsek, et al. (1958) proposed that the vapor bubbles consisting of oxygen, carbon dioxide, and nitrogen are released from blood when it flows through the low pressure, high velocity, stenotic region and that these bubbles would collapse in the distal region where the pressure was higher. They concluded that this process of cavitation would weaken the wall fibers, thereby producing poststenotic dilatation. Rodicsek demonstrated this phenomenon with water flowing through glass models but was unable to confirm this incident in the circulatory system. This theory was supported by Hugh and Fox (1963) who stated that this process was responsible not only for poststenotic dilatation, but also for the associated sounds. However, Burns (1959) was unable to demonstrate cavitation in experimental animals. Furthermore, Roach (1972) states that Harvey's studies (1950) indicate that negative pressures of several atmospheres are needed to create this phenomenon of cavitation in blood.

F. Turbulence

Roach (1963) approached the phenomenon of poststenotic dilatation by experimentally observing the effects of bands around the femoral and carotid arteries of adult dogs. By varying the degree of stenosis, it was concluded that "poststenotic dilatation always develops if turbulence (as shown by the presence of thrills and bruit, and often

eddies visible through the vessel wall) is present distal to the band; a dilatation never develops if there is no turbulence." (Roach, 1963). By using a radiogram technique Roach was able to observe the time course of dilatation in the arteries. "If turbulence was present, the arteries usually started to dilate within 24 hours, reached a steady state within 10 days and then remained essentially unchanged for up to 10 months." (Roach, 1963). It was concluded that vibration of the arterial wall as a result of turbulence was responsible for dilatations. Rodbard, et al. (1967) disagreed with this conclusion, suggesting that if vibrations were present, they would also inhibit the growth of a progressive stenosis.

Pressure-volume curves on the dilated vessels indicated that the dilated distal section was much more distensible than the proximal region (Roach and Burton, 1957). This indicated that the adverse turbulent flow, by some mechanism, was able to affect the material properties of the vessel. However, later studies by Aars (1963) on dilated vessels from rabbits showed no difference in the distensibility curves when compared to the normal ones.

## G. Drag Forces

With steady laminar flow the shear stress is proportional to the mean velocity of the stream while in turbulent flow, the shear stress is proportional to the square

of the mean velocity. Realizing that the presence of the stenosis can transform a laminar stream into a turbulent one, Rodbard, et al. (1967) suggested that poststenotic dilatation was the result of high shear stresses occurring distal to the stenosis. They reasoned that proximal to the stenosis the laminar stream would produce a small drag force on the vessel. As the streamline approached the throat of the stenosis, the velocity would increase, thereby reflecting an increase in the laminar drag force. Immediately distal to the throat, the high velocity streams would deviate from the wall, so that drag would be minimal at this site. However, below this region, the high velocity jet stream was expected to develop into the random motion characteristic of turbulent flow, so that the drag forces had maximal effect upon the vessel. As the flow progressed further downstream, it was postulated that the streamlines regained their laminar appearance and the drag on the vessel decreased. Rodbard concluded that "if the endothelium were sensitive to the magnitude of the drag forces, it could operate to initiate changes in the subjacent layers of the vessel, with sequential modification in the lumen," thereby promoting poststenotic dilatation.

A theoretical study of steady flow through a sharply converging-diverging model supported the concept of high wall shear stresses along the stenosis throat (Lee and Fung, 1970). However, because the study was conducted at below

turbulent conditions (maximum Reynolds number of 25), no significant increase in wall shear stress was detected distal to the constriction. Robicsek, et al. (1958) demonstrated that maximal turbulence occurred in the distal end of a dilated region of glass models. With this finding, it would be reasonable to assume that a region of high shear stress existed there which would propagate downstream with time as the vessel weakened. Consequently, any growth of dilatation would occur in the direction opposite of the stenosis throat.

Numerical studies by Daly (1976) questioned whether endothelial damage could occur distal to the stenotic femoral artery due to turbulent fluctuations. Yet the presence of poststenotic dilatation has been shown to exist (Roach, 1963). In 1967, Fry conducted studies on the thoracic aorta of dogs in an attempt to quantify the acute changes in endothelial lining that are associated with increased blood velocity as a result of the constriction. Two important findings were concluded from this study. He attempted to describe the shear stress which occurred in the stenotic vessel and concluded that endothelial cells could be destroyed by turbulence or by a large shear stress on the cell surface. He also determined a maximum value of shear stress which the cells could withstand before being destroyed.

# CHAPTER III

## DIMENSIONAL ANALYSIS

Utilization of dimensional analysis to describe physical phenomena is a well established practice in engineering studies. Its accuracy is severely restricted by the ability to define and correctly describe all the pertinent variables which will interact to create the phenomena. Because of physical limitations, it is necessary on occasion to omit certain variables. When this occurs, the resulting model is not an exact dimensional replica of the prototype; consequently, the resulting model will reflect distorted predictions. However, judicious analysis of the results can be quite useful in estimating the behavior of the prototype. Such will be the case in this study.

To permit correlation between model and prototype (the constricted artery), (n) measurable pertinent variables were defined, and are itemized in Table 1. Attempts to correctly determine the dynamic modulus of elasticity for the walls of the models resulted in failure, making it impossible to analyze this variable. It was hoped that utilization of the static modulus of elasticity would provide adequate information between the two systems. Care should be exercised when considering the time rate of dilatation as it is expected to be affected by the omission of this variable. Although the effective mass of surrounding tissue and the natural frequency of the effective mass was

TABLE 1

VARIABLES FOR DIMENSIONAL ANALYSIS

| Variable | Variable Definition | Fundamental Dimensions |
|---|---|---|
| $\bar{R}_i$ | inside radius of vessel at mean pressure | L |
| $\bar{R}_o$ | outside radius of vessel at mean pressure | L |
| $R_s$ | inside radius at the throat of the stenosis | L |
| $L_s$ | length of stenosis | L |
| $L_{sd}$ | length from throat of stenosis to start of poststenotic dilatation region | L |
| $L_d$ | length of poststenotic dilatation region | L |
| $R_d$ | outside radius of dilatation region | L |
| $\rho_w$ | density of vessel wall | $ML^{-3}$ |
| $\rho$ | density of fluid | $ML^{-3}$ |
| $\mu$ | absolute viscosity of fluid | $ML^{-1}T^{-1}$ |
| $\nu$ | Poisson's ratio of wall | $M^0L^0T^0$ |
| $E_{st}$ | static modulus of elasticity of wall | $ML^{-1}T^{-2}$ |
| $V_o$ | time average mean velocity | $LT^{-1}$ |
| $V_j$ | modulus of velocity | $LT^{-1}$ |
| $P_o$ | time average pressure | $MT^{-2}L^{-1}$ |
| $P_j$ | modulus of pressure | $MT^{-2}L^{-1}$ |
| $f$ | fundamental driving frequency | $T^{-1}$ |
| $t$ | time | T |

believed to be significant, they were also neglected for this study because of the lack of information in this area. Therefore, for the purpose of this analysis, it was assumed that the prototype was free of any surrounding tissue.

Realizing that the pressure gradient would be an important modeling variable, numerous attempts were made to record it in the models. But lack of a differential pressure transducer, as well as the insufficiency of the laboratory strain gauge pressure transducer to measure very small drops, obstructed the accurate appraisement of this parameter. The pressure-time curve was modeled in this study, and this was considered sufficient to characterize the forces which would be related to the flow.

Three independent quantities (m) were found sufficient to describe this physical problem. These fundamental quantities are mass (M), length (L), and time (T). The dimensionless quantity $\Pi$ is a function of the (n) variables and can be expressed as a product of a dimensionless constant (D) and each of the variables raised to some exponent $C_n$.

$$\Pi = D\Big[(\bar{R}_i)^{C_1}(\bar{R}_o)^{C_2}(R_s)^{C_3}(L_s)^{C_4}(L_{sd})^{C_5}(L_d)^{C_6}$$
$$(R_d)^{C_7}(\rho_w)^{C_8}(\rho)^{C_9}(\mu)^{C_{10}}(\nu)^{C_{11}}(E_{st})^{C_{12}}$$
$$(V_o)^{C_{13}}(V_j)^{C_{14}}(P_o)^{C_{15}}(P_j)^{C_{16}}(f)^{C_{17}}(t)^{C_{18}}\Big]$$

where the $C_n$'s are real numbers such that the net dimension of $\Pi$ is unity. Substitution of the fundamental dimensions

from Table 1 into each variable and collecting exponents gives

$$\Pi = D\Big[(M)^{C_8+C_9+C_{10}+C_{12}+C_{15}+C_{16}}$$

$$(T)^{-C_{10}-2C_{12}-C_{13}-C_{14}-2C_{15}-2C_{16}-C_{17}+C_{18}}$$

$$(L)^{C_1+C_2+C_3+C_4+C_5+C_6+C_7-3C_8-3C_9-C_{10}-C_{12}+C_{13}+C_{14}-C_{15}-C_{16}}\Big]$$

The quantity $\Pi$ will have the dimensions of unity if each of the fundamental dimensions' exponents are equal to zero. Thus,

$$\begin{bmatrix} 0+0+0+0+0+0+0+C_8+C_9 \\ C_1+C_2+C_3+C_4+C_5+C_6+C_7-3C_8-3C_9 \\ 0+0+0+0+0+0+0+0+0 \end{bmatrix}$$

$$\begin{bmatrix} -C_{10}+C_{12}+0+0+C_{15}+C_{16}+0+0 \\ -C_{10}-C_{12}+C_{13}+C_{14}-C_{15}-C_{16}+0+0 \\ -C_{10}-2C_{12}-C_{13}-C_{14}-2C_{15}-2C_{16}-C_{17}+C_{18} \end{bmatrix} = \begin{bmatrix} 0 \\ 0 \\ 0 \end{bmatrix}$$

We have three algebraic equations with 18 unknowns.

The Buckingham Pi Theorem states that the number of independent and non-dimensional quantities required to describe some physical system is equal to the number of pertinent variables (n) minus the rank (r) of the (m x n) dimensional matrix above. Consider the minor which consists of columns 9, 10, and 12, from which the rank (r) of the matrix was calculated to be three. According to the Buckingham Pi Theorem,

$$\text{Number of Pi Terms} = 18 - 3 = 15$$

Thus 15 independent and non-dimensional terms will be required to describe this phenomenon.

To evaluate these Pi terms, 15 of the coefficients were assigned real values, while solving for the other three.

For the first term $\pi_1$, let $C_{10} = -1$ and $C_2 = C_3 = C_4 = C_5 = C_6 = C_7 = C_8 = C_{12} = C_{14} = C_{15} = C_{16} = C_{17} = C_{18} = 0$. Substitution of these values into the equations gives $C_1 = C_9 = C_{13} = 1$; therefore,

$$\pi_1 = \frac{V_o \bar{R}_i \rho}{\mu}$$ ; one half of the Reynolds Number which is defined as being proportional to the ratio of the inertial effects to viscous forces.

For $\pi_2$, let $C_{15} = 1$ and $C_2 = C_3 = C_4 = C_5 = C_6 = C_7 = C_8 = C_{10} = C_{12} = C_{14} = C_{16} = C_{17} = C_{18} = 0$. Solving for the unknowns gives $C_9 = 1$, $C_{13} = -2$ and $C_1 = 0$. Hence,

$$\pi_2 = \frac{P_o}{\rho V_o^2}$$ ; the Euler Number which is defined as the ratio of static pressure forces to the dynamic pressure.

For $\pi_3$, let $C_1 = 1$ and $C_3 = C_4 = C_5 = C_6 = C_7 = C_8 = C_9 = C_{10} = C_{12} = C_{14} = C_{15} = C_{16} = C_{18} = 0$. Solving for the unknowns gives $C_{13} = -1$, $C_{17} = 1$ and $C_2 = 0$. Hence,

$$\pi_3 = \frac{f \bar{R}_i}{V_o}$$ ; the Strouhal Number which determines the time available for vortex formation to occur.

As pointed out by McDonald (1960) the dimensionless parameter $\alpha$, which relates pressure-flow relations of oscillatory flow (Womersley, 1955), is related to $\pi_1$ and $\pi_3$

by

$$\alpha^2 = 2k(\pi_1)(\pi_3) = \bar{R}_i^2 \frac{\omega\rho}{\mu}$$

where k is 3.1416. By following a similar process the remaining $\pi$ terms were determined:

$$\pi_4 = \frac{R_d}{\bar{R}_o} \quad ; \quad \text{relative dilatation radius}$$

$$\pi_5 = \frac{L_s}{\bar{R}_s} \quad ; \quad \text{stenosis length ratio}$$

$$\pi_6 = \frac{\bar{R}_i}{\bar{R}_o} \quad ; \quad \text{relative inside radius}$$

$$\pi_7 = \frac{L_d}{\bar{R}_o} \quad ; \quad \text{dilatation length ratio}$$

$$\pi_8 = \frac{R_d}{\bar{R}_s} \quad ; \quad \text{stenosis dilatation ratio}$$

$$\pi_9 = \frac{L_{sd}}{\bar{R}_o} \quad ; \quad \text{dilatation location ratio}$$

$$\pi_{10} = \frac{\rho_w}{\rho} \quad ; \quad \text{density ratio}$$

$$\pi_{11} = \frac{P_o}{P_j} \quad ; \quad \text{pressure ratio}$$

$$\pi_{12} = \nu \quad ; \quad \text{Poisson's ratio}$$

$$\pi_{13} = \frac{E_{st}}{P_o} \quad ; \quad \text{pressure-elasticity ratio}$$

$$\pi_{14} = ft \quad ; \quad \text{frequency time product}$$

$$\pi_{15} = \frac{V_o}{V_j} \quad ; \quad \text{velocity ratio}$$

To permit correlation between the model and prototype, it is desirable to have $\pi_m = \pi_p$ for each $\pi$ term, where the subscripts p and m refer to the prototype and model, respectively. Hence, from $\pi_1$

$$\pi_p = \pi_m$$

$$\frac{(V_o)_p(\bar{R}_i)_p(\rho)_p}{(\mu)_p} = \frac{(V_o)_m(\bar{R}_i)_m(\rho)_m}{(\mu)_m}$$

or

$$\frac{(V_o)_m}{(V_o)_p} = \frac{(\bar{R}_i)_p}{(\bar{R}_i)_m} \cdot \frac{(\rho)_p}{(\rho)_m} \cdot \frac{(\mu)_m}{(\mu)_p}$$

which can be written as $K_{V_o} = K_{\bar{R}_i}^{-1} K_\rho^{-1} K_\mu$ where K is the scale factor ratio of the model over the prototype for some given variable. The last equation is defined as the model law for the first Pi term. The following Table 2 contains all the modeling laws for this physical system. A true model exists when all the model laws are satisfied. That is, when all the Pi terms in the prediction equation for the prototype are equal to the corresponding Pi terms for the model. Otherwise, the model is distorted. In the present investigation, the modeling laws were generally satisfied with the exception of those determined from $\pi_{13}$ and $\pi_{15}$, as will be discussed in Chapter IV.

TABLE 2

PI TERMS WITH MODELING LAWS

| Pi Term | Ratio | Modeling Laws |
|---|---|---|
| $\pi_1$ | $\frac{V_o \bar{R}_i \rho}{\mu}$ | $K_{V_o} = K_{\bar{R}_i}^{-1} K_\rho^{-1} K_\mu$ |
| $\pi_2$ | $\frac{P_o}{\rho V_o^2}$ | $K_{P_o} = K_\rho K_{V_o}^2$ |
| $\pi_3$ | $\frac{f \bar{R}_i}{V_o}$ | $K_{V_o} = K_\omega K_{\bar{R}_i}$ |
| $\pi_4$ | $\frac{R_d}{\bar{R}_o}$ | $K_{R_d} = K_{\bar{R}_o}$ |
| $\pi_5$ | $\frac{L_s}{R_s}$ | $K_{L_s} = K_{R_s}$ |
| $\pi_6$ | $\frac{\bar{R}_i}{\bar{R}_o}$ | $K_{\bar{R}_i} = K_{\bar{R}_o}$ |
| $\pi_7$ | $\frac{L_d}{\bar{R}_o}$ | $K_{L_d} = K_{\bar{R}_o}$ |
| $\pi_8$ | $\frac{R_d}{R_s}$ | $K_{R_d} = K_{R_s}$ |
| $\pi_9$ | $\frac{L_{sd}}{\bar{R}_o}$ | $K_{L_{sd}} = K_{\bar{R}_o}$ |
| $\pi_{10}$ | $\frac{\rho_w}{\rho}$ | $K_{\rho_w} = K_\rho$ |
| $\pi_{11}$ | $\frac{P_o}{P_j}$ | $K_{P_o} = K_{P_j}$ |
| $\pi_{12}$ | $\nu$ | $K_\nu = 1$ |

TABLE 2 (Continued)

| Pi Term | Ratio | Modeling Laws |
|---|---|---|
| $\pi_{13}$ | $\frac{E_{st}}{P_o}$ | $K_{P_o} = K_{E_{st}}$ |
| $\pi_{14}$ | ft | $K_f = K_t^{-1}$ |
| $\pi_{15}$ | $\frac{V_o}{V_j}$ | $K_{V_o} = K_{V_j}$ |

# CHAPTER IV

## COMPARISON OF PROTOTYPE AND MODEL VARIABLES

The fact that blood flows through vessels in one direction was first recognized by Harvey (1628). Since that time extensive studies have been conducted to better understand the properties of these vessels. Thus, in order to model a canine femoral artery, it is necessary to review these studies. Although it would have been desirable to examine all modeling variables for a stenotic artery, published results are usually for normal arteries and thus have been used herein.

### A. Vessel Elasticity

1. Review of material properties of arteries. Blood vessels are visco-elastic tubes which are composed of four important types of tissue -- the smooth muscle, the collagen fibers, the elastin fibers, and the endothelial cells. The endothelial cells may be deformed with very little force; thus they play a small role in the total elasticity of the vessel (Burton, 1972). Smooth vascular muscle produces active tension under physiological control, but because of its circumferential arrangement, its effect upon the total elasticity of the vessel is minimized. Elastin fibers have a very low elastic modulus, of the order of $1 \times 10^6$ dynes/$cm^2$ (Bergel, 1966); thus they can easily be stretched and

are able to undergo great strains before they reach their elastic limit. As they are stretched, their elasticity will increase to approximately $5 \times 10^6$ dynes/cm$^2$ (Bergel, 1966). On the other hand, the collagen fibers have a much higher elastic modulus; studies in tendons give values of $10^8 - 10^9$ dynes/cm$^2$ (Burton, 1954). The collagen fibers are "loosely strung" through the vessel wall, permitting the elastin fibers to stretch. Once the collagen fibers are stretched out of their "loosely strung" shape, they will exert tension on the vessel. This permits the vessel to undergo strains before major resistance is offered by the vessel.

These four tissues are arranged in three concentric layers through the blood vessel's wall. The first section, tunica interna, consists of flat endothelial cells which line the inside of the vessel wall. The tunica interna is the thinnest layer of the wall with the major function of offering selective permeability to materials passing from the blood stream to the tissue and to provide a smooth internal surface for the blood to flow through. The middle layer of the blood vessel wall, tunica media, consists of smooth muscle, collagen fibers and elastin fibers. The tunica media, being the thickest layer in the vessel, provides support for the vessel and is a significant contributor to the elasticity of the vessel wall. The outermost coat, tunica externa, consists of collagen fibers and elastin fibers. This layer merges with the surrounding

tissue and contains a high proportion of collagen, thus responsible for the elasticity at large strains.

Bergel (1960, 1961a,b) attempted to obtain quantitative knowledge of the mechanical properties of arteries by performing a series of static and dynamic experiments on an isolated segment of dog arteries. The method chosen by Bergel to measure the stress and strain properties was a photo-electric one. Excised dog arteries were held at constant *in vivo* lengths in the path of a collimated light beam. Changes in intraluminal pressure resulted in varying diameter changes which in turn caused a variation in the amount of light passing by the tube. This change was detected by a photo-multiplier tube which was calibrated with a series of metal rods of known radius.

In performing the static experiment, Bergel recorded the radius at each step of 20mm Hg between 0 and 240mm Hg with a pause of 2 minutes after each change to allow for the completion of stress relaxation. In all the vessels tested the pressure-radius relationships were non-linear, becoming less distensible as the internal pressure was increased. Bergel's results were not tabulated but rather presented on curves. However, Hutchison (1974) tabulated successive measurements of radius with variation in internal pressure for the canine carotid artery and these data are shown in Table 3. To analyze these non-linear results, Bergel defined and calculated an "incremental modulus of elasticity" as:

TABLE 3

COMPARISON OF INTERNAL PRESSURE AND RESULTING RADIUS FOR THE CANINE CAROTID ARTERY (HUTCHISON, 1974)

| Pressure (mm Hg) | $R_o$ (cm) |
|---|---|
| 5 | .169 |
| 10 | .179 |
| 20 | .189 |
| 30 | .201 |
| 40 | .213 |
| 50 | .220 |
| 60 | .227 |
| 70 | .231 |
| 80 | .235 |
| 100 | .240 |
| 120 | .244 |
| 140 | .246 |

$$E_{inc_{P_2}} = \frac{P_3 - P_1}{R_{o_3} - R_{o_1}} \left[ \frac{2(1 - \nu^2) R_{i_2}^2 R_{o_2}}{(R_o^2 - R_i^2)} \right] \qquad (1)$$

where the subscripts 1, 2, 3 represent successive measurements of pressure and radius. This equation compares increments of stress and strain for small deformation about some mean extension ($P_2$), and is referred to as the incremental modulus of elasticity ($E_{inc}$) for this particular extension ($P_2$). It should be noted at this point that some of the symbols used in this section (Section A), while in general agreement with those presented in the List of Symbols, may

have somewhat different meanings. However, their meanings should be clear from the context in which they are presented.

The mean values for the incremental modulus at various pressures for the femoral and carotid artery are displayed in Figure 1. The curve by Bergel (1961a) was taken directly from his plots for arteries held at constant *in vivo* lengths, while the curve by Hutchison (1974) was derived from his data (Series B) using Equation (1). The wall thickness was given as 0.024 cm at 100mm Hg and successive wall thicknesses were extrapolated by assuming isovolumetric expansion. The dashed line on each of the curves represents the normal physiological range. As can be seen, the incremental modulus becomes progressively higher as the stress is increased. This is what would be expected to occur as the collagen fibers offer more and more resistance, thus making the vessel stiffer as it is extended.

Elastomers are defined as elastic materials with low Young's modulus of elasticity and whose elasticity is governed by certain molecular arrangements (Bergel, 1972). An ideal elastomer will undergo deformation instantly when stress is applied and recover its shape instantly when it is removed. For elastomers, stress is a function of strain only. Materials whose stress is a function of the rate at which the strain is applied are referred to as viscous materials. Materials showing properties of both elastomer

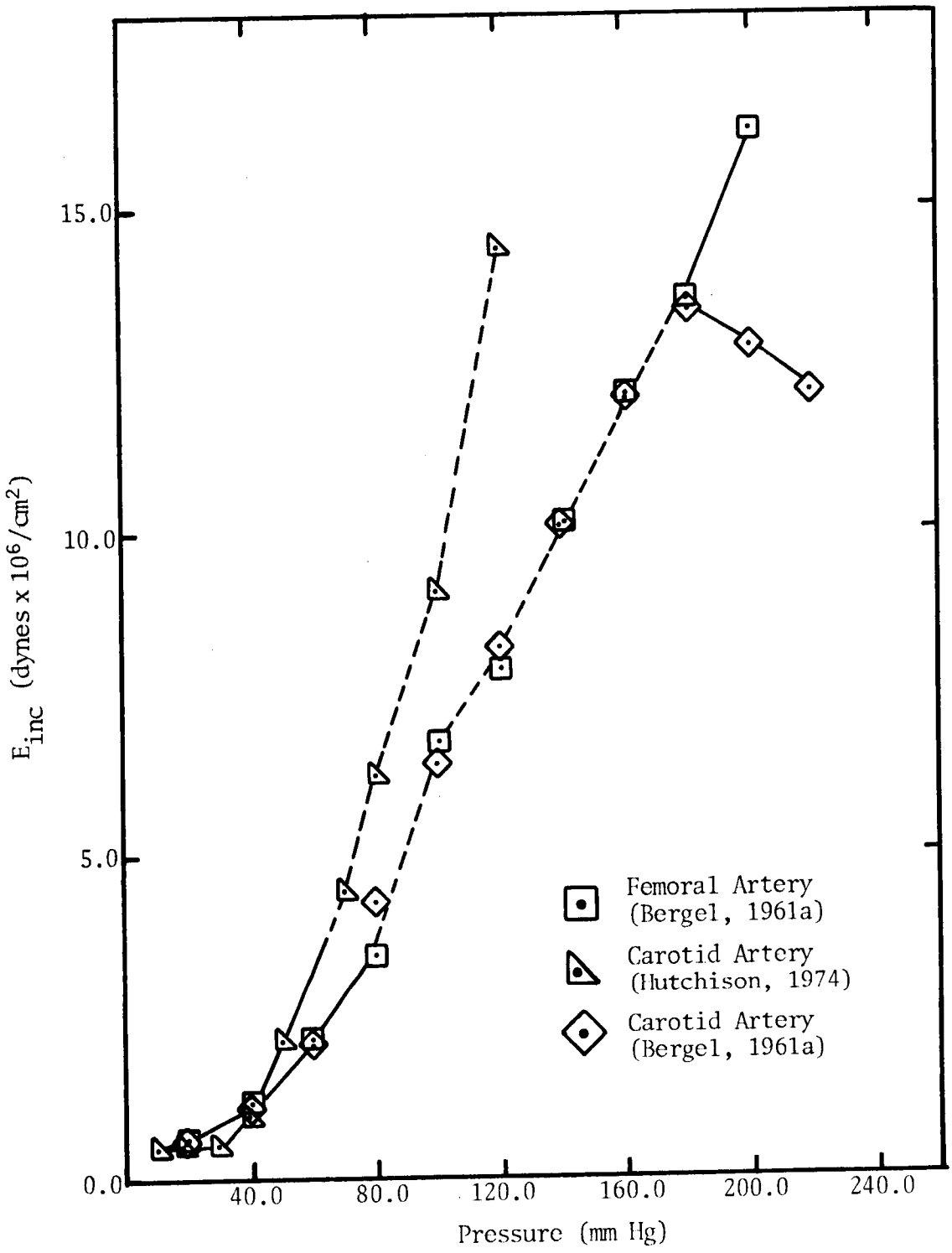


Figure 1. Incremental Modulus ($E_{inc}$) of Two Types of Artery

The curves were derived from plots of Bergel (1961a) and data from Hutchison (1974).

solids and viscous fluids are termed visco-elastic materials. In the case of blood vessels, visco-elastic behavior has been shown to exist (Patel, 1972; Gow and Taylor, 1968; Bergel, 1960).

By subjecting the *in vitro* vessels to sinusoidal variations in volume and recording pressure and radius changes, Bergel (1961b) was able to determine the dynamic elastic properties of the arterial wall. The dynamic elastic modulus was recorded as

$$E' = \frac{\Delta P}{\Delta R_o}\left[\frac{2(1 - \nu^2)\, R_o\, R_i^2}{(R_o^2 - R_i^2)}\right] \tag{2}$$

which was resolved into two components: the elastic component

$$E_{dyn} = E' \cos \phi \tag{3}$$

and the viscous component

$$\eta\omega = E' \sin \phi \tag{4}$$

where $\phi$ was the phase angle between pressure changes ($\Delta P$ leading) and radius changes ($\Delta R_o$). Bergel (1961b) found the viscous component to be small for the arteries studied, thus permitting $E_{dyn} \simeq E'$. It was shown that the vessels had an abrupt increase in the ratio of dynamic to static modulus from 0 to 2 Hz, with little further change at higher frequencies. The mean value of the dynamic elasticity for the femoral artery was recorded as $(12.0 \pm 0.81) \times 10^6$ dynes/cm$^2$ for a frequency of 2 Hz, while the mean value of

the static elasticity was recorded as $(6.4 \pm 1.0) \times 10^6$ dynes/cm$^2$.

Using anesthetized dogs, Peterson, et al. (1960) determined the mechanical properties of arteries *in vivo*. His studies involved the simultaneous recordings of intraluminal pressure and arterial diameter from a variety of sites along the arterial tree. The diameter was measured directly by a differential transformer transducer. The results were expressed as pressure-strain moduli, defined as

$$E_P = \frac{\Delta P \, R_o}{\Delta R_o} \tag{5}$$

which is independent of wall thickness. He concluded that major changes in the mechanical properties of arteries may occur by neuro-humoral influences upon smooth muscle in the arterial wall. Also, the mass of the arterial wall does not play a significant role in determining the stress and strain but the elastic and viscous moduli are the predominant parameters. The mean value of the pressure-strain elastic modulus for the femoral artery was determined as $3.69 \times 10^6$ dynes/cm$^2$.

Gow and Taylor (1968) obtained the dynamic elastic and viscous moduli of the arterial wall in anesthetized dogs. A low-friction caliper was employed to measure pulsatile diameter changes. Using the same equation as Bergel (Equation (2)), the dynamic elastic modulus was determined. For mean blood pressures ranging from 90 to 130mm Hg and frequencies from .96 to 2.75 Hz, the mean value of the

dynamic elastic modulus for eleven femoral arteries was determined as $(12.3 \pm 1.2) \times 10^6$ dynes/cm$^2$. Gow and Taylor pointed out the difficulty in determining the wall thickness to outside radius ratio ($\gamma$) and the variability of this value. Some values of the modulus of elasticity are tabulated in Table 4.

TABLE 4

ELASTIC MODULUS FOR THE FEMORAL ARTERY
(dynes/cm$^2$) x $10^6$

| Author | $E_{inc}$ | $E_p$ | |
|---|---|---|---|
| Bergel (1961a) | 6.9 ± 1.00(a) | 1.69 | (a,c) |
| | 12.0 ± 0.81(b) | | |
| Gow and Taylor (1968) | 12.3 ± 1.20(b) | 2.06 - 3.41 | (a,c) |
| Peterson, et al. (1960) | 9.33 (b,d) | 3.26 | (a,c) |

(a) Static value.

(b) Dynamic value.

(c) Calculated by McDonald (1960) using author's data.

(d) Calculated from Peterson's data using Gow and Taylor's Equation (2) (1968).

2. Latex as an arterial model. In order to simulate some of the previously mentioned properties of arteries, latex models were constructed. Latex is a concentration of water and rubber solids preserved in their liquid state by ammonia and possibly other unknown preservatives. The exact molecular structure of the rubber solids was not determined,

but it was expected to strongly resemble natural rubber. The molecular structure of natural rubber, which has the chemical name cis-1,4 polyisoprene, is given below.

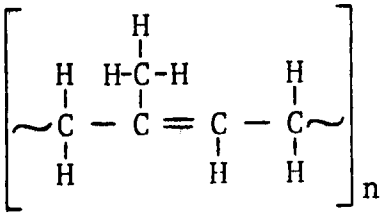

cis-1,4 polyisoprene
(natural rubber)

The n represents a value of about 20,000 (Morton, 1973), thus creating a long chain of cis-polyisoprene molecules. Breaking the double bond and permitting reattachment of bonds between two adjacent chains will greatly restrict movement between two chains and therefore make the rubber harder and stronger. This process is referred to as cross-linking. To help promote this, sulfur, which will form bridges between different chains, is used in a process called vulcanization. Increasing the curing temperature will also promote cross-linking.

The final vulcanized latex molecules are long chain-like affairs which are loosely coiled much like a spring. When initial stress is applied, the material will undergo strain with relatively little resistance. This will continue until the chain is straightened out, at which time the material will offer more and more resistance to further stress. The more cross-linkages that are present, the sooner this limit will be reached.

Based upon the above considerations, it appeared that latex might be a suitable material with which to

construct models of arteries, if the correct amount of cross-linkage could be obtained. Thus a method of making latex models of stenosed arteries was developed (Appendix A).

The latex models are essentially elastomers at low stresses, just as collagen and elastin are elastomers. But, because of the method by which the models were prepared, the latex wall is only a one-phase, homogeneous material, whereas artery walls are multi-phasic in structure with at least three components: collagen, elastin and smooth muscle. Latex is isotropic since the properties will be the same in any direction, whereas the three different wall components of arteries make the arteries anisotropic since one direction has different properties than other directions in the wall (Attinger, 1968).

To determine the material properties of the latex models, a photo-electric method similar to Bergel's (1961b) was used (see Chapter V). The models were held at constant non-stretched lengths in the path of a collimated light beam. Changes in diameter were detected by a photoelectric cell. Values for intraluminal pressure and resulting diameters are given in Appendix D for most of the models. By utilizing Equation (1), the incremental moduli of elasticity were determined for the models, and these results are also presented in Appendix D. A representative set of these values is shown in Figure 2 for one of the models.

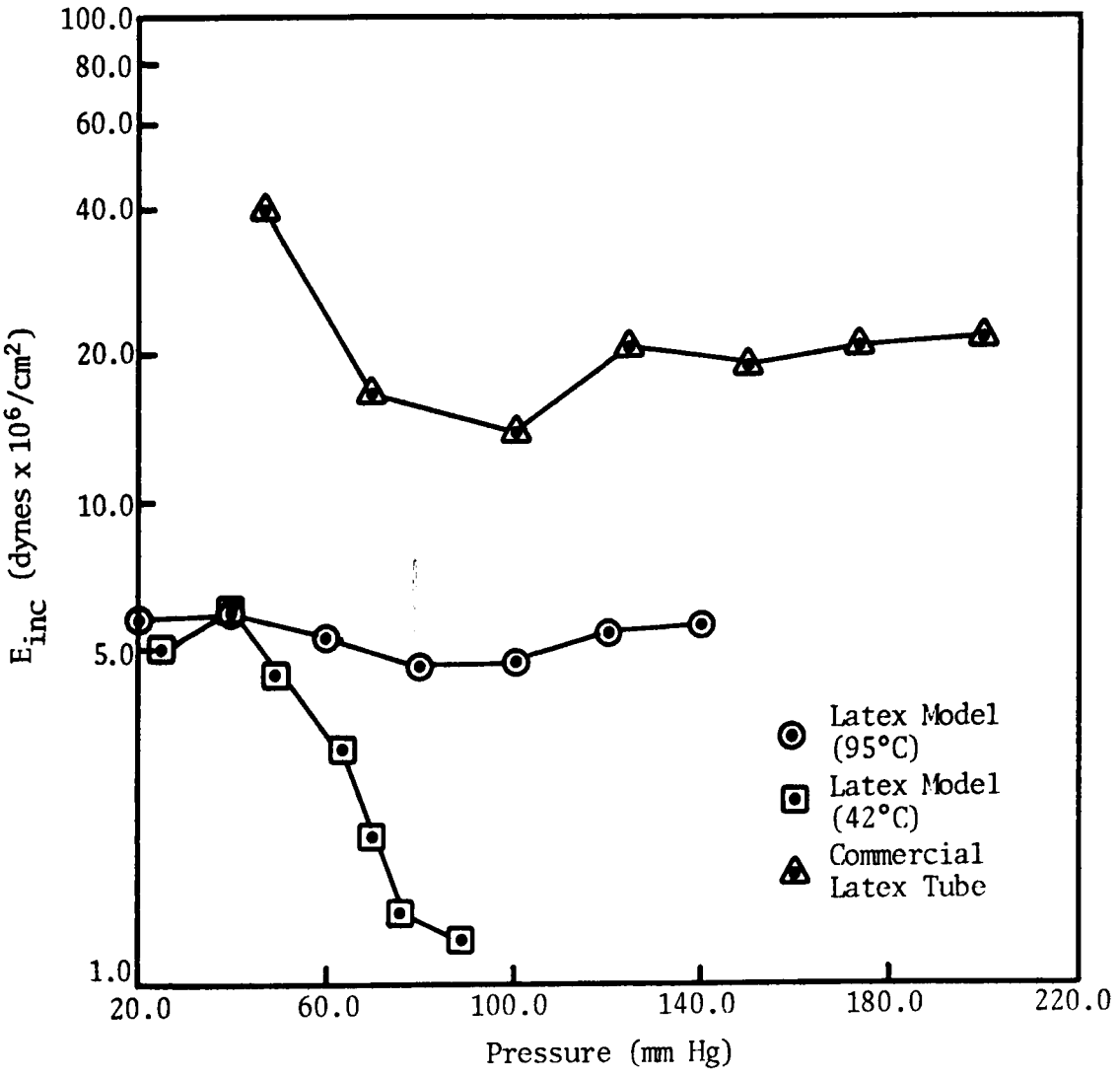


Figure 2. Incremental Modulus ($E_{inc}$) of Three Types of Latex Tubes

In constructing the models, different temperatures were used to increase the strength of the vessel. As can be observed from Figure 2, the elasticity of the vessel increased as the curing temperature was raised from 42°C to 95°C. Obviously, the latex model cured at 42°C is not nearly as strong as the 95°C model. The commercial latex tube was purchased from Rubber Latex Products. Although this tube has a modulus four times greater than the 95°C model, the two curves do have similar shapes. The exact vulcanization procedure is unknown for the commercial tube.

There is a major difference between the commercial latex tube and the constructed tube cured at 95°C which is not apparent from the curves of Figure 2. The commercial tube, if subjected to higher pressures, would show an increase in the elastic modulus, whereas the constructed tube was on the verge of yielding.

All modeling experiments were conducted with the 95°C cured latex for the following reasons: (a) The incremental moduli of elasticity for this material were close to those shown in Table 4; (b) The incremental moduli were relatively constant over the range of pressures of interest; (c) It was possible to "build in" the constriction into the model artery using the liquid latex, but this was not possible using the commercial latex tubes.

3. Relationships from thick-walled theory. From information presented in the preceding two sections, it is apparent that the results obtained for (and thus the comparisons of) the material properties of blood vessels and models of these vessels are dependent upon the method of analysis. Thus it is advantageous to examine the development of these equations, and to look for any other relationships which might depict the behavior of the models with respect to the prototype.

When the stress function depends on the radial direction only, the equation of compatibility can be reduced to give zero shear stress. To describe the resulting stresses produced in the wall of such a vessel by an internal pressure, it is necessary to consider an infinitesimal section of the wall, Figure 3.

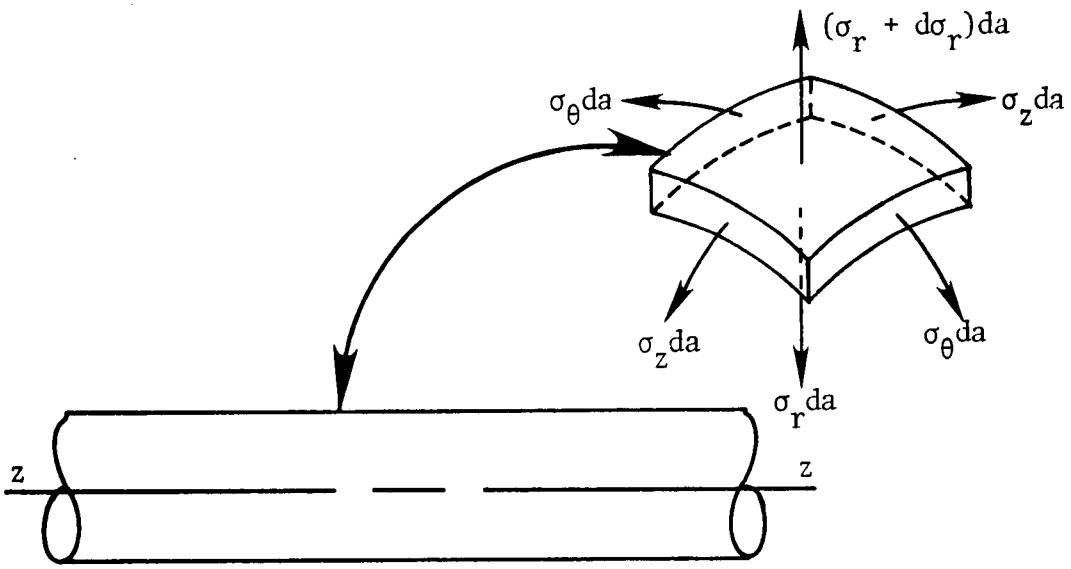


Figure 3. Stresses in the Vessel Wall

The stress component in the circumferential direction is denoted by $\sigma_\theta$, the component in the radial direction by $\sigma_r$ and the longitudinal direction as $\sigma_z$. By applying Newton's Second Law of Motion to this section, the stress terms can be evaluated.

In determining the expression for incremental modulus of elasticity, Bergel (1972) used a thick-walled, homogeneous isotropic tube of fixed length. For these conditions, the full expressions for the wall stresses are (Love, 1927):

$$\sigma_r = \frac{P_i R_i^2 - P_o R_o^2}{R_o^2 - R_i^2} - \frac{P_i - P_o}{R_o^2 - R_i^2} \frac{R_o^2 R_i^2}{R^2} \tag{6a}$$

$$\sigma_\theta = \frac{P_i R_i^2 - P_o R_o^2}{R_o^2 - R_i^2} + \frac{P_i - P_o}{R_o^2 - R_i^2} \frac{R_o^2 R_i^2}{R^2} \tag{6b}$$

$$\sigma_z = \frac{\lambda}{\lambda + G} \frac{P_i R_i^2 - P_o R_o^2}{R_o^2 - R_i^2} + e\frac{(3\lambda + 2G)G}{\lambda + G} \tag{6c}$$

where $\nu = \frac{\lambda}{2(\lambda + G)}$ ; $\lambda = \frac{\nu E}{(1 + \nu)(1 - 2\nu)}$ ; $G = \frac{E}{2(1 + \nu)}$ (7)

The quantities E and G are the modulus of elasticity in tension and compression and the modulus of elasticity in shear respectively, $\nu$ is Poisson's ratio, e is the longitudinal extension, and the quantities $\lambda$ and G are Lame's constants. The pressure at the internal boundary ($R = R_i$) is $P_i$, and $P_o$ is the pressure at the external boundary ($R = R_o$).

Assume that the ends of the vessel are closed by a flat plate so that the longitudinal tension will be balanced by the forces on the plate. Thus,

$$\sigma_z \pi(R_o^2 - R_i^2) = \pi(R_i^2 P_i - R_o^2 P_o) \tag{8}$$

which gives the longitudinal extension (strain) as

$$e = \frac{1}{3\lambda + 2G} \frac{R_i^2 P_i - R_o^2 P_o}{R_o^2 - R_i^2} \tag{9}$$

Substituting in terms of the elastic modulus E and Poisson's ratio $\nu$ for Lame's constants $\lambda$ and G we find

$$e = \frac{1 - 2\nu}{E} \frac{R_i^2 P_i - R_o^2 P_o}{R_o^2 - R_i^2} \tag{10}$$

Hence, if the Poisson's ratio is equal to 0.5, the longitudinal extension e will be zero (recall in the test system that the ends of the model were fixed).

Setting $P_o$ equal to zero and considering a point on the external boundary such that $(R = R_o)$, the outside wall stresses will reduce to

$$\sigma_r = 0 \tag{11a}$$

$$\sigma_\theta = \frac{2 P_i R_i^2}{R_o^2 - R_i^2} \tag{11b}$$

$$\sigma_z = \frac{2\nu P_i R_i^2}{R_o^2 - R_i^2} \tag{11c}$$

when $\nu = 0.5$.

The total strains in the circumferential direction may be expressed in cylindrical coordinates as (Timoshenko and Goodier, 1970):

$$\varepsilon_\theta = \frac{1}{E}\left[\sigma_\theta - \nu(\sigma_r + \sigma_z)\right] = \frac{\Delta R_o}{R_o} \qquad (12)$$

where $\Delta R_o$ is the radial displacement of some point at the external boundary ($R = R_o$). Substituting the stress relationships (11a,b,c) into Equation (12) and setting $\nu = 0.5$,

$$E = \frac{1.5\, P_i\, R_i^2\, R_o}{(R_o^2 - R_i^2)\, \Delta R_o} \qquad (13)$$

which is the same result obtained by Bergel (1972) for a Poisson's ratio of 0.5. Notice that the $(R_o^2 - R_i^2)$ term will be constant because of incompressibility and constant length. Also, if $\Delta P_i$ is substituted for $P_i$ in Equation (13) we obtain Equation (1), which is the Bergel's equation for the incremental modulus of elasticity (1961a).

This equation was based upon the assumption of Poisson's ratio equal to 0.5 and isotropic material, which is not strictly true when considering arterial walls (Bergel, 1961a). Hence, this will be a source of some error.

Lack of data on the pressure-radius relationships for the femoral artery necessitated comparison of the model with an alternate artery. The carotid was selected because of the availability of data and its close comparison to the femoral elasticity through the physiological range (Bergel, 1961a). Utilizing the equations for stress and strain (11b,

12) for thick-walled theory, values for the carotid artery (Hutchison, 1974) and various small models were determined (Appendix D). Figure 4 shows a curve of these values for a number of vessels. It can be seen at once that the carotid artery has a non-linear relationship, becoming less distensible as the stress is increased. Through the physiological range (dashed line) an approximation to Young's Modulus is ($6.3 \times 10^6$ dynes/cm$^2$). The latex models show a more linear behavior at low stresses, and in this range Young's Modulus is also approximately $6.3 \times 10^6$ dynes/cm$^2$. However, at higher strains where the models operated in the *in vitro* tests, the Young's Modulus is approximately $8.3 \times 10^6$ dynes/cm$^2$. It is important to note the low yield point which exists in the small latex models. To prevent plastic deformation, care was exercised to perform all small model experiments below $12.0 \times 10^5$ dynes/cm$^2$ stress.

From dimensional analysis,

$$K_{P_o} = K_E = \frac{8.3}{6.3} = 1.3$$

with $(P_o)_p$ = 107mm Hg. Hence, $(P_o)_m$ = 139mm Hg, with maximum systolic pressure of 220mm Hg. These values would exceed the yield point of the model; thus it was necessary to distort this Pi term. Values between one-half and one were chosen for $K_{P_o}$, such that all the pressure values would be below this maximum stress.

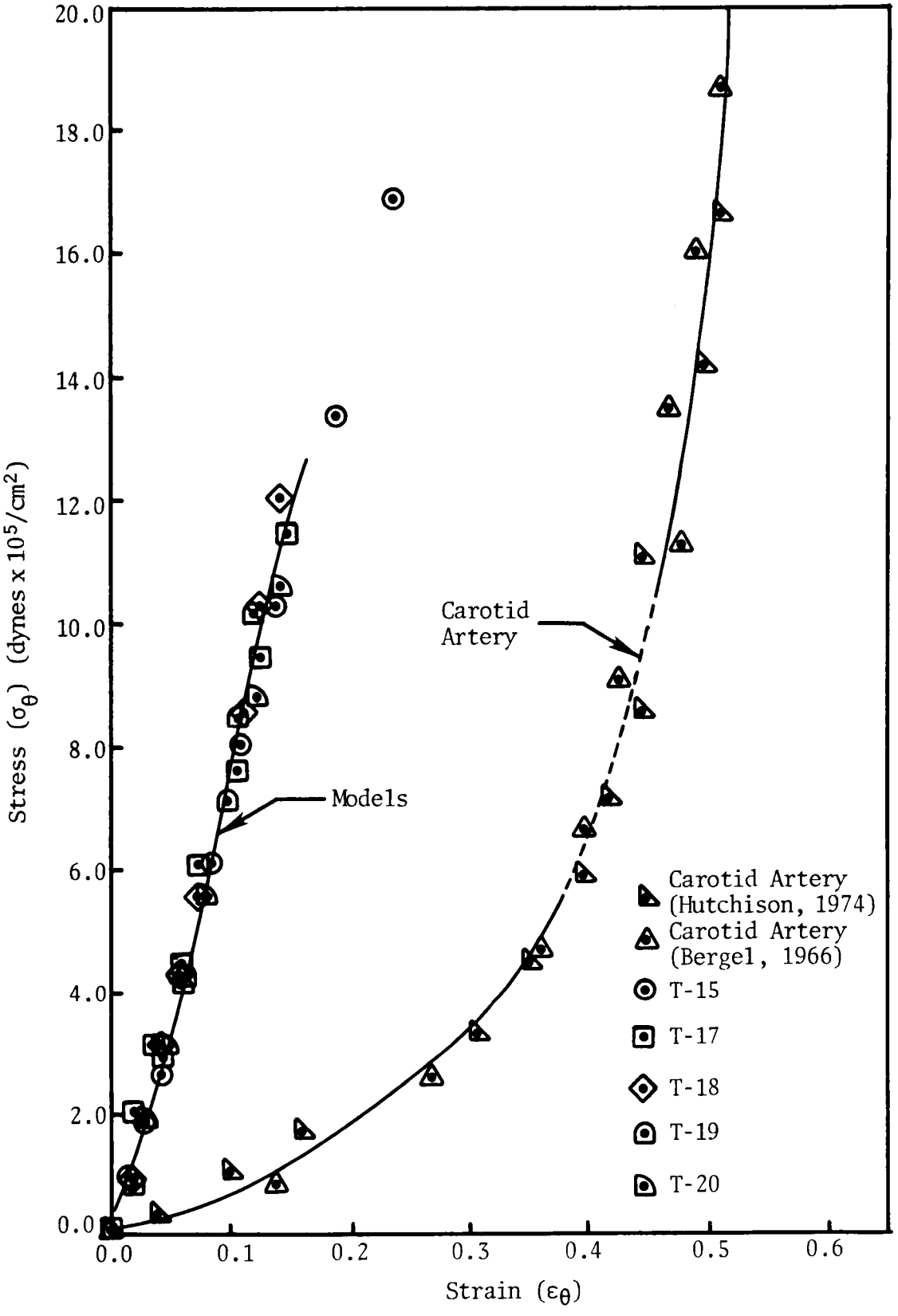


Figure 4. Stress-Strain Curve for Carotid Artery Based Upon Thick-Walled Theory

4. Relationships from thin-walled theory. The pressure-strain modulus ($E_p$) has the limitation of not including a measurement of wall thickness; thus the values calculated are more of a function of experimental set up rather than the actual stresses in the wall. On the other hand, the incremental modulus ($E_{inc}$) incorporates a new wall thickness at each calculation based upon isovolumetric expansion. The major limitation of this approach is the difficulty in determining the wall thickness (Peterson, et al., 1960; McDonald, 1960). An alternative to these two approaches would be to determine an incremental modulus based upon thin-walled theory.

Assuming thin-walled theory, the stress ($\sigma$) and strain ($\varepsilon$) in the wall of any thin-walled, homogeneous and isotropic vessel can be calculated. The use of the thin-walled theory is justified when the wall thickness is less than 10% of the radius. This condition is nearly met in the majority of data recorded for the femoral artery (as can easily be observed in Section B). Although the model has a wall-thickness radius ratio greater than 10%, this assumption will be applied as an approximation to allow comparison with thick-walled theory.

Consider the longitudinal and transverse plane of a thin-walled pressure vessel under a pressure $P_i$, as shown in Figure 5. Since the vessel is in static equilibrium,

$$\sum F = 0$$

$$\sum F = \int_0^{\pi} P_i R_i \, d\theta \, (\sin \theta) \, L \; - \; 2 \int_{\text{area}} \sigma_\theta \, da \qquad (14)$$

Hence,

$$\sigma_\theta = \frac{P_i R_i}{h} \qquad (15a)$$

If the vessel has closed ends, the longitudinal stress $\sigma_z$ can be determined by passing a plane through the cylinder normal to its z-axis. Using a free-body diagram,

$$\sigma_z = \frac{P_i R_i}{2h} \qquad (15b)$$

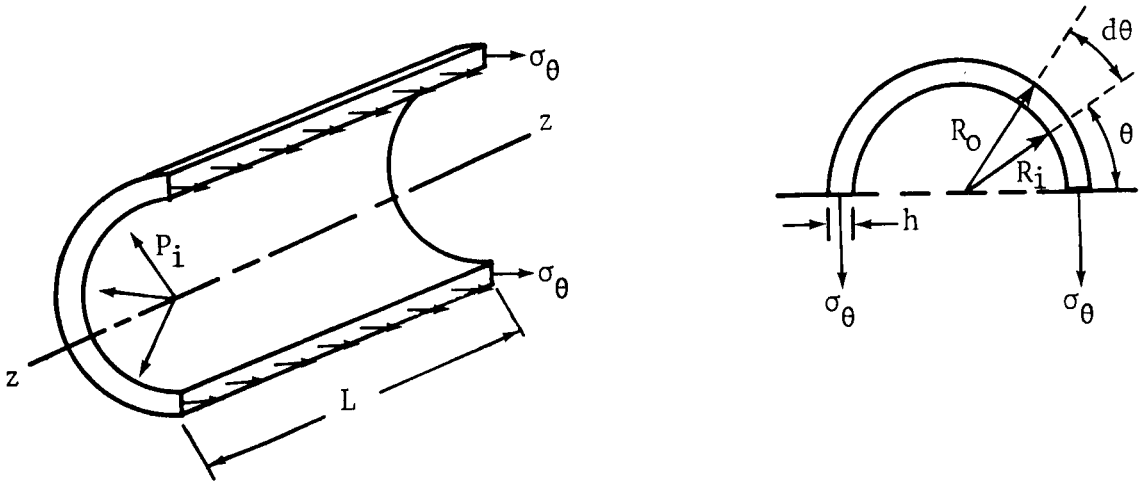


Figure 5. A Thin-Walled Vessel

The radial stress is due to the compressive effects of the pressure $P_i$. If the outside pressure is equal to zero, then

$$\sigma_r = -P_i \qquad (15c)$$

This radial stress is obviously an order of magnitude lower than the circumferential and longitudinal stress for thin-walled vessels, thus the radial stress will be neglected.

To determine the strain relationships, consider an infinitesimal transverse section of this vessel, which has been deformed by the pressure $P_i$. It is assumed that the circumferential planes remain concentric and that the change in wall thickness is negligible.

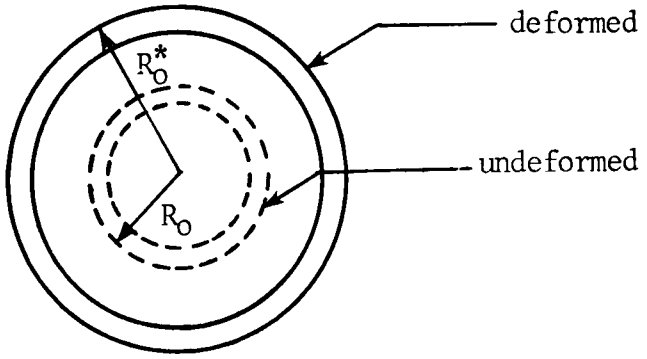


From the above figure the circumferential strains are

$$\varepsilon_\theta = \frac{2\pi R_o^* - 2\pi R_o}{2\pi R_o} = \frac{R_o^* - R_o}{R_o} = \frac{\Delta R_o}{R_o} \qquad (16)$$

As with thick-walled theory, the total strain in the circumferential direction may be expressed in cylindrical coordinates as

$$\varepsilon_\theta = \frac{1}{E}\left[\sigma_\theta - \nu(\sigma_r + \sigma_z)\right] = \frac{\Delta R_o}{R_o} \qquad (17)$$

Substituting the thin-walled stress relationships and

solving for the elastic modulus E, gives

$$E = 0.75 \frac{P_i}{\Delta R_o} \frac{R_i R_o}{h} \tag{18}$$

where $\nu = 0.5$. This equation is similar to the expression used by Patel (1972) and Gosling and King (1974). Because of constant wall thickness, h will be defined as

$$h = 0.1 \bar{R}_o \tag{19}$$

where $\bar{R}_o$ is the outside radius at the mean pressure over the range in which the vessel is tested. Also, for thin-wall theory $R_i \simeq .9R_o$.

Thus, equation (18) becomes

$$E = 6.75 \frac{P_i}{\Delta R_o} \frac{R_o^2}{\bar{R}_o} \tag{20}$$

Equation (20) will be modified for an incremental approach similar to that of Bergel (1961a) to facilitate its application to materials having a non-linear stress-strain behavior:

$$E_{inc_t} = 6.75 \frac{P_3 - P_1}{R_{o_3} - R_{o_1}} \frac{R_{o_2}^2}{\bar{R}_o} \tag{21}$$

The subscripts 1, 2, 3 represent successive measurement of internal pressure and outside radius. The equation gives the incremental modulus which exists at pressure ($P_2$) for an incremental strain from $R_{o_1}$ to $R_{o_3}$. This equation provides the necessary expression for the wall thickness term (when h is approximately $0.1\bar{R}_o$), yet it eliminates the difficult task of determining the exact value.

To compare these three approaches, it is necessary to convert the pressure-strain modulus ($E_p$) (Peterson, et al., 1960) to an incremental modulus similar to that of Bergel (1961a). This may be expressed as

$$E_{inc_p} = \frac{P_3 - P_1}{R_{o_3} - R_{o_1}} R_{o_2} \qquad (22)$$

Figure 6 illustrates the comparison between these values. It can be seen that the $E_{inc}$ and $E_{inc_p}$ curves differ dramatically in magnitude for the carotid artery as the $E_{inc_t}$ curve approximates $E_{inc}$ much better. The nearer the vessel is to thin-walled conditions the better the approximation. This explains the large difference that exists with the thick-walled model curves. Also, the magnitudes of $E_{inc_t}$ are affected by the assumed wall thickness ratio (equation (19)). A more realistic approach might be to determine h in terms of $\bar{R}_o$ for the vessels and use that relationship to determine the expression for $E_{inc_t}$. Further work is needed before definite conclusions can be drawn regarding the various methods of evaluating the model with respect to the prototype.

B. Radius

As a result of the oscillatory intraluminal forces, both the inside and outside radii are continuously changing. To simplify calculations the radius was defined as that radius which existed at the mean pressure. By extracting data (Bergel, 1961a; Gow and Taylor, 1968; Peterson,

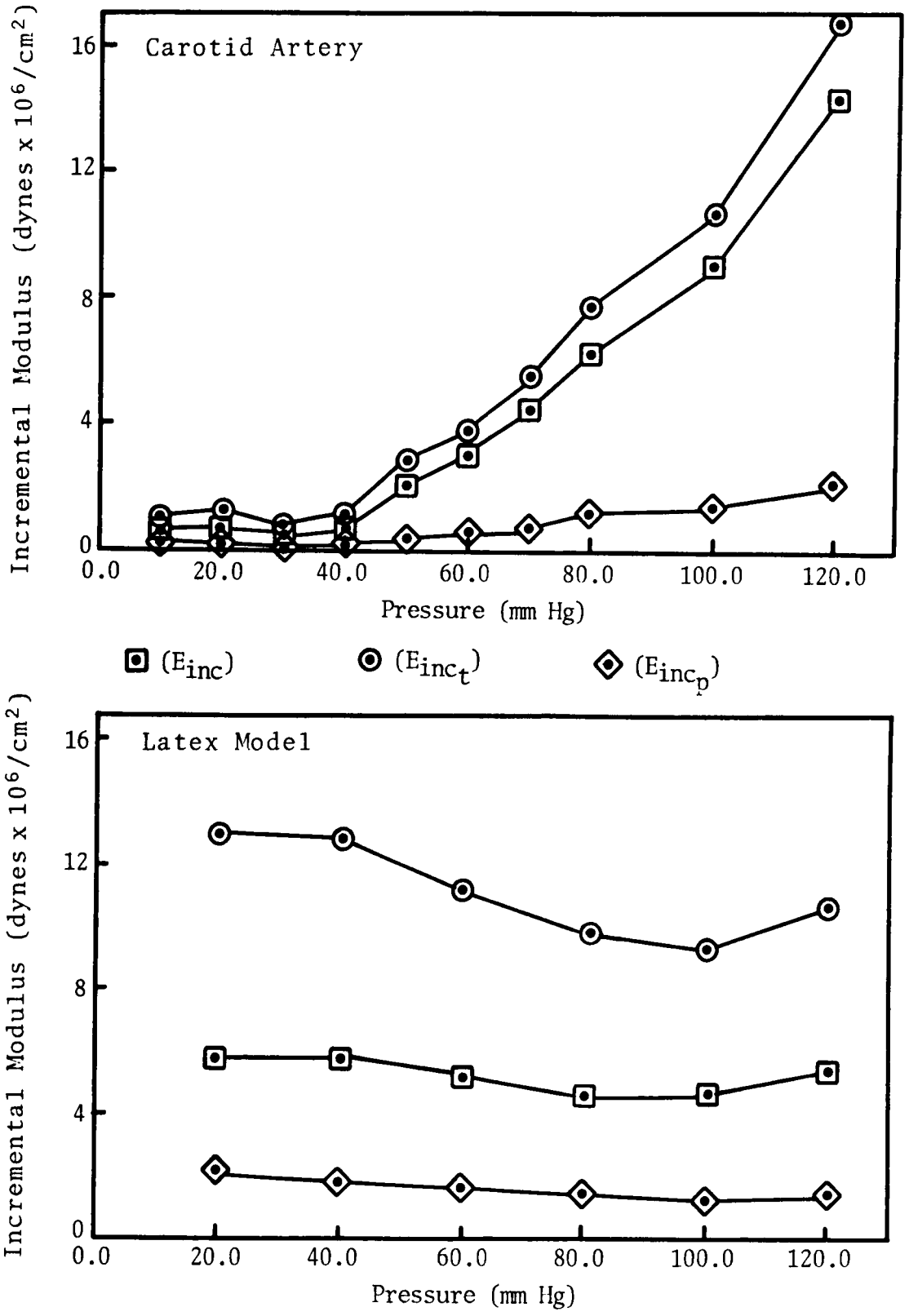


Figure 6. Pressure Elasticity Curves for Three Different Types of Incremental Modulus

et al, 1960) it was possible to obtain a mean radius for the femoral artery, while the mean radii for the models were determined directly by a photoelectric system. The values for each of the vessels for a given mean pressure are shown in Table 5.

C. Wall Thickness

Due to the pulsatory pressure, isovolumetric expansion and surrounding connective tissue, it is difficult to accurately measure *in vivo* arterial wall thickness. Thus, estimations of wall thickness have been calculated *in vitro* at constant *in situ* lengths. By assuming incompressibility and knowing the weight of the vessel and the density of the wall, the wall thickness was determined by several authors (Bergel, 1960; Peterson, et al., 1960; Gow and Taylor, 1968). The comparative mean values for the relative wall thickness ($\gamma$) defined as the ratio of the wall thickness to outside radius were calculated and are displayed in Table 5. The thickness was calculated by multiplying the relative wall thickness by the mean outside radius.

The thickness of the latex models was determined by measuring the latex coated mandrels (see Appendix A) with a micrometer and subtracting the known diameter of the mandrels. Estimations of mean pressure wall thickness values were determined by assuming isovolumetric expansion. Comparative values of the relative wall thickness ($\gamma$) for several models are also displayed in Table 5. The variations shown

TABLE 5

RADII AT MEAN PRESSURE

| Sample | Mean Pressure (mm Hg) | $\gamma$ ($h/\bar{R}_o$) | $\bar{R}_o$ (cm) | $\bar{R}_i$ (cm) | h (cm) | Author |
|---|---|---|---|---|---|---|
| Femoral Artery | 100. | 0.115 ± 0.0096 (11) | 0.197 | 0.174 | 0.023 | Bergel (1960a) |
| | 124. | 0.130 ± 0.0320 (12) | 0.218 | 0.190 | 0.028 | Gow and Taylor (1968) |
| | -- | 0.190 ± 0.5400 (7) | 0.203 | 0.165 | 0.038 | Peterson, et al. (1960) |
| Value Used in Study | 107. | 0.112 | 0.206 | 0.185 | 0.022 | |
| Small Latex Models | 60. | 0.186 ± 0.0040 (3) | 0.312 | 0.254 | 0.058 | |
| | 100. | 0.175 ± 0.0060 (3) | 0.323 | 0.266 | 0.057 | |
| Large Latex Models | 60. | 0.100 ± 0.0140 (8) | 1.030 | 0.930 | 0.103 | |
| | 100. | 0.075 ± 0.0160 (8) | 1.100 | 1.096 | 0.089 | |

in the table are the standard deviations of means. Figures in parentheses are the number of measurements.

## D. Poisson's Ratio

The ratio of the magnitude of the lateral strain to the magnitude of the axial strain is defined as Poisson's ratio ($\nu$). This constant may be determined by considering the bulk modulus, which may be written in terms of Poisson's ratio as

$$K = \frac{E}{3(1 - 2\nu)} = \frac{PV_o}{\Delta V} \qquad (23)$$

where K, the bulk modulus, is the ratio of compressive stress P to the relative change in volume $\frac{\Delta V}{V_o}$.

Lawton (1954) and Bergel (1960) showed isovolumetric expansion to occur for small strains in the arterial wall. From the above equation, it can be seen that this will occur only when the Poisson's ratio has a value of 0.5. The Poisson's ratio for the models was not determined directly, but recorded values (Popov, 1968) of 0.5 are shown for rubbers.

## E. Viscosity

Blood is essentially a suspension of proteins, erythrocytes, leukocytes and platelets in an aqueous solution called plasma. About 97% of the total cell volume consists of erythrocytes, thus the removal of leukocytes and platelets from whole blood is unlikely to make measurable changes in the viscosity level (Cokelet, 1972). Measurement of the

relationships between stress and rate of strain is difficult because of the varying rheological properties of blood. Factors such as temperature, flow oscillation, tube diameter and percent haematocrit all have an effect upon the viscous properties.

It has been shown experimentally (Merrill, et al., 1963; Bugliarello, et al., 1965) that blood behaves as a non-Newtonian fluid with asymptotic Newtonian behavior. Such a fluid has a non-linear relationship between the shear stress and shear rate at low shear rates, but at higher values it becomes linear. The Newtonian viscosity of canine blood is reported as being 3.196 centipoise at 38°C (Albritton, 1952).

The blood analog was a clear glycerol-water solution whose viscosity was measured with a Hoppler-Viscosimeter. The absolute Newtonian viscosity of the analog was determined from a measurement of the time required for a glass ball to fall through a column of the analog enclosed in a precision glass tube. The viscosity was calculated in accordance with the following formula:

$$\mu = T \times (S_b - S_f) \times B$$

where $\mu$ = absolute Newtonian viscosity in centipoise,

$T$ = time interval of the falling ball,

$S_b$ = specific gravity of the glass ball (2.4157),

$S_f$ = specific gravity of the analog, and

$B$ = ball constant (.01745).

Samples of the blood analog fluid were tested at 25°C, the temperature at which experiments were performed.

F. Wall Density

The wall density of the femoral artery was determined experimentally by extracting an artery from a ten month old male collie weighing 48 lb. The wall volume was determined by placing the artery in distilled water and measuring the amount of displaced fluid. Weight of the vessel was established by using a microbalance. Calculation of mass over volume resulted in a wall density of 1.16 $gm/cm^3$. This agrees with other recorded values of 1.0 - 1.2 $gm/cm^3$ (Kirkeeide, et al., 1975). Using the same method, the mean value for the wall density of the models was calculated as 1.1 $gm/cm^3$.

G. Density of Fluid

The specific gravity of canine blood is reported as 1.052 - 1.056 for adults and 1.045 for younger dogs at 22 - 26 °C referred to water at 4°C (Aldritton, 1952; Ditter, 1961), from which the mean density was calculated as 1.05 $gm/cm^3$. In like manner, the specific gravity of the blood analog was measured with a hydrometer at 25°C, and the density was calculated.

H. Pressure Wave Shape

The pressure wave in the femoral artery is of periodic nature which may be described in terms of the Fourier series

$$P = P_o + \sum_{1}^{n} P_j \cos (j\omega t - \phi_j) \qquad (24)$$

with

$$\phi_j = \tan^{-1}\left(\frac{B_j}{A_j}\right) \; ; \quad P_j = \sqrt{A_j^2 + B_j^2} \qquad (24a,b)$$

where $P_o$ is the mean pressure and $P_j$ is called the pressure modulus, or amplitude, of the oscillation and $\phi_j$ its phase angle. The values of $A_j$ and $B_j$ are the Fourier coefficients.

By extracting data points from the femoral pressure pulse (McDonald's Figure 6.2, 1960) and performing a Fourier analysis, the coefficients were determined (Appendix E). Values of the first five harmonic components are given in Table 6.

In Figure 7, the canine femoral artery pressure curve is illustrated as well as the theoretically derived curves to be modeled. These curves were used as a reference or standard to be duplicated experimentally for modeled physiological conditions. They were determined using the Fourier analysis by first specifying the desired ratio $(P_o)_m/(P_o)_p$, and thus $(P_j)_m/(P_j)_p$, and then using the modeling laws to obtain the fundamental angular frequency $(\omega)_m$ for the model.

For the small arterial models, a cam-driven, variable frequency piston-operated pump was designed and constructed to simulate the modeled pressure and flow of the canine femoral artery. Problems resulting from wave reflection and capacitance of this elastic circulatory system required

TABLE 6

HARMONIC COMPONENTS FOR THE FEMORAL PRESSURE CURVE

| Harmonic | $A_j$ (cosine) | $B_j$ (sine) | $P_j$ (mm Hg) | $\phi$ (radians) |
|---|---|---|---|---|
| 1 | - .23 | 28.92 | 28.92 | 1.58 |
| 2 | -24.83 | 1.69 | 24.89 | 3.07 |
| 3 | - 2.74 | - 7.24 | 7.74 | 4.35 |
| 4 | 1.05 | - 1.94 | 2.21 | 5.21 |
| 5 | 0.26 | - 0.07 | 0.27 | 6.01 |

$P_o$ (mean pressure) = 107.7

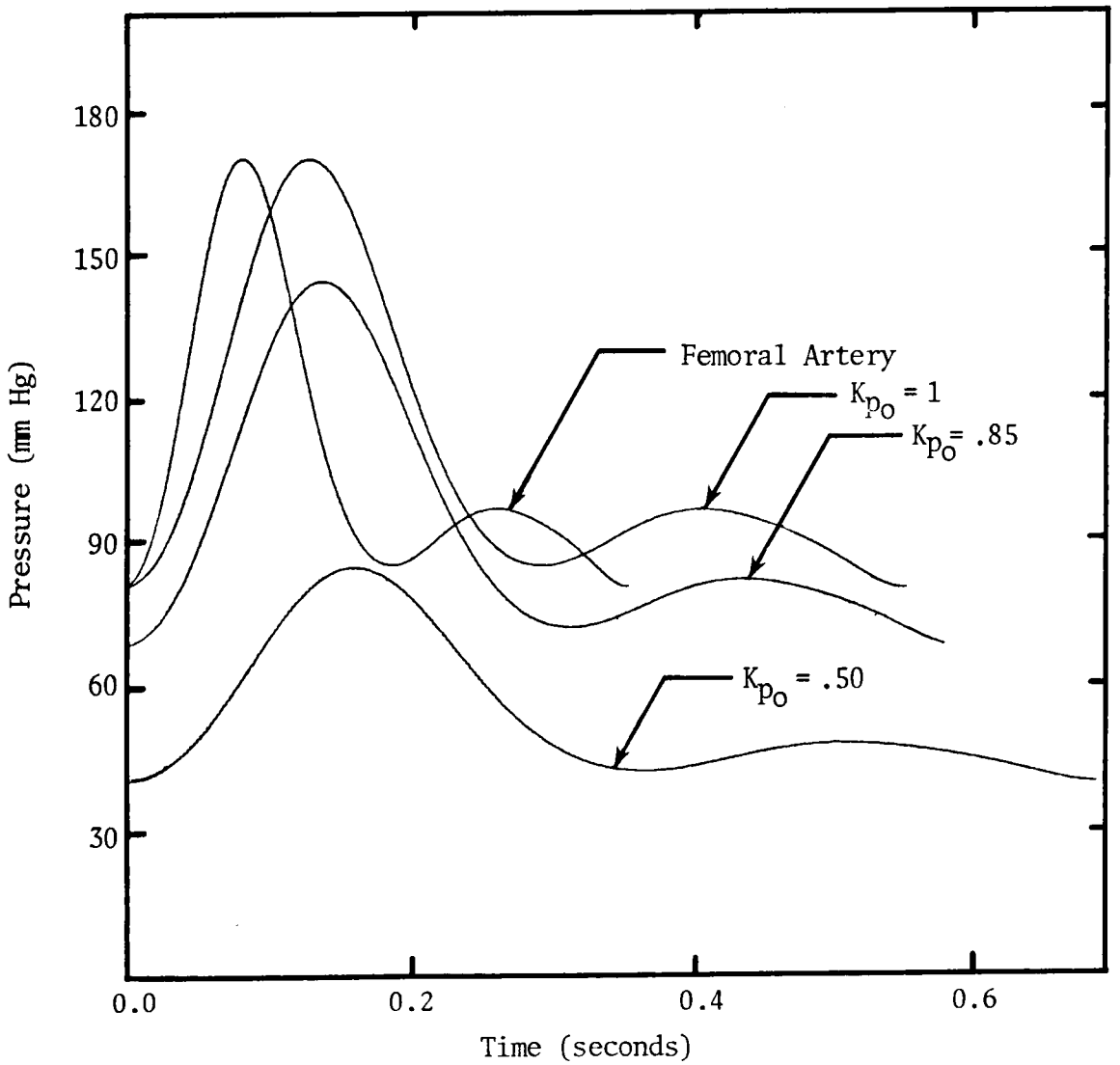


Figure 7. Femoral Artery Pressure Curves and Scale Factors for the Small Models

consideration. After considerable effort and time had been spent in investigating these problems and carrying out successive tests, cam profiles were obtained which produced conformable pressure curves. Figure 8 illustrates the parallelism between a desired theoretical curve and actual pressure wave shape from this mechanical system as well as from the large arterial model system.

## I. Mean Velocity Wave Shapes

Just as pressure, the velocity of propagation of blood through the systemic system has pulsatile characteristic. By continuous measurement of the volume flow rate Q through the canine femoral artery (McDonald, 1960), the mean spacial velocity V may be determined as a function of time. The mean spacial velocity is defined as:

$$V = \frac{Q}{\pi \bar{R}_i^2} \tag{25}$$

where $\bar{R}_i$ is the inside radius which exists at mean pressure. To model this wave it is convenient to express the velocity in terms of the Fourier series as:

$$V = V_o + \sum_{n=1}^{n} V_j \cos (j\omega t - \phi_j) \tag{26}$$

where $V_o$ is the time average mean velocity and $V_j$ is the velocity modulus and $\phi_j$ its phase angle. By modifying the pressure Fourier series program (Appendix E), it was possible to determine the Fourier coefficients of this curve, Table 7.

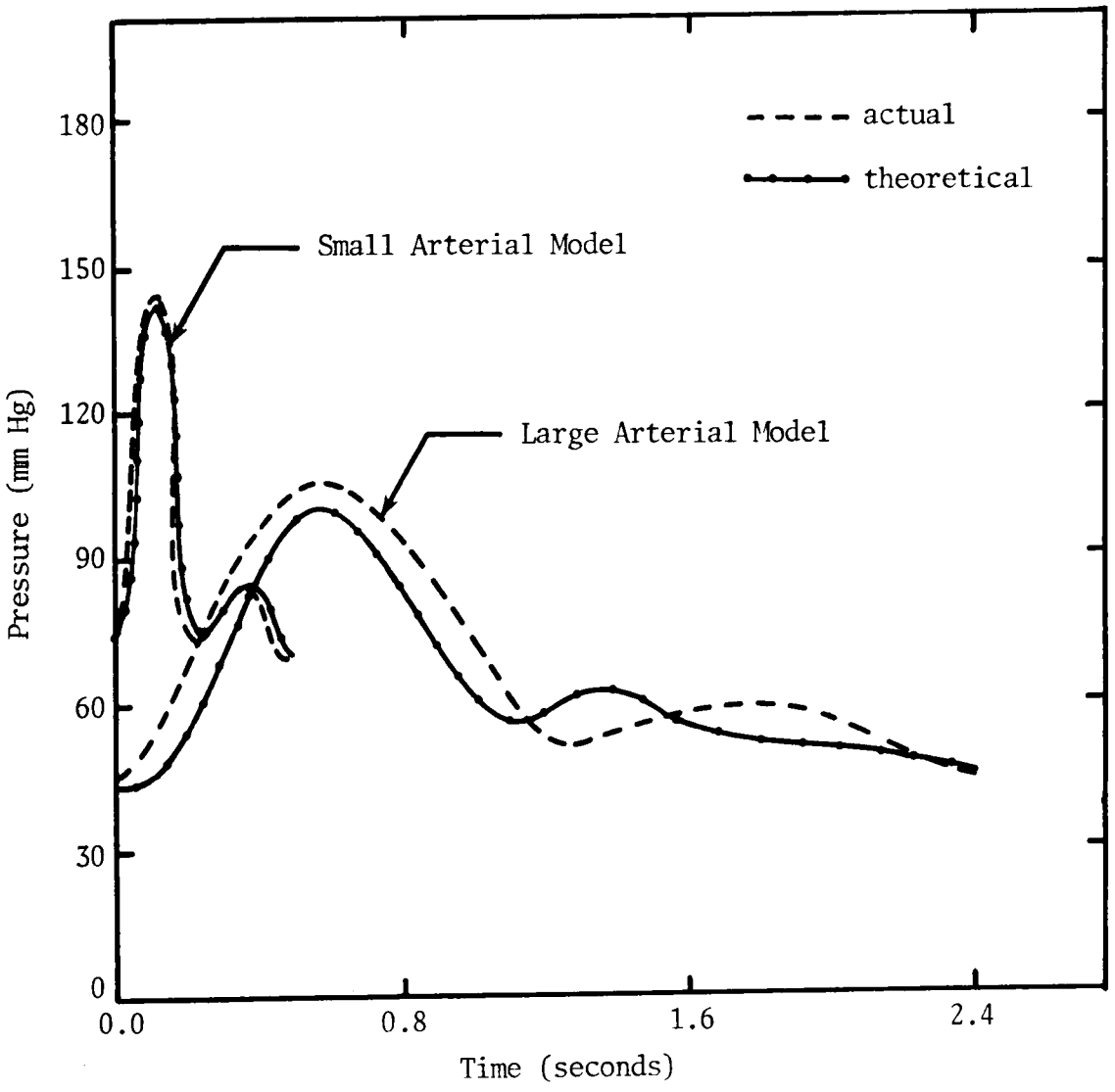


Figure 8. Theoretical and Actual Pressure Curves for the Small and Large Arterial Model Systems

TABLE 7

HARMONIC COMPONENTS FOR MEAN VELOCITY CURVE

| Harmonic | $A_j$ (cosine) | $B_j$ (sine) | $V_j$ (cm/sec) | $\phi$ (radians) |
|---|---|---|---|---|
| 1 | 19.6850 | 12.2271 | 23.17 | 58.15 |
| 2 | -25.7646 | 12.5263 | 28.65 | 154.07 |
| 3 | -11.3864 | - 6.4273 | 13.08 | 209.44 |
| 4 | - 2.0830 | - 6.2214 | 6.56 | 251.49 |
| 5 | 2.6020 | - 2.3647 | 3.52 | 312.26 |

$V_o$ (mean velocity) = 12.3

In the mock circulatory system it was insurmountable to exactly duplicate both the pressure and velocity wave shapes. Thus it was necessary to model one wave shape as accurately as possible while holding the other at its mean value. Because of the ability to accurately measure the instantaneous pressure inside the model, it was decided to model the pressure wave while holding the velocity at its mean value. Figure 9 indicates the degree of error between the theoretical curve and actual velocity wave shape in one of the small models (T-18) by following this practice.

## J. Geometry of the Stenosis

A stenosis is a lesion or narrowing of a passage or orifice such as in arteries or veins of the body. This type of constriction may be caused by either intravascular or extravascular deformation, as shown in Figure 10 (Rodbard, 1966). When fatty substances are transported into the vessel wall by plasma they become trapped within the wall. An excessive quantity of these entrapped fatty substances will pile up, thus initiating the development of atherosclerotic lesions (Spain, 1966). Deformations may also occur when platelets attach themselves to the vessel wall as a result of injury to the tunica interna or by the impingement of ligaments or spurs on the vessel wall (Hardin, 1965). The geometry of the stenosis will vary in degree of narrowing as well as shape, depending on the method of deformation.

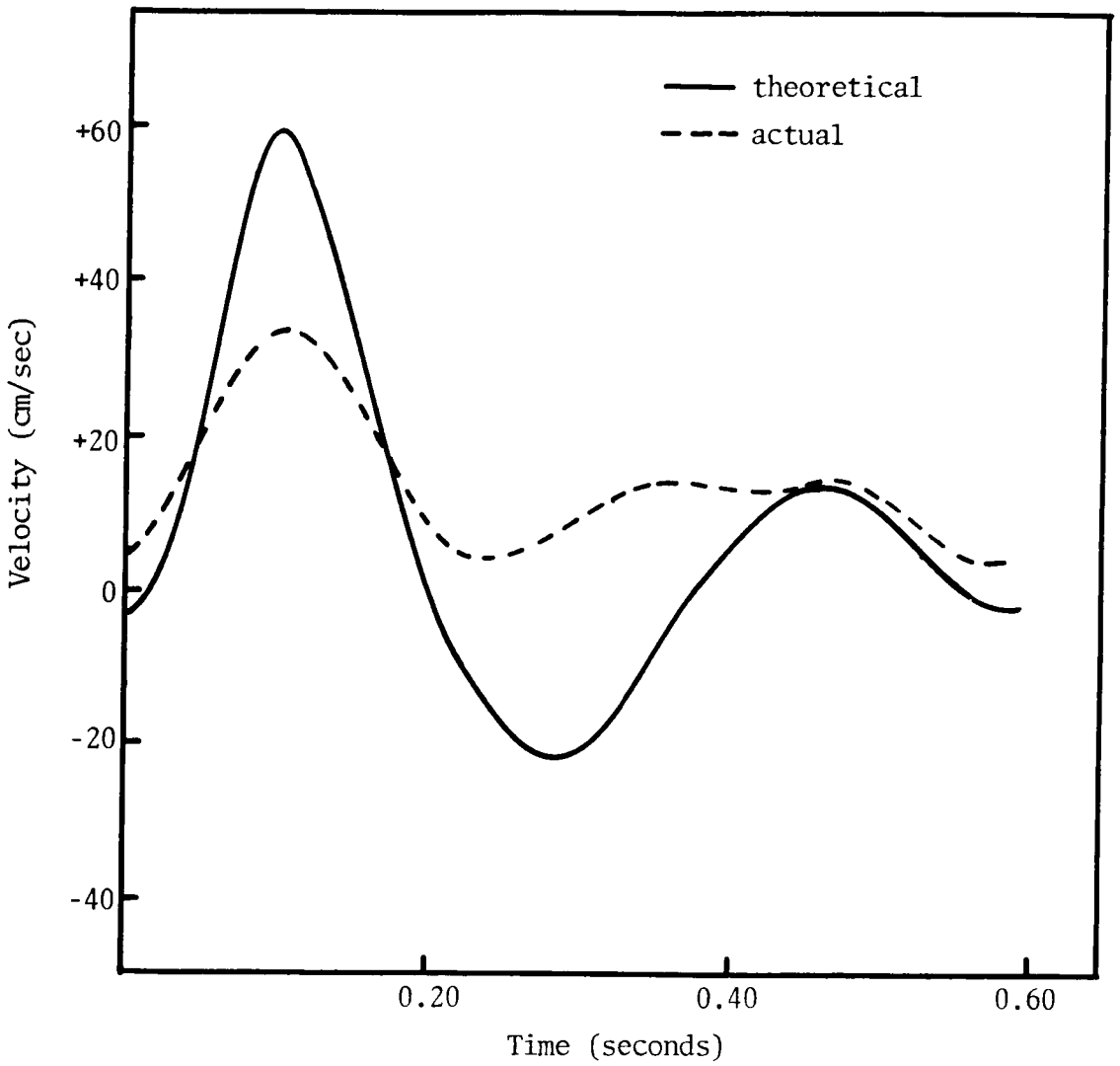


Figure 9. Comparison of Theoretical and Actual Velocity Curves in Model T-18

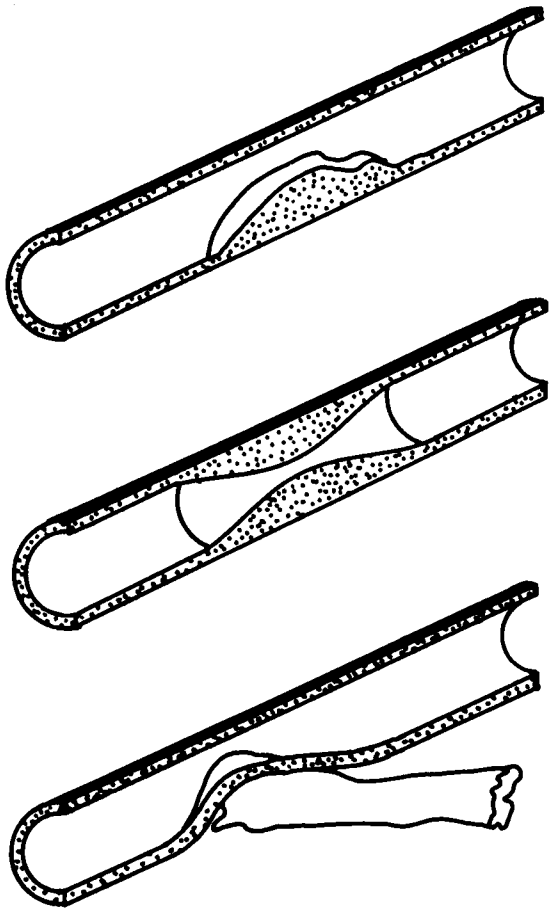


Figure 10. Possible Methods by Which the Stenosis Might Develop

The geometry of the models, Figure 11, was the same as that studied by Lee and Fung (1970) and Kozman and Forrester (1972) and is described by the equation:

$$\frac{r_i}{R_i} = 1 - \left(\frac{H}{R_i}\right) \exp\left[\frac{-16z^2}{L_s^2}\right] \qquad (27)$$

where

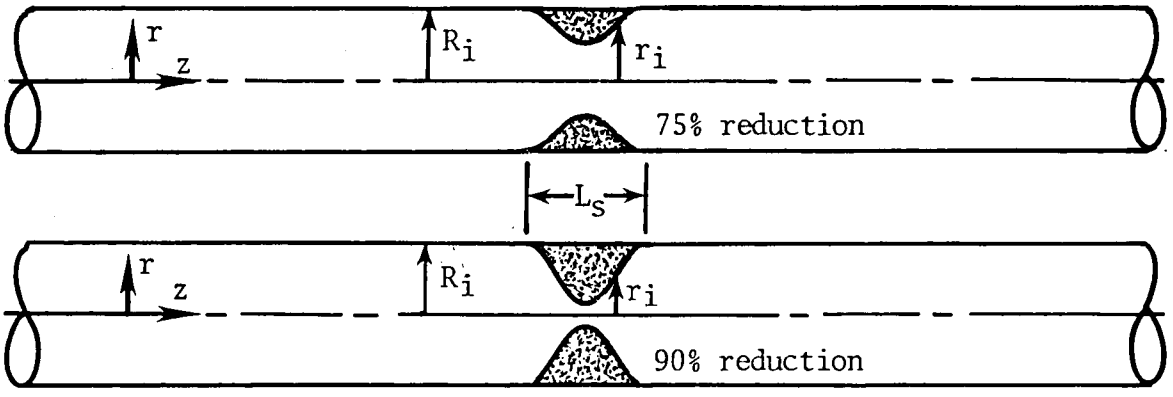


$$\frac{r_i}{R_i} = 1 - \left(\frac{H}{R_i}\right) \exp\left[\frac{-16z^2}{L_s^2}\right]$$

Figure 11. Geometry of the Models

$R_i$ = radius of the straight tube proximal to the stenosis at atmospheric pressure,

$r_i$ = local radius of the tube,

$z$ = axial coordinate, measured from the throat of the stenosis,

$H$ = height of stenosis, and

$L_s$ = stenosis length.

This normalized bell-shape geometry was originally selected because of its conformal mapability to simplify theoretical work. It was used here so that comparison between rigid and flexible models could be made. The severity of the constriction is controlled by $L_s$ and H. In the present study, $L_s = 2R_i$ and H was chosen to provide area reductions of either 75% or 90% at mean pressures as shown in Figure 11.

## K. Dilatation Length Scale

The remaining variables to be discussed are the length from throat of stenosis to start of poststenotic dilatation region ($L_{sd}$), outside radius of poststenotic dilatation region ($R_d$) and length of poststenotic dilatation ($L_d$). Experimental studies by Roach (1963) on the femoral artery of adult dogs has permitted determination of these variables. It was found that the radius of dilatation ($R_d$) is greatly affected by the type of stenosis (Table 8). The values shown are the maximum ones obtained by Roach at the time of sacrifice, which varied from 24 hours to 10 months.

TABLE 8

EXPERIMENTAL RESULTS BY ROACH (1963) ON THE EFFECT OF TYPE OF STENOSIS AND RADIUS OF DILATATION

| Type of Stenosis | % Decrease in Lumen | Number of Poststenotic Dilatations | Number of Prestenotic Dilatations | Relative Radius (cm/cm) | $R_o$ .75 cm distal (cm) | $R_o$ .75 cm Proximal (cm) |
|---|---|---|---|---|---|---|
| Minimum | 5 - 35 | 6 | 0 | .89 - .94 | .47 | .52 |
| Moderate | 23 - 76 | 24 | 0 | 1.1 - 1.45 | .55 | .50 |
| Severe | 85 - 100 | 0 | 4 | .78 - .83 | -- | -- |

The radius has been expressed as relative radius which is the ratio of distal radius over proximal radius. It is obvious that no poststenotic dilatation occurred unless the relative diameter was greater than one. The severe stenosis was defined as a ligation so tight that a pulseless distal section existed at the time of operation. In all four of the cases, a prestenotic dilatation developed with a collapsed distal section. Roach contributed this to the increase in proximal pressure. After several days collateral circulation caused the proximal and distal diameters to return toward normal.

By placing a moderate stenosis around one femoral artery and a minimum stenosis around the other of six dogs, Roach was able to relate the degree of constriction to the length of dilatation. These values have been tabulated in Table 9 as well as depicted graphically in Figure 12. It can be seen that for the moderate stenosis, $L_d$ is 2.05 cm long with maximum $R_d$ changes between 0.75 and 1.0 cm from the distal end of the stenosis; thus $L_{sd}$ would equal one-half $L_s$. For the minimum stenosis, no dilatation developed, consequently $L_d$ and $L_{sd}$ will equal zero and infinity respectively.

TABLE 9

RELATIONSHIP BETWEEN THE DEGREE OF CONSTRICTION AND THE LENGTH OF DILATATION ON THE FEMORAL ARTERY, FROM ROACH (1963).

| | Relative Radius* | |
|---|---|---|
| Distance from Edge of Stenosis | Moderate Stenosis | Minimum Stenosis |
| 0.25 | 1.03 | 0.89 |
| 0.55 | 1.10 | 0.89 |
| 0.75 | 1.08 | 0.89 |
| 1.05 | 1.07 | 0.89 |
| 1.25 | 1.04 | 0.90 |
| 1.55 | 0.97 | 0.86 |
| 1.75 | 0.93 | 0.86 |
| 2.05 | 0.92 | 0.87 |

*Relative radius is expressed as ratio of distal radius over proximal radius.

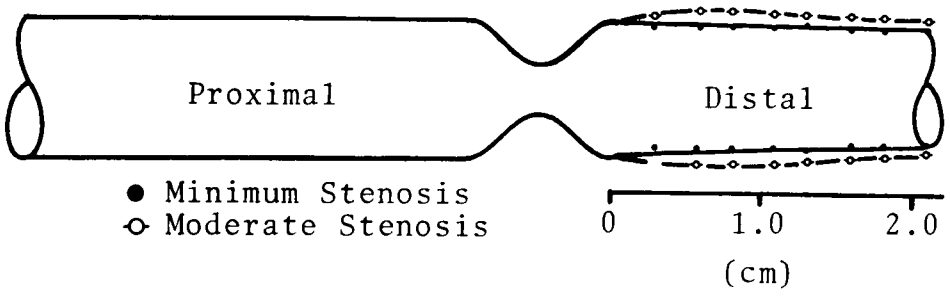


Figure 12. Relationship between Degree of Constriction and Size of Dilatation

## L. Summary of Values for the Prototype Variables

To facilitate comparisons between model and prototype, values of the prototype variables and the resulting Pi terms have been tabulated in Table 10.

TABLE 10

VALUES OF THE PROTOTYPE VARIABLES

| Variable | Prototype Value | Pi Term | Value |
|---|---|---|---|
| $\bar{R}_o$ (cm) | 0.206 | $\pi_1$ | 150 |
| $\bar{R}_i$ (cm) | 0.185 | $\pi_2$ | 902 |
| $L_s$ (cm) | * | $\pi_3$ | 0.042 |
| $L_d$ (cm) | * | $\pi_4$ | * |
| $R_d$ (cm) | * | $\pi_5$ | * |
| $L_{sd}$ (cm) | * | $\pi_6$ | .90 |
| $R_s$ (cm) | * | $\pi_7$ | * |
| $\rho_w$ (g/cm$^3$) | 1.16 | $\pi_8$ | * |
| $\rho$ (g/cm$^3$) | 1.05 | $\pi_9$ | * |
| $\mu$ (C.P.) | 3.2 | $\pi_{10}$ | 0.91 |
| $\nu$ | 0.5 | $\pi_{11(j=1)}$ | 3.72 |
| $E_{st}$ (dynes x 10$^6$/cm$^2$) | 6.3 | $\pi_{11(j=2)}$ | 4.33 |
| $V_o$ (cm/sec) | 12.3 | $\pi_{11(j=3)}$ | 13.91 |
| $V_{j=1}$ (cm/sec) | 23.17 | $\pi_{11(j=4)}$ | 48.73 |
| $V_{j=2}$ (cm/sec) | 28.65 | $\pi_{12}$ | 0.5 |
| $V_{j=3}$ (cm/sec) | 13.08 | $\pi_{13}$ | 1.3 |
| $V_{j=4}$ (cm/sec) | 6.56 | $\pi_{14}$ | 1.0 |
| $P_o$ (mm of Hg) | 107.7 | $\pi_{15(j=1)}$ | 0.53 |
| $P_{j=1}$ (mm of Hg) | 28.92 | $\pi_{15(j=2)}$ | 0.43 |
| $P_{j=2}$ (mm of Hg) | 24.89 | $\pi_{15(j=3)}$ | 0.94 |
| $P_{j=3}$ (mm of Hg) | 7.74 | $\pi_{15(j=4)}$ | 1.88 |
| $P_{j=4}$ (mm of Hg) | 2.21 | | |
| f (Hz) | 2.78 | | |
| t (sec) | 0.36 | | |

*Must be determined from text.

# CHAPTER V

# EXPERIMENTAL APPARATUS

This study necessitated two separate mock circulatory systems (Figures 13 and 14), one for the small models (nominal diameter of 0.64 cm) and another for the larger ones (nominal diameter of 2.1 cm). This was necessary primarily because of the difference in frequency ranges of the pumps and because of the difficulty in obtaining a good physiological wave shape with the large mock circulatory system over long periods. By designing the small system with a piston-cam arrangement as well as a relatively low volume of fluid (one half liter as compared to eight liters for the large system), it was possible to obtain good consistent physiological wave shapes for several days.

## A. Large Mock Circulatory System

The experimental apparatus for the large models is shown in Figure 13 and illustrated in the schematic diagram of Figure 15. It was designed to provide steady flow, pulsatile flow, or pulsatile superimposed on steady flow through the arterial models. For this study, the pulsatile and steady flow systems were used. The equipment shown has been labeled so that its function may be reviewed.

By simulating the left ventricle of the heart, the Silastic Diaphragm Pump (A) generated a pulsatile wave shape. This diaphragm pump consisted of an acrylic dome

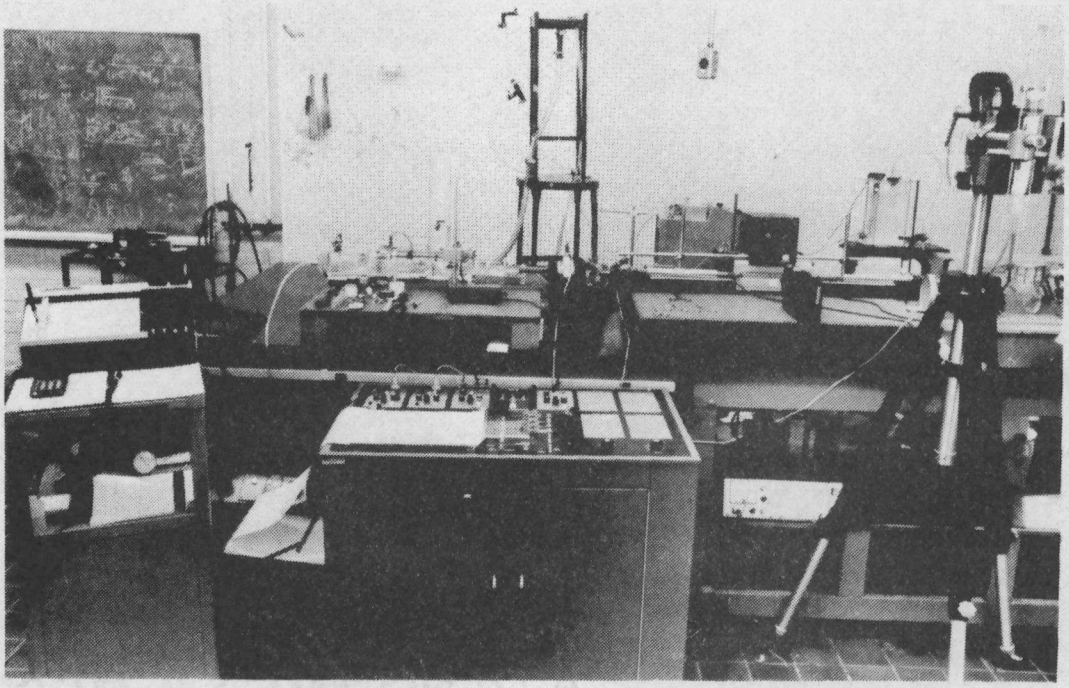

Figure 13. Experimental Apparatus for the Large System

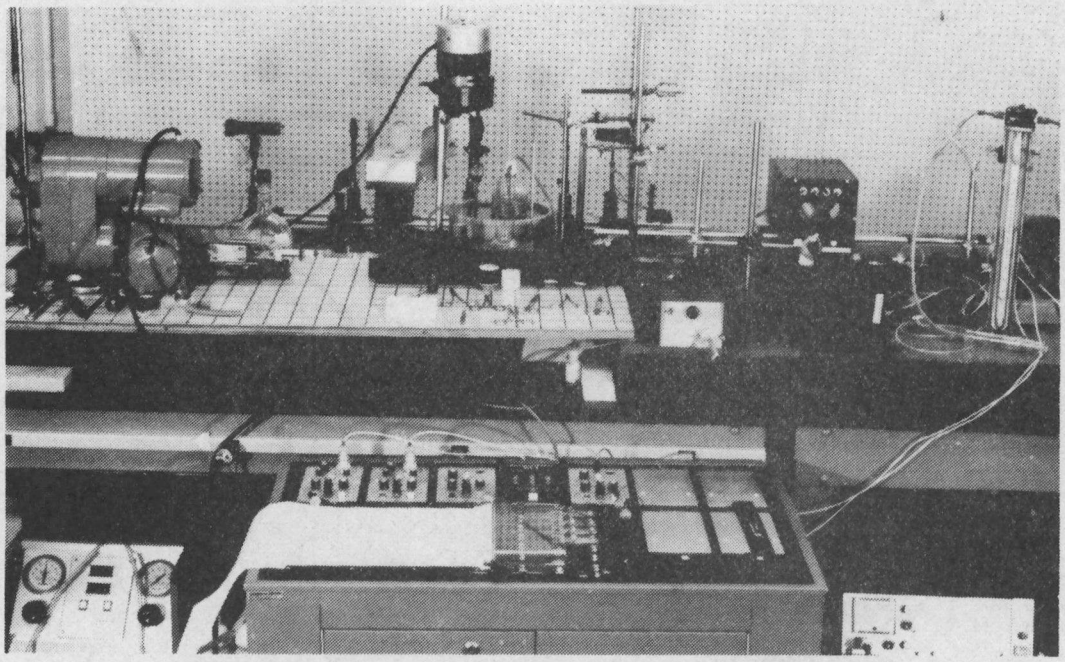

Figure 14. Experimental Apparatus for the Small System

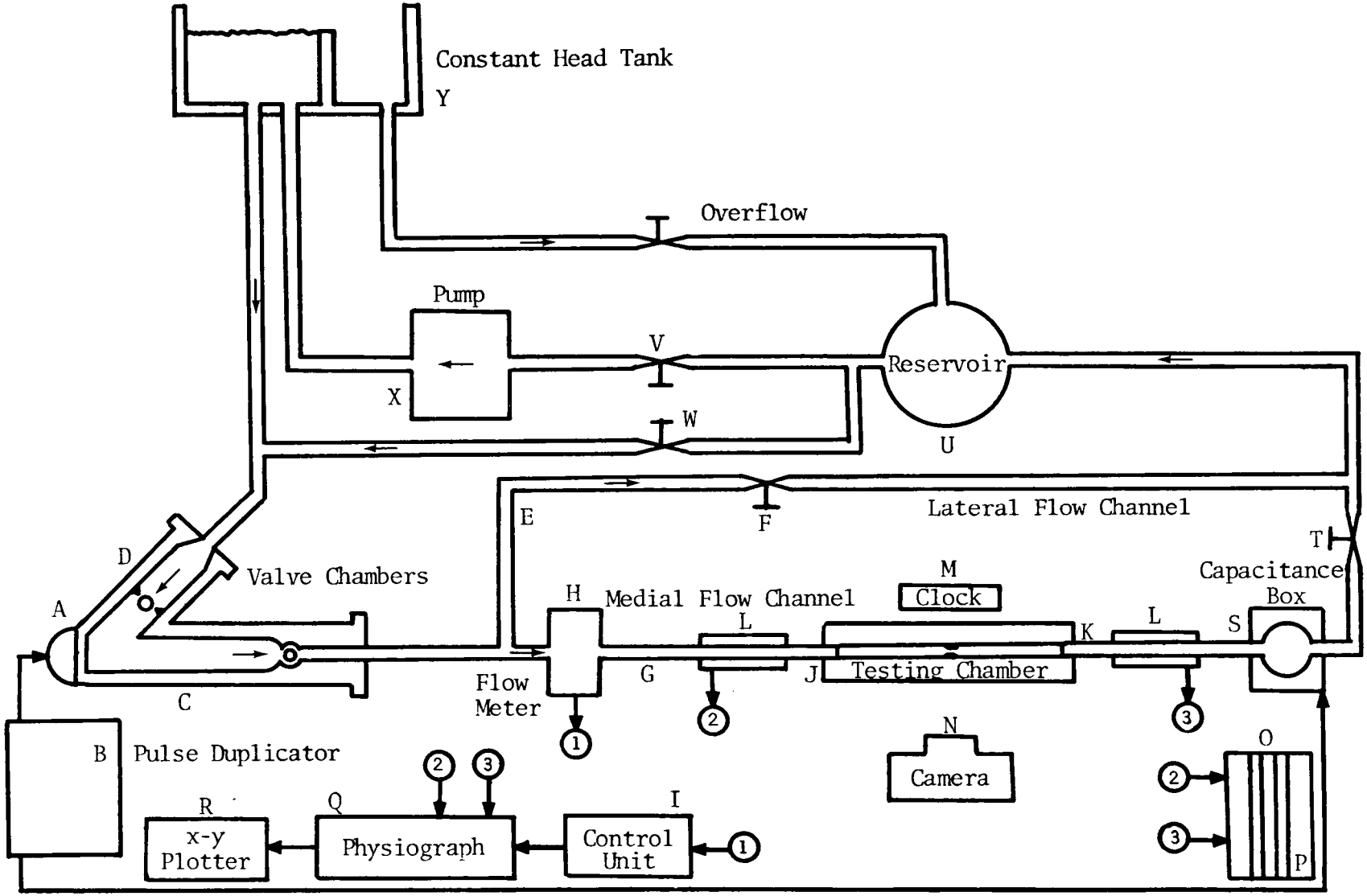


Figure 15. Large Mock Circulatory System

with air pressure connector and a silastic diaphragm. The Vitamek Pneumatic Pulse Duplicator (B) provided positive and negative pressure to drive the silastic diaphragm. This pulse duplicator provided pulse rates from 0 to 120 pulses per minute with variable systolic duration from 0 to 690 milliseconds under positive pressure from 0 to 175 mm Hg, and negative pressure from 0 to 75 mm Hg. The outlet of the Silastic Diaphragm Pump was connected to the aortic valve chamber (C) which housed a Starr-Edwards Aortic prosthetic valve. The mitral valve chamber (D) was connected to the inlet of the pump. This pump system was similar to that of Wieting (1969) and Cliff (1976) and provided pulse shapes which were approximately physiological. The systemic bilateral flow system was located downstream from the aortic valve chamber. The lateral flow channel (E) was unobstructed except for the adjustable valve (F). The amount of fluid flowing through the medial flow channel (G) was controlled by means of this adjustable valve. Downstream from the bilateral branch in the medial channel was located a 5/8 in. inside diameter electromagnetic flow meter transducer (H) which was connected to a Biotronix BLT-610 control unit (I). The flow meter had excellent linearity, sensitivity and stability as shown by Lambert and Henry (1975). The flow meter was calibrated by measuring the time required to collect a given volume of fluid at the end of the medial flow channel.

The model testing chamber (J) housed the arterial model (K) as well as provided support for the pressure catheters (L) and digital clock (M). The testing chamber was made out of Plexiglas to permit photographing of the model by a 16 mm motion camera (N), with the digital clock placed in the field of view. The chamber was lined its entire length with a soft sponge to provide support for the model.

The pressure catheters, Appendix C, were located proximal and distal to the stenosis. Each consisted of a probe 28 cm long made from 0.73 mm diameter stainless steel tubing with a single side hole made perpendicular to the flow 5 mm from the end which had been closed off with epoxy. This probe was attached to a 3.0 cm outside diameter aluminum collar which enclosed a 1.65 cm inside diameter by 42 cm long copper tube. As the flow passed through the copper tube it was possible to slide the stainless steel collar up and down, thus permitting relocation of the probe inside the arterial model from 0 to 11 cm beyond the end of the copper tube. A metric scale located below the collar permitted location of the probe within the model. The external end of the probe was coupled to a three way stopcock.

For the steady flow experiments the stopcocks were attached to two 1/8 inch inside diameter piezometer columns (O) by a 0.32 cm inside diameter by 190 cm long rubber tube. A cathetometer (P) consisting of a telemicroscope mounted on a micrometer slide was used for the pressure-drop

measurements. The total system was mounted vertically on an adjustable camera stand. This arrangement permitted measurement of 0.0001 inch of fluid pressure drop. Water was used in the system instead of the glycerol-water solution for the steady flow experiments. Approximately 15 minutes were spent in allowing the water solution in each piezometer tube to reach its equilibrium position. This position was defined as that location where no noticeable displacement of fluid occurred for a period of one minute.

For pulsatile flow experiments the stopcocks were attached to a strain gage manometer, Narco Bio-Systems Inc., RP-1500. They featured ultralow volume displacement ($9 \times 10^{-5}$ $mm^3/mm$ Hg) and high frequency response (1.5 KHz with 20 gauge 1.5 inch needle). To insure accuracy the vessel and the pressure transducer mounting levels were approximately the same. Before and after each experiment the transducers were calibrated by applying a reference pressure with a mercury manometer. Outputs from the pressure transducers as well as the Biotronix Control Unit were recorded on a six channel physiograph (Q) from Narco Bio-Systems. To increase the resolution of the pressure curves, an X-Y plotter (R) was attached to the physiograph. It was possible to obtain a 0.6 mm to 1 mm Hg displacement relationship with this system.

Distal to the model testing chamber was a pneumatic capacitance box (S); its function was to absorb much of the pulse, simulating the natural capacitance and resistance of

the systemic circulatory system. The capacitance was achieved by two silastic diaphragms whose resistance to movement was regulated by air pressure. During diastole the air pressure causes the silastic diaphragms to be compressed thus maintaining a good diastolic pressure, whereas during systole the systolic pressure causes the silastic diaphragms to expand. An air pressure valve controls the amount of steady pressure applied to the silastic diaphragms from the pneumatic pulse duplicator. The resistance of the medial flow channel was achieved by varying the degree of opening of the metal clamp (T) which was attached to the capacitance box. The medial flow channel now rejoined the lateral flow channel at the T-connection before the fluid emptied into the reservoir (U).

The reservoir was capable of maintaining two liters of fluids under controlled temperature and pressure by using a 25 watt water heater and pressure tight fittings. The fluid temperature was maintained at 25°C for all the experiments conducted while the pulsatile pressure was varied from 0 to 170 mm of mercury. When pulsatile flow was being examined the fluid flowed directly from the reservoir into the mitral valve chamber. This was achieved by cutting off all flow through the steady flow system with the adjustable clamp (V) on the tygon tube. When steady flow was observed the adjustable clamp (W) was used to stop all flow through this channel.

The steady flow system consisted of a Sarns Model 350 roller pump (X) which pumped the fluid from the reservoir to the constant head tank (Y) which was about 1.5 meters above the model testing chamber. The liquid was pumped from the reservoir up to the constant-head tank at sufficient rates to always provide some overflow back to the reservoir so that a constant-head supply was maintained. This constant-head tank not only provided the pressure head needed to move the fluid through the system, but also smoothed the pulsations from the Sarns roller pump. The fluid then flowed to the mitral valve chamber where the cycle was repeated. Connections to various parts of the system were made with 3/4 inch tygon tubing.

B. Small Mock Circulatory System

As illustrated in Figures 14 and 16, the small system has many characteristics similar to the large mock circulatory system. Other than size the basic differences were in the pumping units, the elastic tubing used for connections, and the absence of a steady flow system. This equipment shown has been labeled so that its function may also be reviewed.

The pumping unit consisted of a one-half horsepower varidrive motor (A) with speeds from 64 to 384 revolutions per minute. An irregularly shaped cam (B), Appendix B, revolved on the constant-speed shaft and imparted motion to a roller follower (C). The follower was held in contact

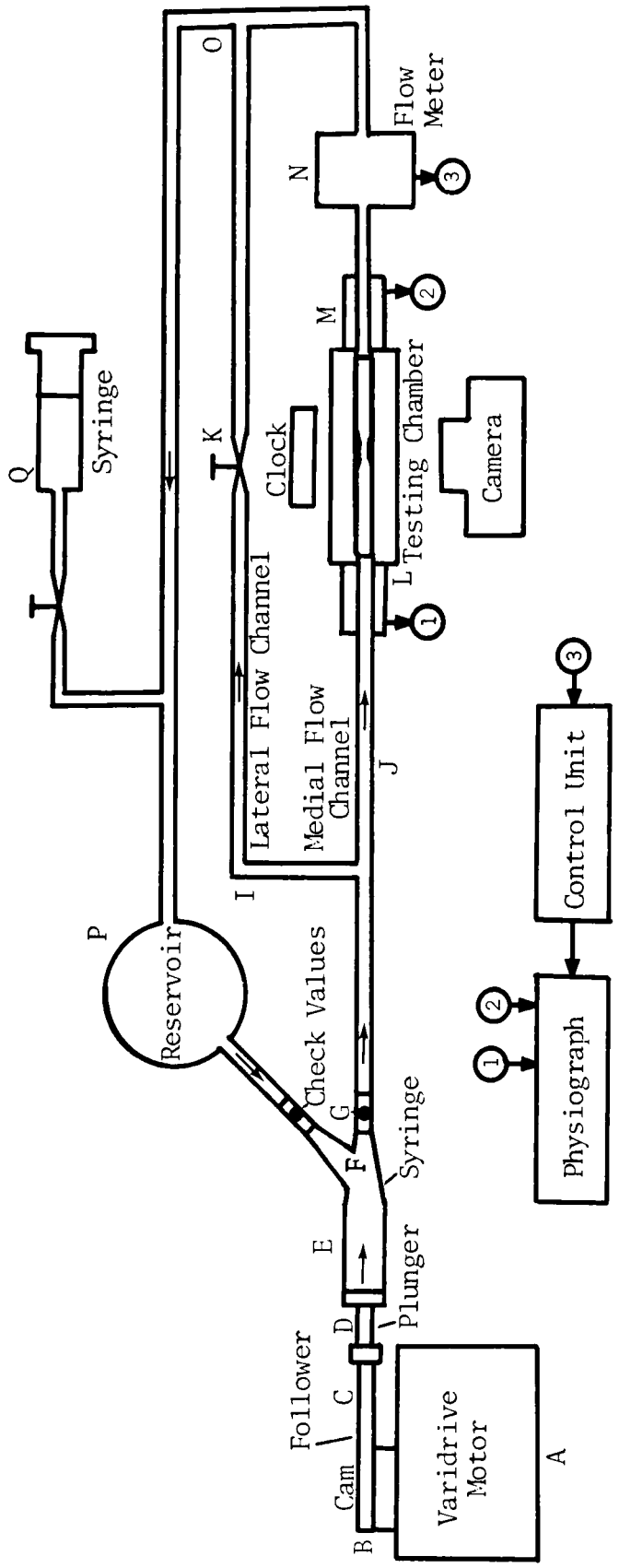


Figure 16. Small Mock Circulatory System

with the profile of the cam by means of two springs located above and below the follower. The follower operated in a plane perpendicular to the axis of the cam shaft. A syringe plunger (D) was connected to the end of the follower and the volume displacement was proportional to the cross-sectional area of the syringe barrel (E). Several different syringes were used to allow for variation in stroke volume.

The syringe barrel was connected to a branch connector (F) which was equipped with two check valves. Each check valve consisted of a 32 mm diameter metal ball placed between two specially shaped pieces of polypropylene tubing, which were secured in the branch connector. The outlet valve (G) was designed to permit the fluid to move out of the branch connector while stopping backflow, thus serving the same function as the aortic valve. The inlet valve (H) operated as the mitral valve, permitting fluid to enter the branch connector but stopping fluid from leaving. The systemic bilateral flow system was located downstream from the branch connector. As with the large mock circulatory system, the lateral flow channel (I) controls the amount of fluid entering the medial flow channel (J) by means of the adjustable valve (K). The first element encountered on the medial channel was the model testing chamber (L). Other than being smaller than the larger model testing chamber, there was no difference in these two test cells.

The pressure catheters (M) located proximal and distal to the stenosis consisted of a 6 cm long probe made from 0.73 mm diameter stainless steel tubing with a single hole made perpendicular to the flow 6 mm from the end with the internal end closed off with epoxy. This probe was attached to a piece of copper tubing which was 7.5 cm long by 6 mm inside diameter. Because of size limitation it was not feasible to design the pressure catheter to be movable, thus the probe was epoxied at a set location 2.2 cm beyond the end of the copper tubing. The external end of the probe was coupled to a three way stopcock which in turn was connected to a pressure transducer. After passing through the model testing chamber the fluid passed through a 1.3 cm inside diameter electromagnetic flow transducer (N). Signals from both the pressure and flow transducers were recorded and calibrated in the same manner as in the large mock circulatory system.

The medial channel then rejoined the lateral channel at the Y-connector (O) before emptying into the reservoir (P). This reservoir was capable of maintaining 500 ml of fluid under pressure conditions up to 300 mm Hg. To control the fluid temperature at 25°C, the reservoir was submerged in an isothermal water bath. The fluid was then pumped from the reservoir back into the branch connector where the cycle was repeated. The pressure in the system varied directly according to the volume of circulating fluid, which was controlled by the 50 ml syringe (Q).

C. Photoelectric Elasticity Measuring System

To measure the elastic modulus of the latex model it was necessary to construct a device which would measure the relative diameter change of the model. Certain criteria had to be considered when proposing a device for the above purpose. First, the instrument could not interfere with the tube's normal function and it had to be sensitive as the changes measured were often less than 1% of the diameter of the vessel. It needed to be easily calibrated and have a continuous electrical output linearly related to vessel displacement. Finally, it was necessary that the output would not drift appreciably.

The apparatus used is shown diagrammatically in Figure 17. The vessel was positioned (A) in the path of a collimated light beam (1 cm high and 0.5 cm wide). Both ends of the vessel were clamped to the metal stand to insure constant length and tension throughout the test. The collimated light was created by placing two slits 25 cm apart (B) in front of a 60 watt filament bulb (C). The filament bulb was powered by a D.C. signal to reduce ripple in the output. The D.C. signal was generated by a bridge rectifier in series with a low pass filter (D). The shadow of the vessel was thrown on a 25 mm lens (E) mounted on the primary sensing head (F). Variations in the vessel size were detected by a 1 inch by 1.5 inch photoelectric cell contained within the sensing head. The light which was permitted to enter the sensing head had to enter at an

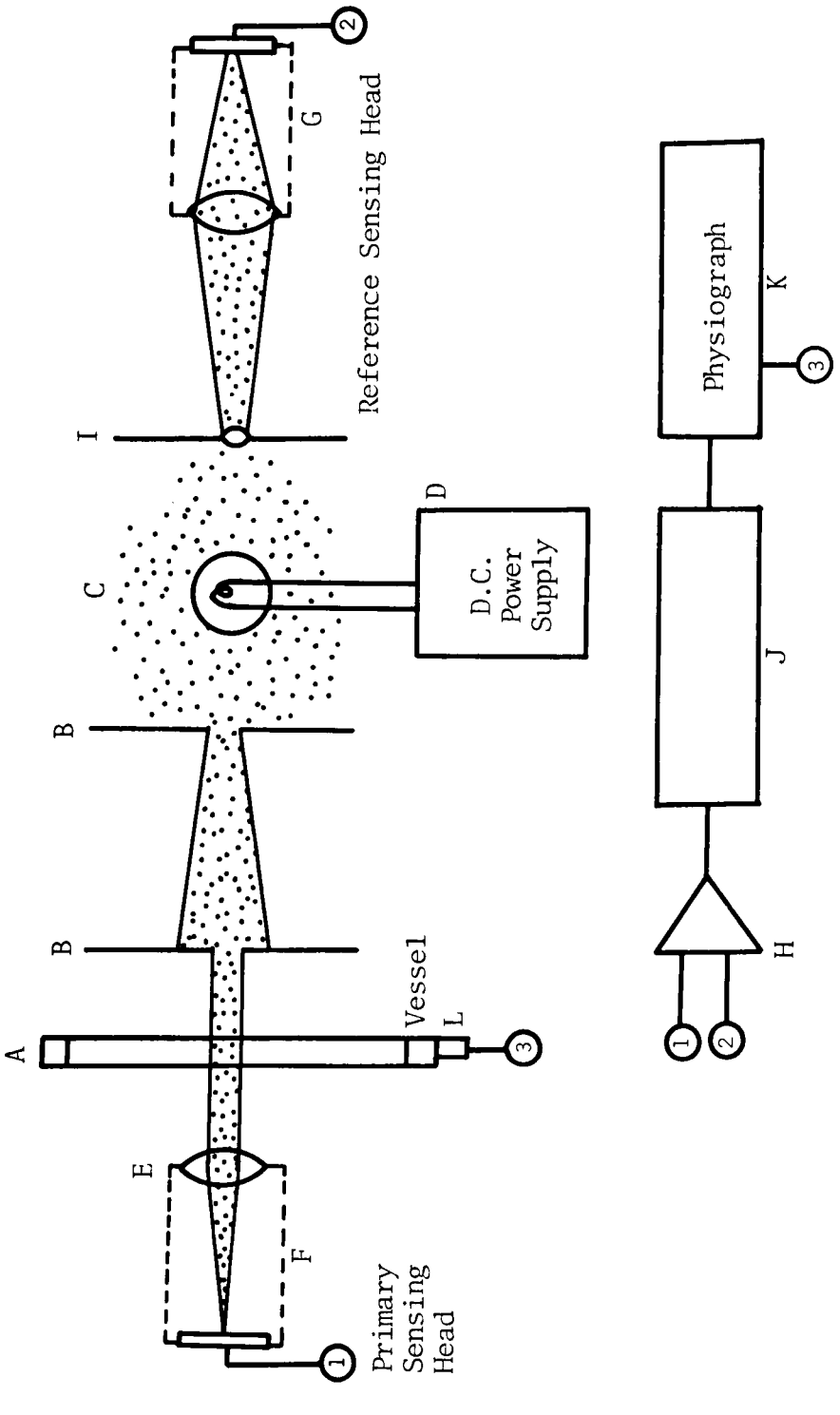


Figure 17. Photoelasticity Measuring System

acceptance angle, which was governed by the lens focal length. As the radius of the specimen increased, the amount of light falling on the photoelectric cell decreased, thus decreasing the voltage output.

To account for any variation in light intensities other than changing diameter a reference sensing head (G) was placed behind the light bulb. Signals from the reference and primary sensing heads were fed into a differential amplifier (H). The difference in the two signals was obtained so that any voltage output from this amplifier was the result of variations in diameter. An adjustable iris diaphragm (I) for regulating the amount of light passed was placed between the reference sensing head and light bulb permitting adjustment of the system so that the instrument could be calibrated. Signals from this differential operation were amplified (J) and recorded on the physiograph (K).

Before and after each experiment the instrument was calibrated with a series of metal rods of known radii mounted in the position of the vessel. A linear relationship between voltage output and diameter of the metal rod was shown to exist for all values tested. The pressure changes were detected by a strain gage transducer (L).

# CHAPTER VI

# RESULTS AND DISCUSSION

## A. Small Arterial Models

Several experiments were performed on the small mock circulatory system as described in Chapter V. To facilitate comparisons between these experiments, the variables considered for each model have been tabulated in Table 11, along with general comments, cam used in the system, and total time of experiment in Table 12. Seven of the models have been described graphically in Figures 18 through 24 so that a more meaningful appraisement might be made. Each drawing approximately depicts the model and the resulting dilatation with respect to the rigid Plexiglas stenosis which had been inserted in the latex tube. Particular attention should be drawn to the reference axis located at the throat of the stenosis. While the horizontal axis is to scale, the vertical axis has been doubled to improve graphical representation of the vessel. The respective location of each pressure tap, with reference to the stenosis, may also be seen from these drawings. The proximal pressure, distal pressure, volume flow and mean flow versus time tracings, are given below the tube for each of the seven models. Three different time tracings were considered for each of the pressure profiles, representing the start of the experiment, mid-way through the experiment, and moments before rupture. Only one tracing was displayed for

TABLE 11

SMALL MODEL VARIABLE VALUES

| Variable \ Model | T-8 | T-10 | T-13 | T-15 | T-16 | T-17 | T-18 | T-19 | T-20 | T-21 | T-27 | T-28 | T-30 | T-33 |
|---|---|---|---|---|---|---|---|---|---|---|---|---|---|---|
| $\bar{R}_o$ (cm) | .32 | .326 | .336 | .311 | .320 | .307 | .32 | .323 | .323 | .314 | .324 | .323 | .320 | .321 |
| $\bar{R}_i$ (cm) | .263 | .292 | .292 | .268 | .263 | .250 | .263 | .265 | .264 | .262 | .268 | .265 | .265 | .265 |
| $L_s$ (cm) | .54 | .54 | .54 | .54 | .54 | .54 | .54 | .54 | .54 | .54 | .54 | .54 | .54 | .54 |
| $L_d$ (cm) | 1.5 | † | 2.0 | † | † | 2.0 | 2.0 | 2.0 | 4.0 | 2.0 | † | † | † | 2.5 |
| $R_d$ (cm) | ∞ | † | ∞ | ∞ | ∞ | † | ∞ | ∞ | † | ∞ | † | † | ∞ | ∞ |
| $L_{sd}$ (cm) | -.2 | † | +4.0 | -1.0 | -.14 | -.5 | -1.0 | -1.0 | -2.0 | -1.0 | † | † | -5. | -.14 |
| $R_s$ (cm) | .135 | .135 | .135 | .135 | .135 | .135 | .135 | .135 | .135 | .135 | 0.09 | .135 | .135 | .135 |
| $\rho_w$ (g/cm$^3$) | 1.1 | 1.1 | 1.1 | 1.1 | 1.1 | 1.1 | 1.1 | 1.1 | 1.1 | 1.1 | 1.1 | 1.1 | 1.1 | 1.1 |
| $\rho$ (g/cm$^3$) | 1.12 | 1.13 | 1.13 | 1.118 | 1.12 | 1.1 | 1.12 | 1.12 | 1.12 | 1.12 | 1.12 | 1.12 | 1.12 | 1.12 |
| $\mu$ (C.P.) | 4.45 | 5.35 | 5.35 | 4.25 | 4.45 | 3.05 | 4.45 | 4.45 | 4.45 | 4.45 | 4.45 | 4.45 | 4.45 | 4.45 |
| $\epsilon$ | 0.5 | 0.5 | 0.5 | 0.5 | 0.5 | 0.5 | 0.5 | 0.5 | 0.5 | 0.5 | 0.5 | 0.5 | 0.5 | 0.5 |
| $E_{st}$ (dyne x 10$^6$/cm$^2$) | 8.3 | 8.3 | 8.3 | 8.3 | † | 8.3 | 8.3 | 8.3 | 8.3 | 8.3 | 8.3 | 8.3 | 8.3 | 8.3 |
| $V_o$ (cm/sec) | 10.9 | 11.9 | 11.9 | 10.3 | 10.9 | 8.5 | 10.9 | 10.9 | 10.9 | 21.8 | 10.9 | 10.9 | * | 10.9 |
| $V_j$ (cm/sec) | 100% | * | * | * | * | * | * | * | * | * | 100% | 100% | * | 100% |
| $P_o$ (mm Hg) | 91.6 | * | 107.7 | 80.8 | 91.6 | 53.9 | 91.6 | 91.6 | 91.6 | 91.6 | 91.6 | 91.6 | * | 91.6 |
| $P_j$ (% of prototype) | * | * | 100% | 75% | 85% | 50% | 85% | 85% | 85% | 85% | * | * | * | * |
| f (Hz) | 1.69 | 1.66 | 1.66 | 1.58 | 1.69 | 1.38 | 1.69 | 1.68 | 3.38 | 1.71 | 1.69 | 1.69 | 1.69 | 1.69 |
| t (sec) | .59 | .60 | .60 | .63 | .59 | .72 | .59 | .59 | .30 | .59 | .59 | .59 | .59 | .59 |

*: not modeled.
†: undetermined.
∞: complete rupture.

TABLE 12

GENERAL COMMENTS FOR SMALL MODELS

| Model | Cam # | Total Time (hr) | General Comments |
|---|---|---|---|
| T-8 | 7 | 13.8 | Modeled velocity wave shape. |
| T-10 | 1 | 2 | Stopped experiment because of poor pressure wave shape. |
| T-13 | 2 | 21.6 | Simulated decrease in support tissue; poststenotic rupture. |
| T-15 | 5 | 8.3 | Submerged in a neutrally buoyant glycerol solution. |
| T-16 | 16 | 1.7 | Supported vessel on rigid surface; thin proximal wall. |
| T-17 | 16 | 167 | 50% pressure wave shape. |
| T-18 | 12 | 3.6 | 85% pressure wave shape; stenosis in center of model. |
| T-19 | 7 | 16.2 | 85% pressure wave shape; stenosis 5 cm proximal of T-18. |
| T-20 | 7 | 20.8 | Frequency was twice normal modeled rate. |
| T-21 | 11 | 22.3 | Velocity was twice mean modeled rate. |
| T-27 | 1 | 34 | 90% stenosis; modeled velocity; leak in syringe plunger. |
| T-28 | 1 | 19 | Used capacitance box; leak in syringe plunger. |
| T-30 | 7 | 0 | Left clamp on model; caused rupture at start of experiment. |
| T-33 | 7 | 20.3 | Simulated decrease in support tissue with weak proximal wall. |

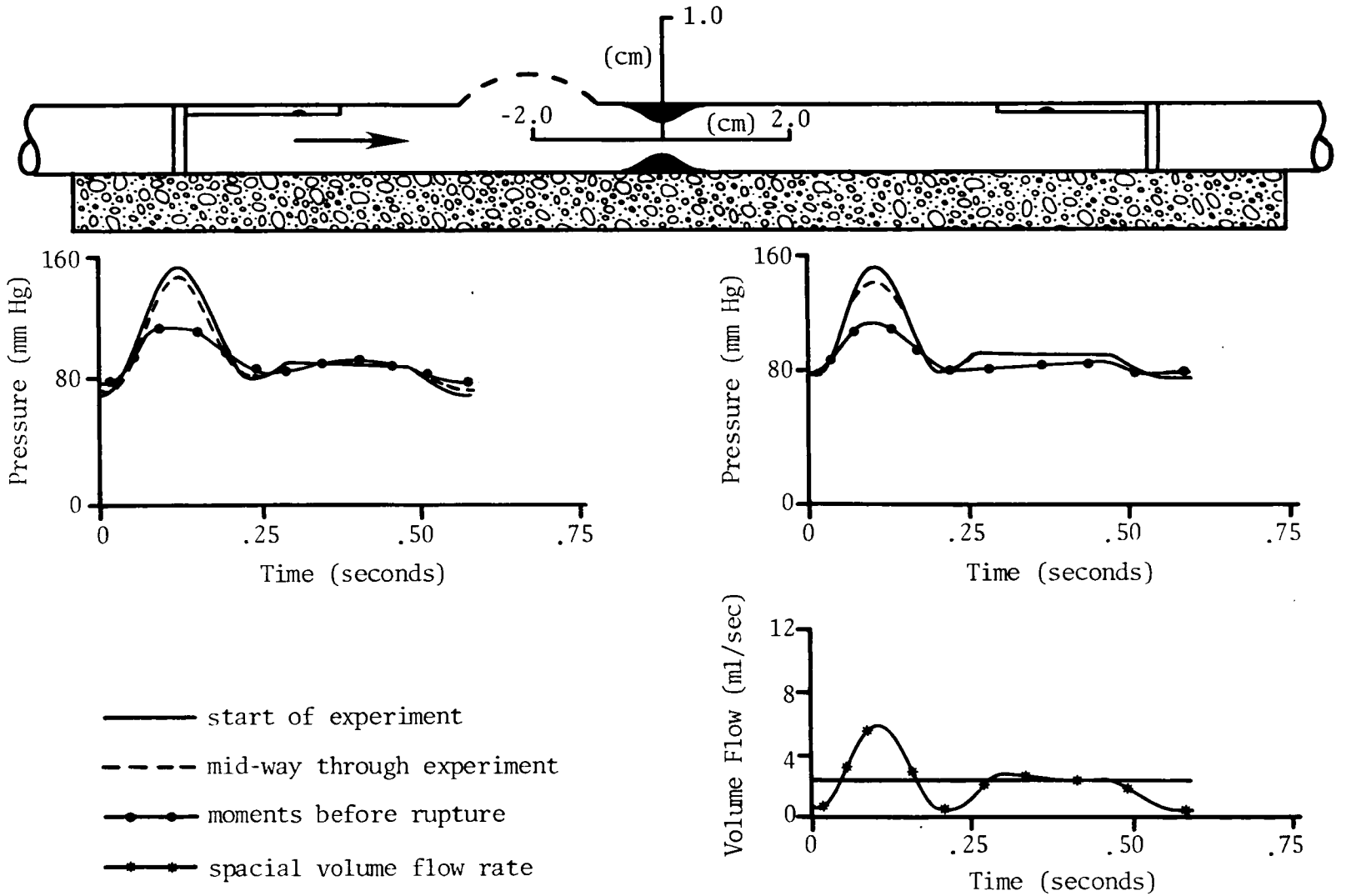


Figure 18. Results for Model T-18

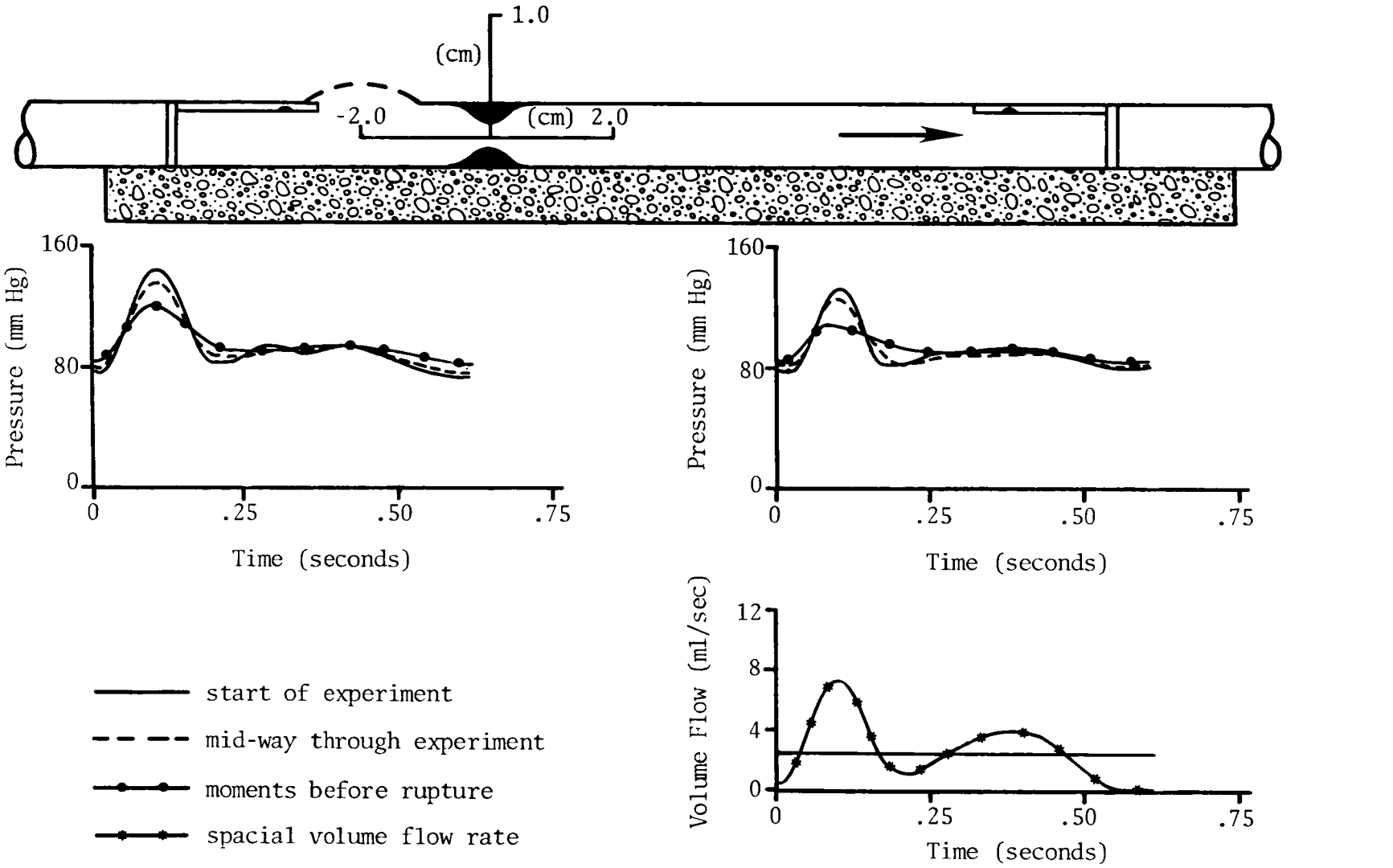


Figure 19. Results for Model T-19

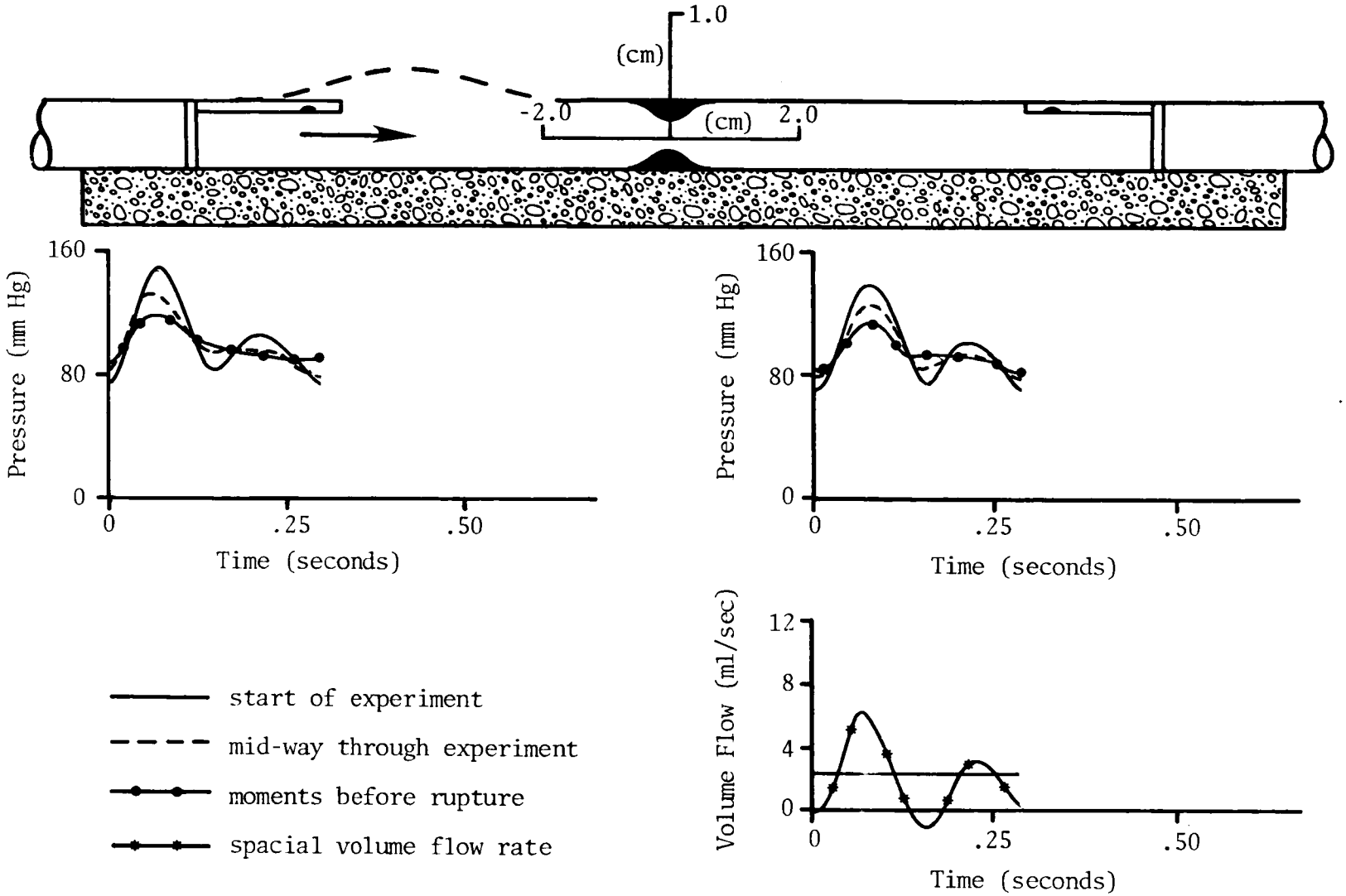


Figure 20. Results for Model T-20

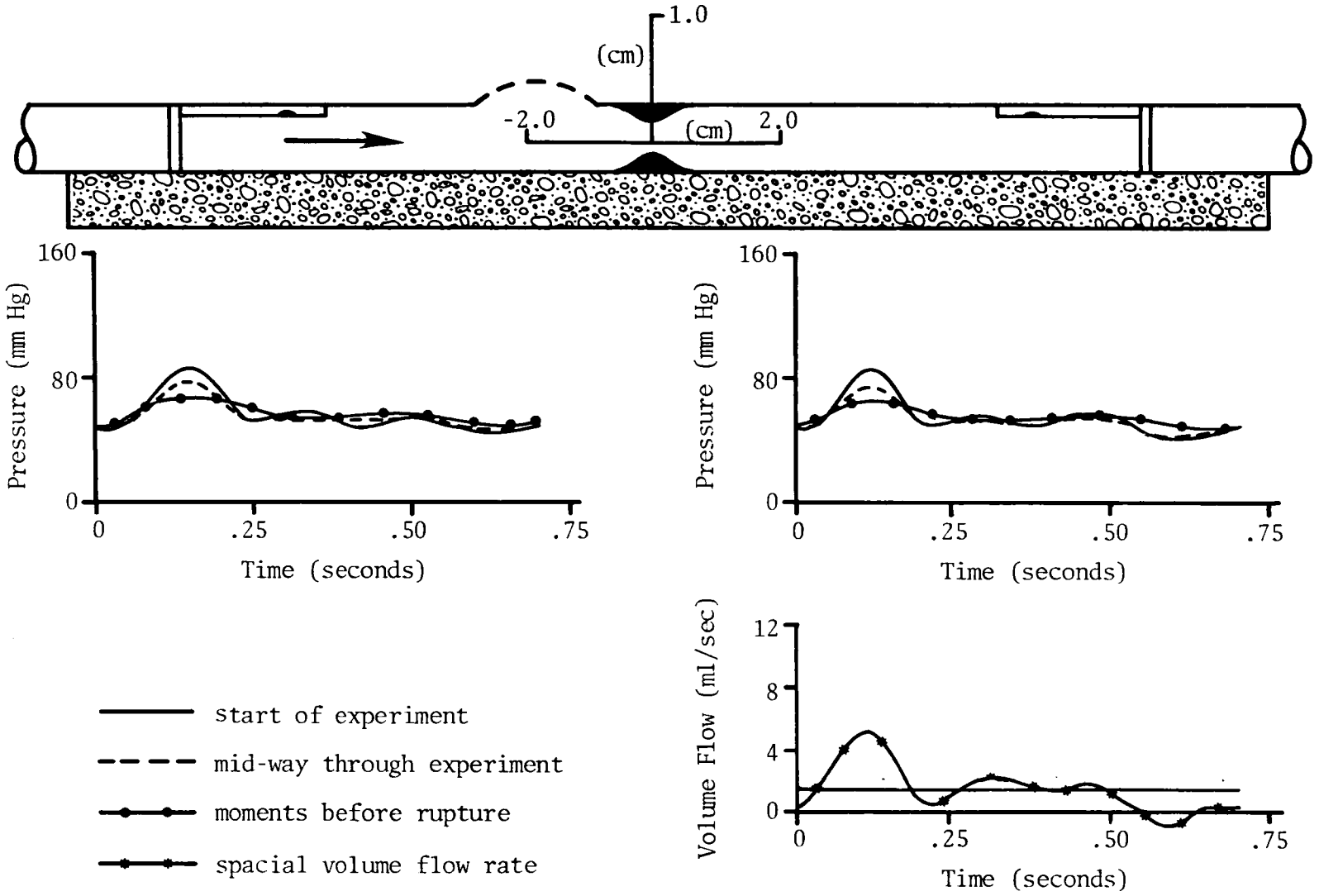


Figure 21. Results for Model T-17

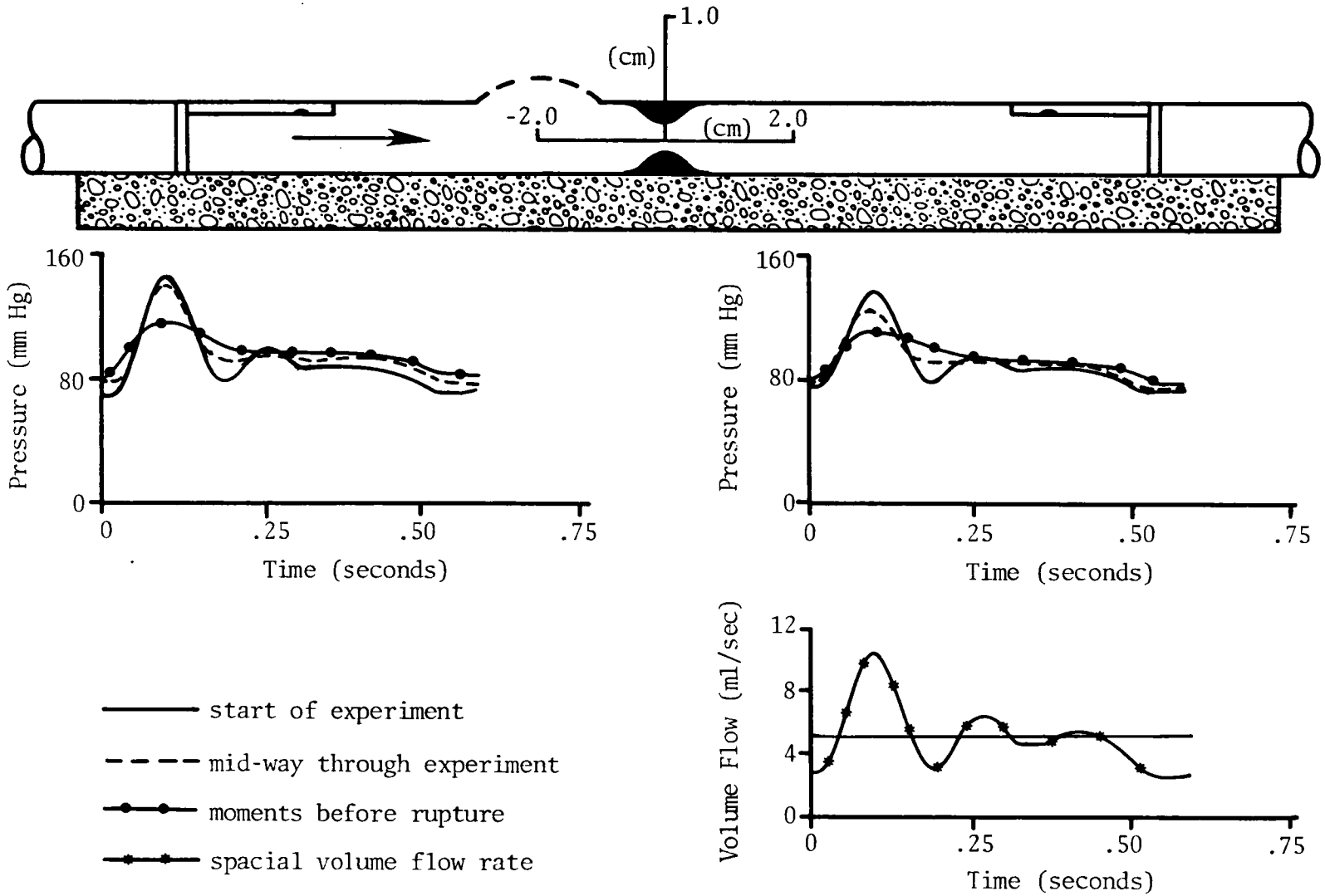


Figure 22. Results for Model T-21

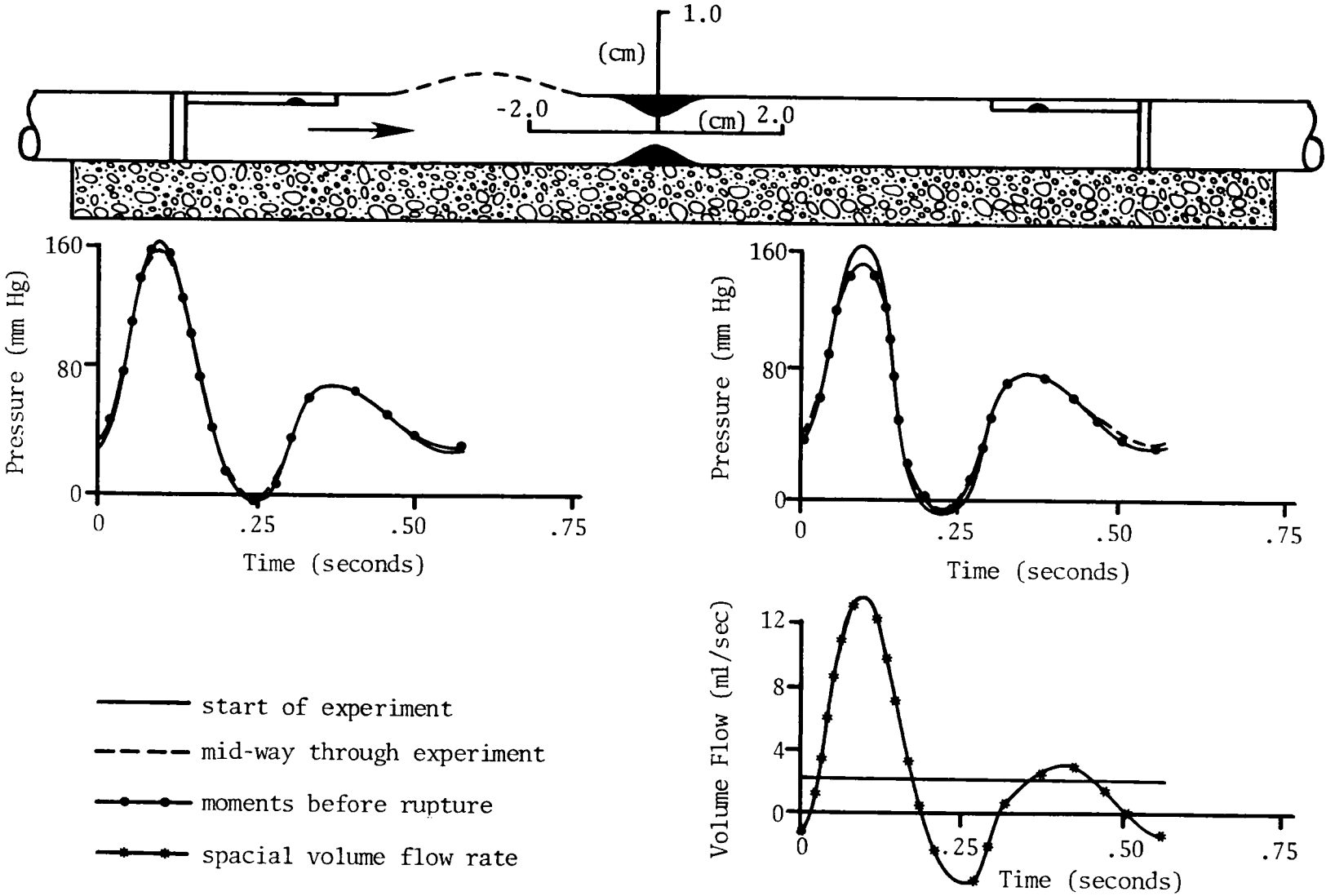


Figure 23. Results for Model T-8

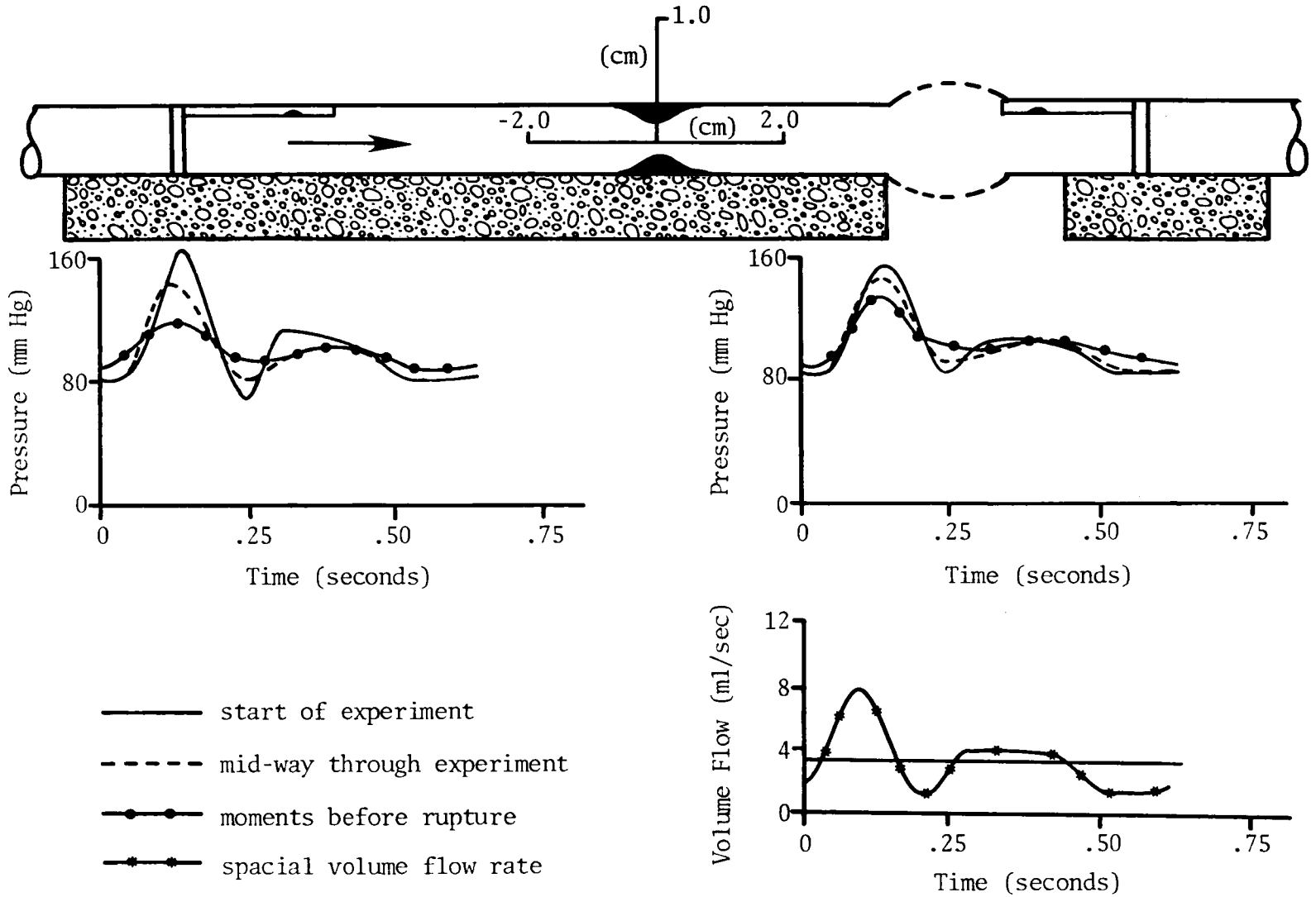


Figure 24. Results for Model T-13

each of the flow curves because of the relative consistency throughout the experiment. Examination and comparison of these profiles revealed several interesting points.

Model 18, Figure 18, was examined under normal physiological conditions, with a 75% reduction in area at the throat of the stenosis. After 0.4 hours of pulsation, a slight bulge appeared two centimeters prestenotically. The bulge continued to grow until rupture occurred 3.2 hours later. The time required for dilatation was only a fraction of the actual time required for arteries to dilate, possibly because of the inability of the arterial model to repair itself as structural fatigue progressed, but more importantly, it was likely the result of modeling the static modulus of elasticity while neglecting the dynamic and fatigue effects. It is realized that these models fall short of being exact models of an *in vivo* artery. Yet it is believed that meaningful information might be obtained when comparing the models under various flow conditions. The rupture of T-18 appeared much as a sacculated aneurysm, with total fatigue occurring on the upper side of the vessel. The ability of the sponge to absorb much of the energy from the pulsatile flow helped to dampen out the force effect on the bottom side of the model.

From the modeled pressure profiles, the expected pressure drop between proximal and distal locations may be observed. As pulsation continues, the amplitude is seen to decrease. This is most noticeable moments before rupture,

and is the result of total fatigue of the vessel, as it offers less resistance to each additional pulse. The decrease in resistance was relatively small when compared to the total system; consequently, no detectable change occurred in the flow rate until moments before rupture.

To test whether the location of the stenosis could affect the location of the dilatation, Model T-19 was tested under nearly the same conditions as T-18, except the stenosis was moved 5 cm upstream. Figure 19 shows that the dilatation again developed approximately 2 cm prestenotically. This suggested that a standing wave as a result of wave reflection might have developed when the pulsatile wave confronted the rigid Plexiglas stenosis.

By placing a high powered light source above the vessel and injecting a concentrated solution of methylene blue through the proximal pressure tap, it was possible to observe the flow pattern. When the dye was injected it promptly moved away from the pressure tap into the fast flowing stream. It was anticipated that a momentary delay in the dye progress would be observed downstream from the stenosis as a result of the turbulent eddy. However, the reverse phenomenon actually occurred (see below). When the dye was injected there was noted just proximal to the constriction a definite delay in its progress downstream. This delay created a ring-shaped pocket of dye around the inside wall of the vessel. The pocket was approximately 0.5 cm long, and extended from the sides of the stenosis

back. During diastole it was observed to move slightly upstream, while returning to the side of the stenosis during the systolic portion of the cycle. Total movement was restricted to 0.75 cm upstream. It was impossible to determine if the pocket was in a rotational or irrotational state, and attempts to determine this through photographic techniques were unsuccessful. This result appears to support the concept of wave reflection as a possible contributor to prestenotic dilatation.

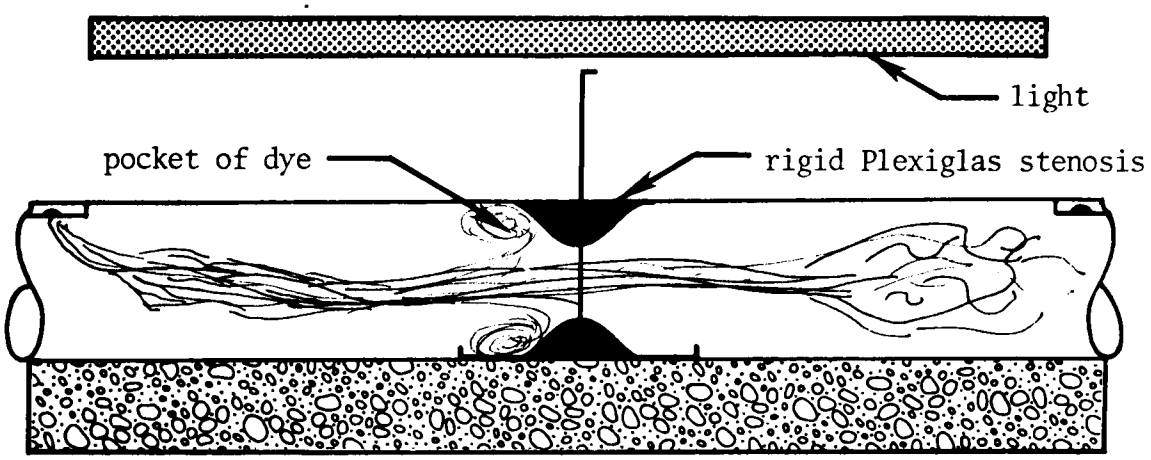


In another experiment, Figure 20, Model T-20 was subjected to pulsations which were twice the normal rate. After 21 hours of pulsation, this model dilated prestenotically, but unlike previous prestenotic dilatations, this one was much longer, covering almost the entire length of the proximal section. Apparently the forces which prompted this dilatation were more evenly distributed along the proximal portion of the latex tubes as compared to the two models previously discussed.

All the aforementioned experiments were conducted at a mean pressure of 92 mm of mercury with the pressure wave variance from 150 to 80 mm of mercury during systole and diastole respectively. Without considering the dynamic elasticity of these vessels, it was possible that the pressures were too great to allow sufficient time for the fluid effects to fatigue the distal region of the model. To test this hypothesis the mean pressure was lowered to 54 mm of mercury, with the pressure wave variance from 94 to 48 mm of mercury on Model T-17, Figure 21. After 167 hours of continuous pulsations, the vessel again dilated 2 cm prestenotically. Before rupture occurred, the model was removed from the testing chamber so that its elastic properties could be rechecked. Tests were conducted on both the distal and proximal section, 2.5 cm from the stenosis throat. Figure 25 shows that the model was more distensible after the experiment than before. It is also obvious that the dilated proximal section is slightly more distensible than the non-dilated section. This suggests that the prestenotic dilatation was made possible by the alteration of material properties, or material properties were altered due to the prestenotic dilatation.

The velocity of the fluid is considered to be one of the more significant factors in stenotic vessels, and especially significant when considering dilatations. The test conducted on Model T-21, Figure 22, was designed to examine the effect increased velocity would have on these

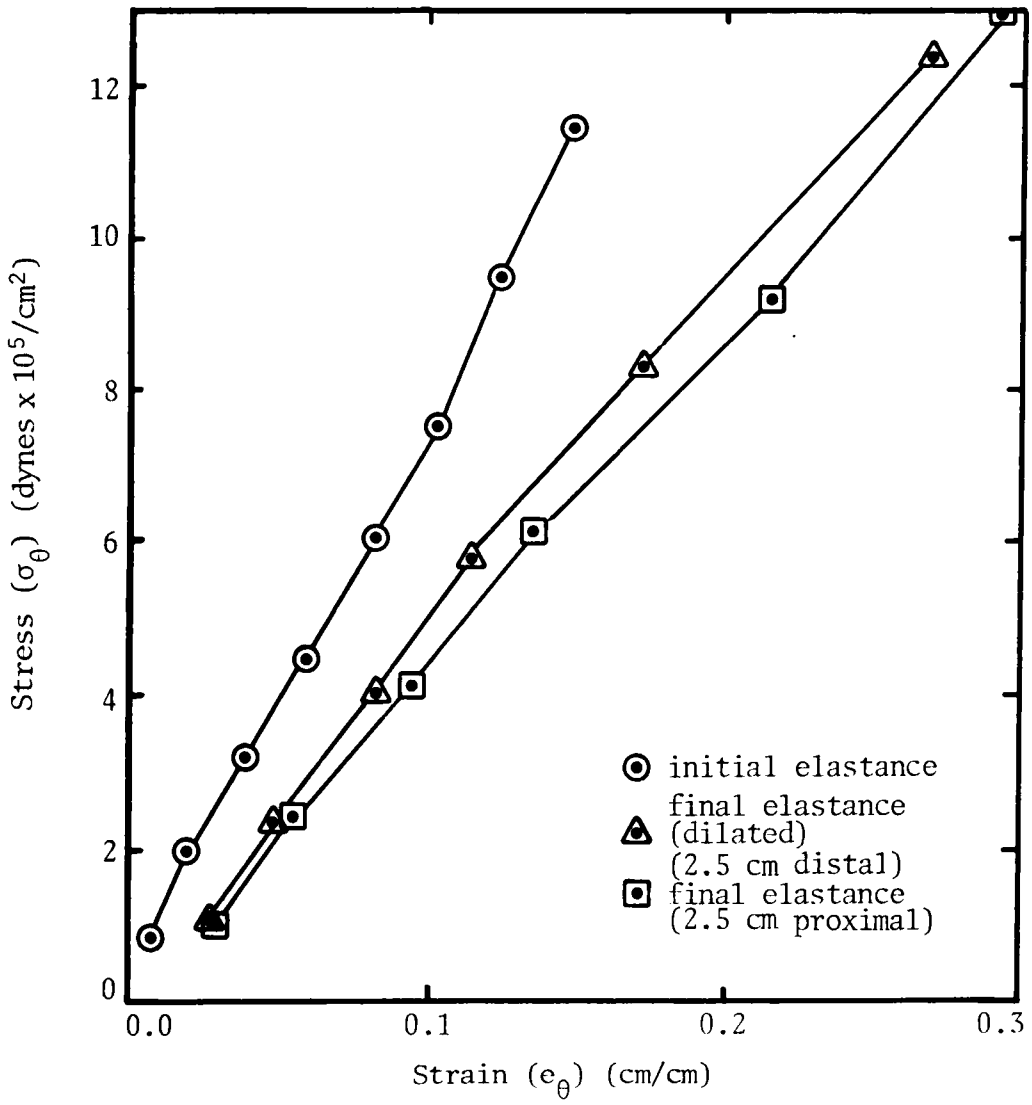


Figure 25. Elastic Properties of Model T-17 Before and After Experiment

arterial models. Holding all variables at normal physiological conditions, the volume rate of flow was increased by a factor of two. Unlike previous models, T-21 did not show a complete reversal of the flow at the end of the systolic cycle. After 22 hours of pulsation, this vessel experienced a complete rupture 2 cm prestenotically.

In previous models the pressure profile and mean volume flow rate were modeled. Conditions were reversed in models T-8, T-27 and T-28, in which the volume flow wave shape and mean pressure were modeled. Figure 23 shows this increased flow rate in T-8 as well as the large fluctuating pressure profile. This model was observed to actually collapse during portions of the diastolic cycle. As with T-18, this model ruptured prestenotically after 14 hours. In model T-28 a capacitance box was placed distal to the model, with the hopes that it would help decrease the large pressure fluctuation. This was partially successful; however the experiment was stopped prematurely because of a leak in the syringe plunger. Model T-27 was similar to T-28 except that the 75% stenosis was replaced with a 90% one. The proximal pressure was much higher while the distal pressure was much lower; again the large fluctuating pressure was apparent. As with T-28, this model also developed a leak in the syringe plunger prior to the completion of this experiment.

If the surrounding tissue of the vessel is damaged either by disease, external injury, or decreased blood

supply, it cannot perform its function of supporting the vessel. When a stenosis exists in an artery it is possible that any of the above might occur. To simulate this decrease in support, Model T-13, Figure 24, was only partially supported on its distal section. As the vessel was being subjected to normal physiological conditions, it was observed that the sponge damped the movement of the vessel on its underside. This damping was not present on the non-support section of the vessel. Consequently, the vessel was able to expand much more freely in this section. After 8.5 hours of pulsation, a poststenotic dilatation started to develop 6 cm from the throat. The dilatation was very symmetrical with respect to the axis of the tube, appearing much as a fusiform aneurysm. Thirteen hours later complete failure of the vessel occurred at this location. To investigate this further, the support device was varied in models T-15, T-16 and T-33. Model T-15 was submerged in a neutrally buoyant aqueous glycerol solution, T-16 was supported on a rigid surface and T-33 was the same as T-13 except the model had a thin proximal wall. In all of these models the vessel ruptured prestenotically.

B. Large Arterial Models

The small arterial model size limitation made it necessary to insert a Plexiglas plug into a straight tube to create the stenotic vessel. As discussed previously it appears that this rigid plug distorted the normal flow

condition anticipated for such a model. To eliminate this, a larger model was constructed completely out of latex (Appendix A). This model had the distinct advantage of homogeneity between stenosis and vessel wall as well as the larger size permitted more sensitivity in photographic determination of dilatation. Photographs of both large and small dilatated models are shown in Figure 26.

As with the small models, the variables considered for each model have been tabulated in Table 13 along with general comments and total time of experiment in Table 14. Models Z-4, Z-1 and Z-8 have been described graphically in Figures 27, 28 and 29, respectively. Each figure depicts the approximate dilatation rate as determined from the photographic method as well as the pressure profile 6 cm distal and proximal to the stenosis throat at the start of the experiment and completion of each experiment. The exact values for the vessel profile have also been tabulated in Tables 15, 16 and 17 for each of these models. Unlike the small models, the corresponding reference axis located at the throat of the stenosis is to scale both in the horizontal and vertical direction. However, because of size limitations it was not possible to display the entire vessel in each figure; consequently, primary emphasis was placed upon the dilated region.

To establish a basis for comparison, Model Z-4 was examined under normal modeled physiological conditions. As depicted in Figures 27 and 30, the model dilated in both the

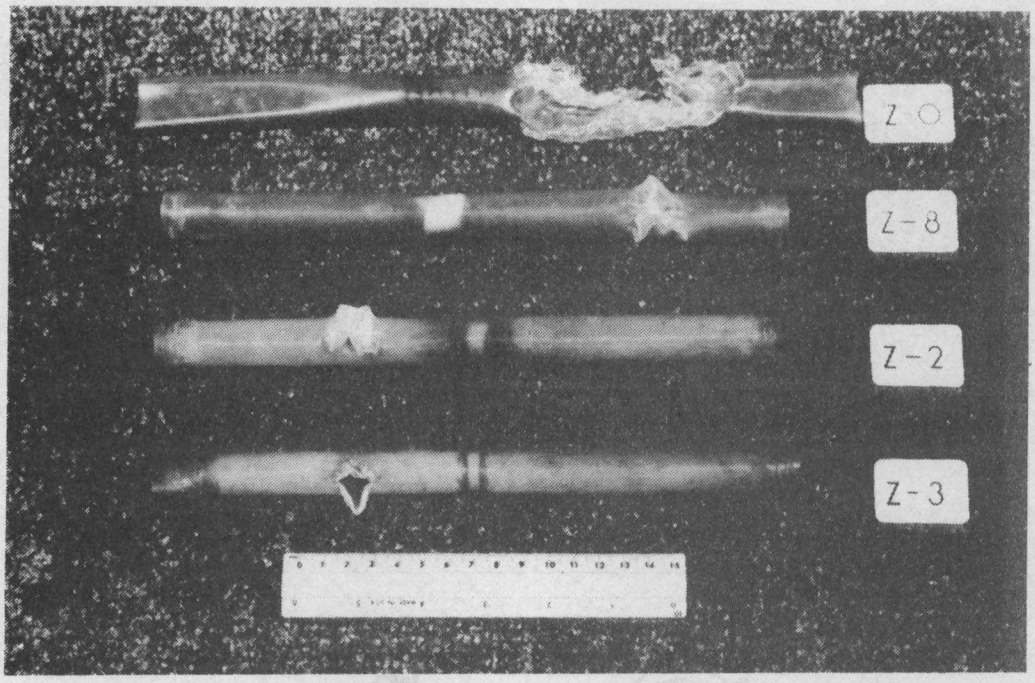


Resulting Rupture on Models Z-0, Z-8, Z-2 and Z-3

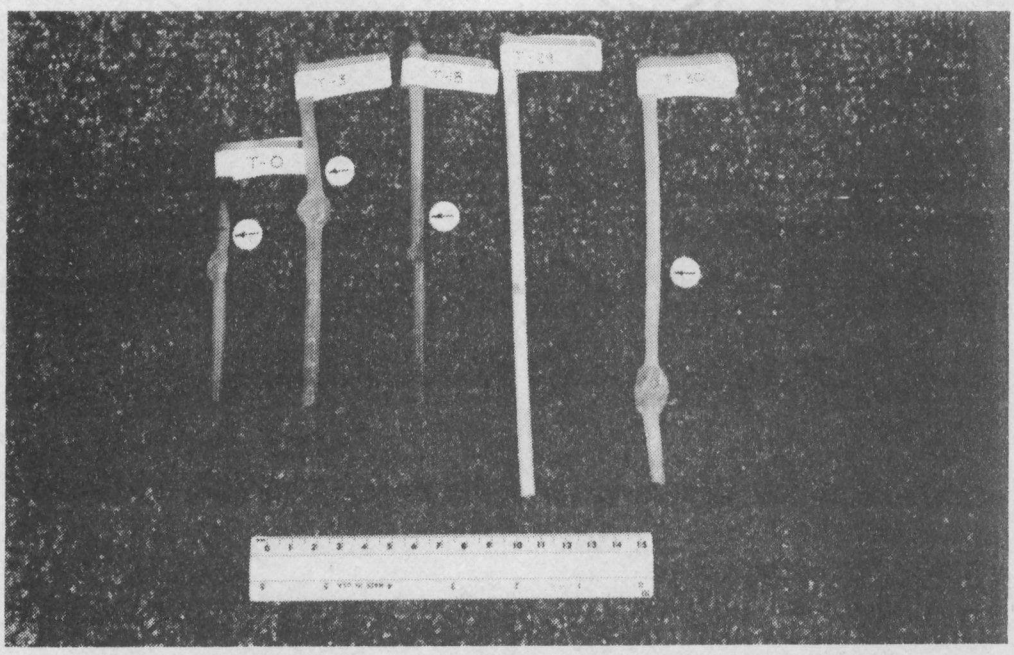


Resulting Rupture on Models T-0, T-3, T-18 and T-30

The arrows indicate the location of the stenosis. Model T-29 was not tested.

Figure 26. Resulting Rupture on Some of the Small and Large Models

TABLE 13

LARGE MODEL VARIABLE VALUES

| Variable \ Model | Z-0 | Z-1 | Z-2 | Z-3 | Z-4 | Z-5 | Z-6 | Z-7 | Z-8 | Z-10 |
|---|---|---|---|---|---|---|---|---|---|---|
| $\bar{R}_o$ (cm) | 1.1 | 1.05 | 1.03 | 1.03 | 1.03 | 1.05 | 1.1 | 1.04 | 1.03 | 1.06 |
| $\bar{R}_i$ (cm) | .99 | .93 | .94 | .93 | .93 | .93 | .98 | .94 | .91 | .91 |
| $L_s$ (cm) | 1.75 | 1.75 | 1.75 | 1.75 | 1.75 | 1.75 | 1.75 | 1.75 | 1.75 | 1.75 |
| $L_d$ (cm) | 9.0 | A | 2.4 | 1.8 | B | † | 4.0 | 3.9 | C | † |
| $R_d$ (cm) | ∞ | A | ∞ | ∞ | B | ∞ | ∞ | ∞ | C | ∞ |
| $L_{sd}$ (cm) | 3.9 | A | -3.5 | -4.2 | B | † | -3.0 | 6.0 | C | † |
| $R_s$ (cm) | .44 | .44 | .24 | .44 | .44 | .44 | .44 | .44 | .44 | .24 |
| $\rho_w$ (g/cm$^3$) | 1.1 | 1.1 | 1.1 | 1.1 | 1.1 | 1.1 | 1.1 | 1.1 | 1.1 | 1.1 |
| $\rho$ (g/cm$^3$) | 1.17 | 1.17 | 1.17 | 1.17 | 1.17 | 1.17 | 1.17 | 1.17 | 1.17 | 1.17 |
| $\mu$ (C.P.) | 14. | 13.2 | 13.2 | 13.2 | 13.2 | 13.2 | 14. | 13.2 | 12.8 | 12.8 |
| $\varepsilon$ | .5 | .5 | .5 | .5 | .5 | .5 | .5 | .5 | .5 | .5 |
| $E_{st}$ (dyne x 10$^6$/cm$^2$) | 8.3 | 8.3 | 8.3 | 8.3 | 8.3 | 8.3 | 8.3 | 8.3 | 8.3 | 8.3 |
| $V_o$ (cm/sec) | V | 9.2 | 9.2 | 13.8 | 9.2 | † | 9.24 | 9.2 | 9.2 | 9.2 |
| $V_j$ (cm/sec) | * | * | * | * | * | * | * | * | * | * |
| $P_o$ (mm Hg) | 64 | 64 | 64 | 64 | 64 | † | 64 | 64 | 64 | 64 |
| $P_j$ (% of prototype) | 60% | 60% | 60% | 60% | 60% | † | D | 60% | 60% | 60% |
| f (Hz) | 6.2 | V | .41 | .41 | .41 | † | .41 | V | 1.54 | V |
| t (sec) | .16 | V | 2.4 | 2.4 | 2.4 | † | 2.4 | V | .65 | V |

A: see Figure 28.
B: see Figure 27.
C: see Figure 29.
D: range increased.
V: varied.
*: not modeled.
†: undetermined.
∞: complete rupture.

TABLE 14

GENERAL COMMENTS FOR LARGE MODELS

| Model | Total Time (hr) | General Comments |
|---|---|---|
| Z-0 | 3.0 | 80% reduction; frequency held at 6.4 times normal value with various velocities; poststenotic dilatation. |
| Z-1 | 2.2 | 78% reduction; varied frequency from .56 to 1.56 times normal value; poststenotic dilatation. |
| Z-2 | .65 | 93% reduction; normal physiological values; prestenotic dilatation. |
| Z-3 | 1.9 | 78% reduction; mean velocity increased 1.5 times normal value; prestenotic dilatation. |
| Z-4 | 2.8 | 78% reduction; normal physiological values; prestenotic dilatation. |
| Z-5 | * | 78% reduction; excessively high pressure at start up resulted in instantaneous rupture. |
| Z-6 | .5 | 80% reduction; normal physiological values, except pressure was allowed to reach values of zero during each cycle; prestenotic dilatation. |
| Z-7 | 4.1 | Straight tube ligated to different degrees and tested under various frequencies (1.0 to 3.0 times normal values); poststenotic dilatation. |
| Z-8 | 3.3 | 78% reduction; frequency increased to 3.75 times normal physiological values; poststenotic dilatation. |
| Z-9 | -- | 93% reduction; not tested. |
| Z-10 | * | 93% reduction; compared pressure profiles with and without epoxy covered vessel under various frequencies. |

*Premature rupture.

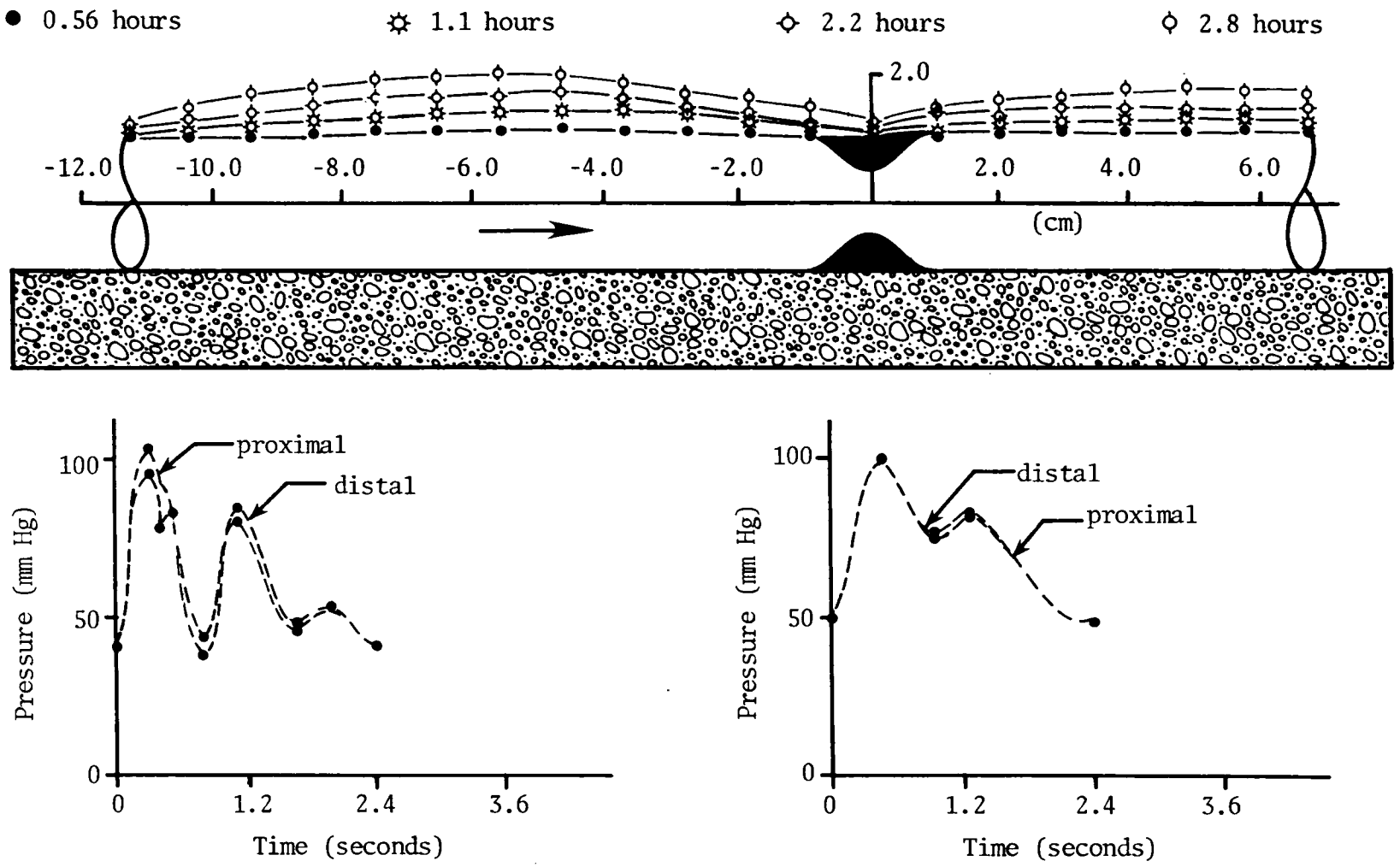


Figure 27. Results for Model Z-4

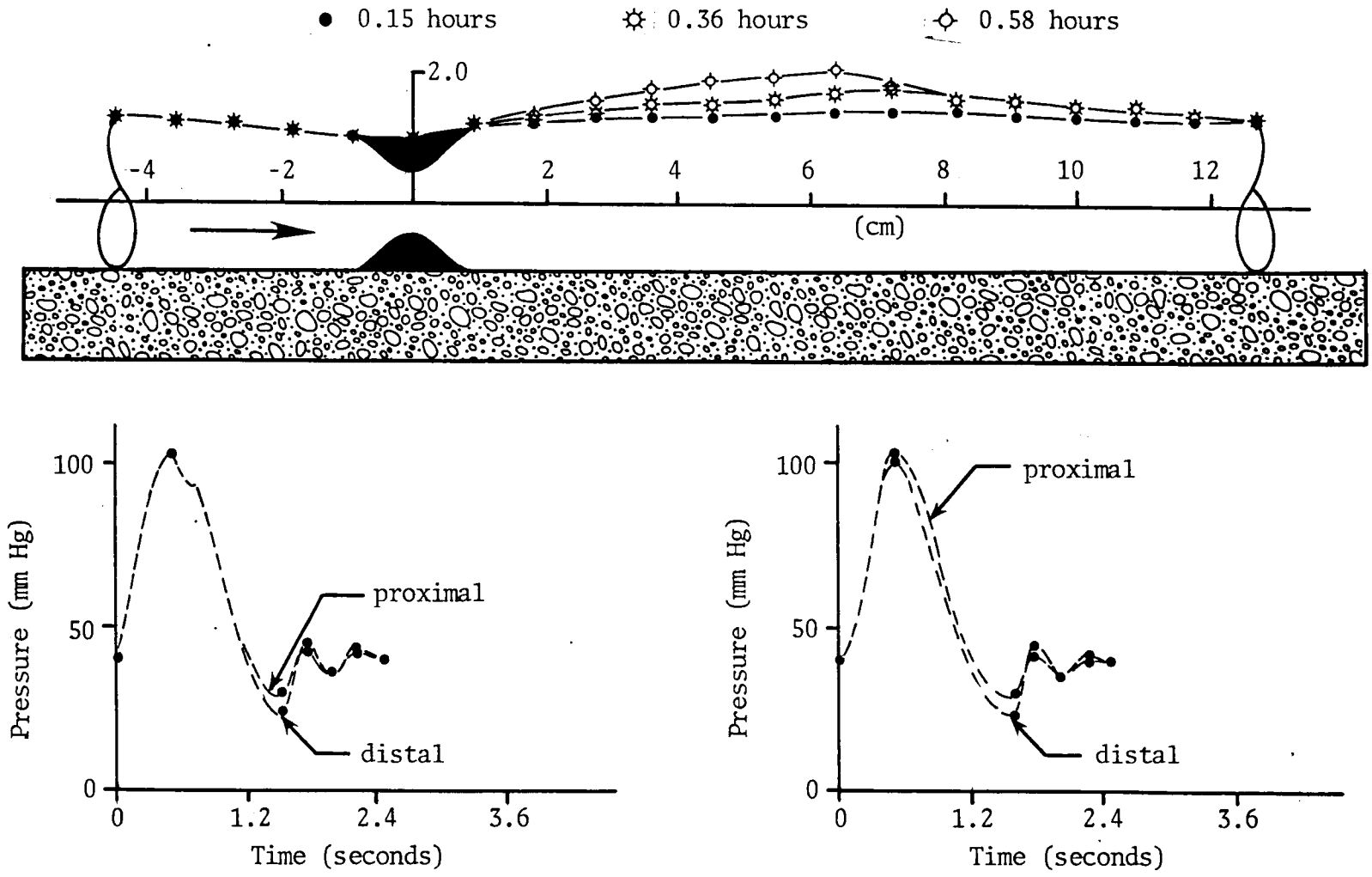


Figure 28. Results for Model Z-1

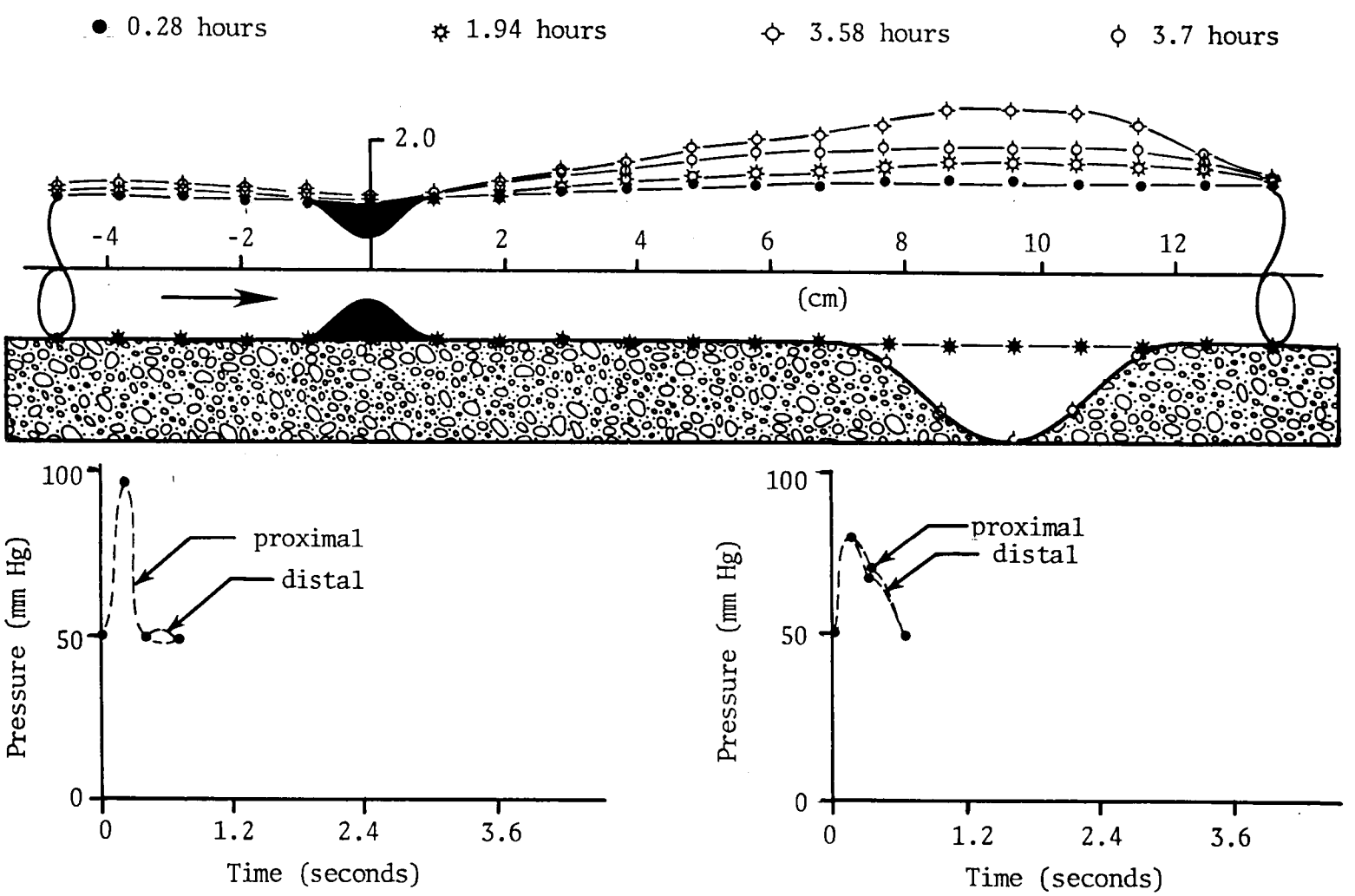


Figure 29. Results for Model Z-8

TABLE 15

DILATATION RATE FOR MODEL Z-4

| Z (cm) Location from Throat | $R_d$ (cm)* | | | |
|---|---|---|---|---|
| | .56 hrs | 1.1 hrs | 2.2 hrs | 2.8 hrs |
| -11.4 | 1.03 | 1.1 | 1.26 | 1.26 |
| -10.45 | 1.03 | 1.18 | 1.35 | 1.54 |
| -9.5 | 1.03 | 1.22 | 1.45 | 1.75 |
| -8.55 | 1.07 | 1.29 | 1.56 | 1.83 |
| -7.6 | 1.14 | 1.34 | 1.64 | 1.92 |
| -6.65 | 1.16 | 1.39 | 1.65 | 1.98 |
| -5.7 | 1.16 | 1.41 | 1.66 | 2.06 |
| -4.75 | 1.18 | 1.45 | 1.68 | 2.0 |
| -3.8 | 1.12 | 1.47 | 1.64 | 1.92 |
| -2.85 | 1.12 | 1.41 | 1.54 | 1.85 |
| -1.9 | 1.07 | 1.29 | 1.45 | 1.73 |
| -.95 | 1.03 | 1.18 | 1.26 | 1.54 |
| 0 | 1.03 | 1.14 | 1.29 | 1.29 |
| .95 | 1.07 | 1.18 | 1.41 | 1.49 |
| 1.9 | 1.07 | 1.26 | 1.35 | 1.64 |
| 2.85 | 1.1 | 1.28 | 1.41 | 1.73 |
| 3.8 | 1.12 | 1.32 | 1.47 | 1.79 |
| 4.75 | 1.12 | 1.33 | 1.49 | 1.83 |
| 5.7 | 1.16 | 1.33 | 1.49 | 1.79 |
| 6.65 | 1.1 | 1.26 | 1.51 | 1.69 |

*The radius below the center of the vessel remained relatively constant at 1.03 cm.

TABLE 16

DILATATION RATE FOR MODEL Z-1

| Z (cm) Location from Throat | $R_d$ (cm)* | | |
|---|---|---|---|
| | .15 hrs | .36 hrs | .58 hrs |
| -4.5 | 1.30 | 1.30 | 1.30 |
| -3.6 | 1.26 | 1.26 | 1.26 |
| -2.7 | 1.21 | 1.21 | 1.21 |
| -1.8 | 1.12 | 1.12 | 1.12 |
| -.9 | 1.05 | 1.05 | 1.05 |
| 0 | 1.03 | 1.03 | 1.03 |
| .9 | 1.21 | 1.21 | 1.21 |
| 1.8 | 1.21 | 1.21 | 1.39 |
| 2.7 | 1.30 | 1.37 | 1.58 |
| 3.6 | 1.30 | 1.48 | 1.74 |
| 4.5 | 1.30 | 1.53 | 1.87 |
| 5.4 | 1.30 | 1.55 | 1.92 |
| 6.3 | 1.33 | 1.66 | 2.01 |
| 7.2 | 1.39 | 1.74 | 1.83 |
| 8.1 | 1.39 | 1.74 | 1.74 |
| 9.0 | 1.30 | 1.57 | 1.57 |
| 9.9 | 1.30 | 1.48 | 1.48 |
| 10.8 | 1.21 | 1.48 | 1.48 |
| 11.7 | 1.21 | 1.38 | 1.39 |
| 12.6 | 1.21 | 1.30 | 1.30 |

*The radius below the center of the vessel remained relatively constant at 1.03 cm.

TABLE 17

DILATATION RATE FOR MODEL Z-8

| Z (cm) Location from Throat | $R_d$ (cm)* | | | | |
|---|---|---|---|---|---|
| | .28 hrs | 1.94 hrs | 3.58 hrs | 3.7 hrs | |
| -5.7 | 1.12 | 1.26 | 1.31 | 1.22 | -- |
| -4.75 | 1.16 | 1.26 | 1.35 | 1.26 | -- |
| -3.8 | 1.16 | 1.26 | 1.35 | 1.31 | -- |
| -2.85 | 1.12 | 1.22 | 1.31 | 1.31 | -- |
| -1.9 | 1.07 | 1.18 | 1.26 | 1.26 | -- |
| -.95 | 1.03 | 1.10 | 1.20 | 1.16 | -- |
| 0 | 1.03 | 1.07 | 1.16 | 1.16 | -- |
| .95 | 1.07 | 1.07 | 1.20 | 1.26 | -- |
| 1.9 | 1.16 | 1.18 | 1.45 | 1.35 | -- |
| 2.85 | 1.22 | 1.28 | 1.58 | 1.54 | -- |
| 3.8 | 1.28 | 1.41 | 1.73 | .164 | -- |
| 4.75 | 1.35 | 1.47 | 1.93 | 1.73 | -- |
| 5.7 | 1.35 | 1.54 | 2.02 | .183 | -- |
| 6.65 | 1.35 | 1.57 | 2.11 | 1.83 | -- |
| 7.6 | 1.41 | 1.64 | 2.21 | 1.94 | -1.31 |
| 8.55 | 1.41 | 1.69 | 2.30 | 1.92 | -2.17 |
| 9.5 | 1.41 | 1.69 | 2.30 | 1.92 | -2.46 |
| 10.45 | 1.39 | 1.68 | 2.21 | 1.92 | -2.08 |
| 11.4 | 1.35 | 1.64 | 2.02 | 1.92 | -1.12 |
| 12.35 | 1.35 | 1.60 | 1.83 | 1.69 | -- |
| 13.3 | 1.35 | 1.45 | 1.45 | 1.64 | -- |

*The radius below the center of the vessel was relatively constant at 1.03 cm except during complete rupture at 3.7 hours.

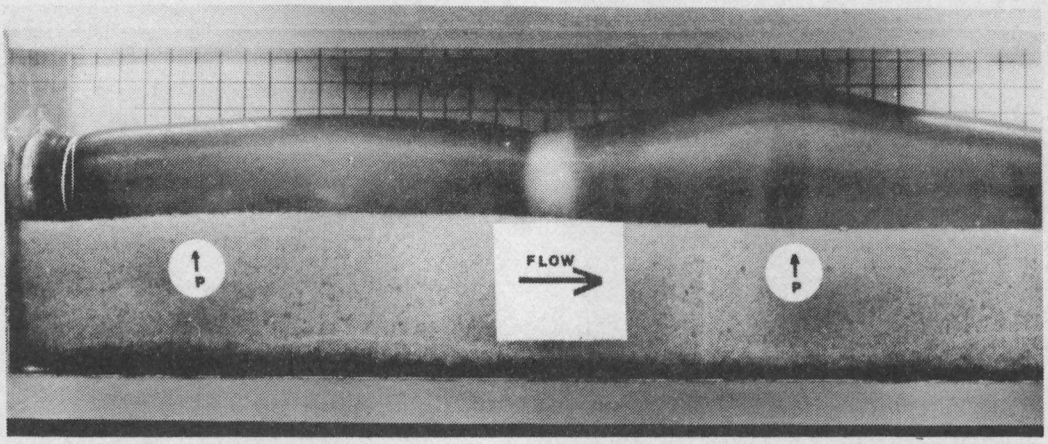


Poststenotic Dilatation with Model Z-1 During Systole

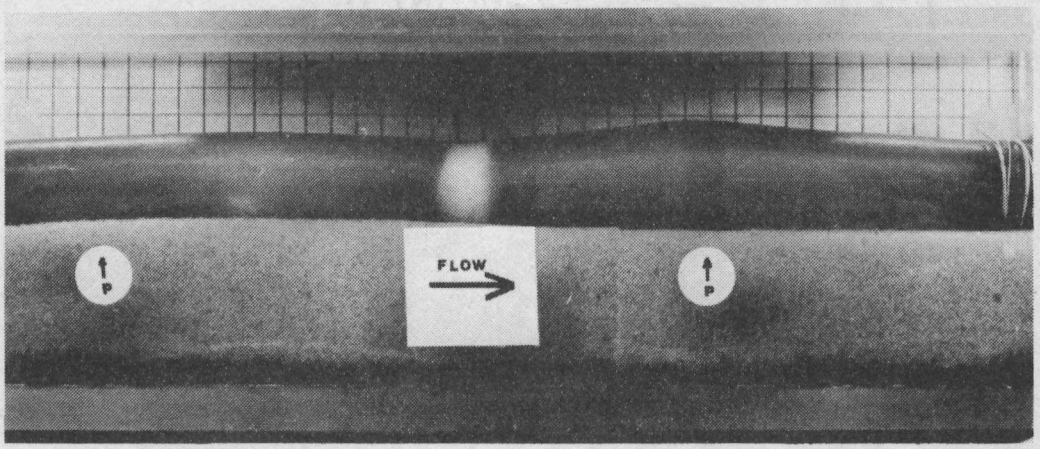


Poststenotic Dilatation with Model Z-1 During Diastole

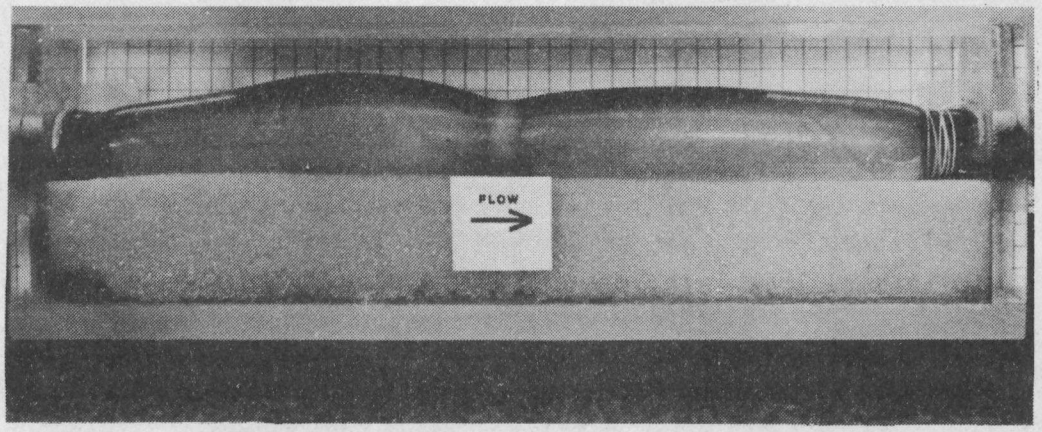


Model Z-4; Prestenotic Dilatation Forming Under Normal Physiological Conditions

Figure 30. Dilatation on Model Z-1 and Z-4

distal and proximal regions; however the proximal dilatation was larger. As with the smaller models, the time for dilatation was much less than an actual arterial dilatation. It is interesting to note that initially there was a sudden drop in each pressure profile approximately 40% of the way through each cycle. However, as the vessel is weakened it tends to do a better job of damping, thereby removing this sudden drop in both profiles.

Experiments were performed on Model Z-0 under a frequency 6.4 times normal physiological conditions. The volume flow rate was varied such that the effects of varying velocities might be determined. Mean volume rates of flow of 2.4, 5.5, 7.1, 8.9, 9.4, 11.8, 13.4, 14.1 and 15.7 ml/sec were examined, which respectively correspond to velocities of .26, .60, .77, .96, 1.0, 1.3, 1.5 and 1.7 times greater than normal physiological conditions for the large arterial model. After two hours a slight bulge appeared poststenotically. It continued to grow until rupture occurred one hour later. As with the small model the dilatation was much more noticeable on the top of the vessel than on the supported bottom side. It was not until moments before rupture that any detectable change occurred on the lower side. However, when rupture did occur, it was very symmetrical with respect to the axis of flow, appearing much as a fusiform aneurism, Figure 26. The final rupture was 4 cm from the throat of the stenosis with a total dilatation length of 9 cm. It is interesting to note

that the dilated region became twice as large as the non-dilated region within the first three hours, yet when complete failure occurred the dilated region became approximately 10 times larger in a matter of seconds. Unfortunately instrumentation problems with the Physiograph eliminated any possibility of comparing pressure and velocity profiles for this experiment.

In the previous experiment both the frequency and the velocity variables were distorted. Consequently it was impossible to determine whether the high frequencies and/or varying velocity promoted the development of the post-stenotic dilatation. With Model Z-1 the time-averaged mean velocity was held at its normal value while the frequency was varied at .56, .76, 1.0, 1.16, 1.4, and 1.56 times the normal modeling frequency. Figure 28 shows that the dilatation again developed poststenotically approximately 1 cm from the stenosis throat with a final dilatation length of 12 cm. This vessel showed very little change in the proximal region with the major dilatation occurring on the upper distal side. As the experiment progressed the point of maximum dilatation appeared to be moving backward toward the stenosis throat. Figure 30 shows the difference in dilatation size between systolic and diastolic portions of the cycle.

Pressure readings were taken at 1 cm intervals both distal and proximal to the throat of Model Z-1. A slight pressure drop was recorded between distal and proximal

regions for a given frequency. However, no localized increase or decrease in pressure was detected for the frequencies examined. The two pressure profiles, Figure 28, below the model and to the left represent the normal modeling frequency, 6 cm proximal and distal to the stenosis throat at the beginning of the experiment. While there is a slight difference in profile, no major pressure differential was detected early in the experiment. This suggests that some type of normalizing effect exists in a flexible model which tends to equate the pressures. After the model was tested under all the various frequencies, the dilatation had become quite noticeable distal to the stenosis. The frequency was then reduced back to the normal modeling condition and a second profile was obtained. This profile is shown in the lower right pressure curve.

To test whether a high mean velocity could promote poststenotic dilatation, Model Z-3 was tested with the mean velocity increased to 1.5 times the normal value while all other variables were held at normal physiological conditions. After 1.9 hours of pulsation this model dilated prestenotically. This tends to support the concept that Model Z-0 sustained a poststenotic dilatation because of the excessively high frequency and not as a result of a high velocity. This finding was also supported by Model Z-1. The dilatation formed in Model Z-3 was much shorter in length as well as restricted to the upper side of the proximal section, Figure 26.

In another experiment Model Z-6 was examined under the same conditions as Z-4 (that is, normal conditions) except the pressure profiles reached a value of zero momentarily during each cycle. When this occurred the vessel was able to collapse completely with each beat. Again the dilatation was prestenotic; however the time of rupture was much less for this model than Z-4 (.5 hours compared to 2.8 hours). It is apparent that these large pressure variations are much more destructive to the vessel wall.

To confirm the effect of high frequencies on poststenotic dilatation development, Model Z-8 was examined under a frequency of 3.75 times higher than normal physiological conditions. Figure 29 shows that a dilatation occurred poststenotically with the center occurring 12 cm from the stenosis throat. As with Model Z-0 it is interesting to observe that the initial dilatation was confined to the upper distal region of the vessel until moments before complete rupture. Because of soft sponge support, when complete rupture occurred the dilatation was able to force itself downward toward the bottom of the testing chamber.

From the pressure profiles it is obvious that very little difference exists between the two regions throughout the experiment. It should be noted that the pressure profiles shown were taken some time before the vessel was able to dilate downward into the sponge. When this occurred, the distal pressure not only dropped considerably, but it also lost most of its pulsatile shape.

In all the aforementioned large model experiments the vessel was either reduced 78% or 80% at the throat of the stenosis. To test the effect of further reduction Models Z-2 and Z-10 were reduced to 93% and tested under normal conditions. In both cases the model ruptured prestenotically shortly after the experiment began. However, unlike the 78% and 80% reduced models there was a significant pressure drop between proximal and distal regions.

Examination of all the previous experiments has demonstrated the importance of frequency and degree of constriction on each of the models. To better understand some of these principles an additional test was performed on a straight latex tube which had been banded to various degrees by a nylon suture. Ligations formed in this manner tend to create folds and buckles on the inside wall of the vessel so that the percent reduction in area may have been greater than recorded. Care should be exercised when attempting to compare this model to previous ones. The severity of these folds and buckles was demonstrated by a plaster cast which was made of the lumen at the completion of this experiment.

First, the model was constricted to a throat reduction of 53, 62, 71, 79 and 83% and tested under normal physiological conditions. Figure 31 shows the resulting pressure profile 6 cm distal and proximal to the throat under each constriction. While pressure profiles were obtained at 1 cm intervals in both the distal and proximal

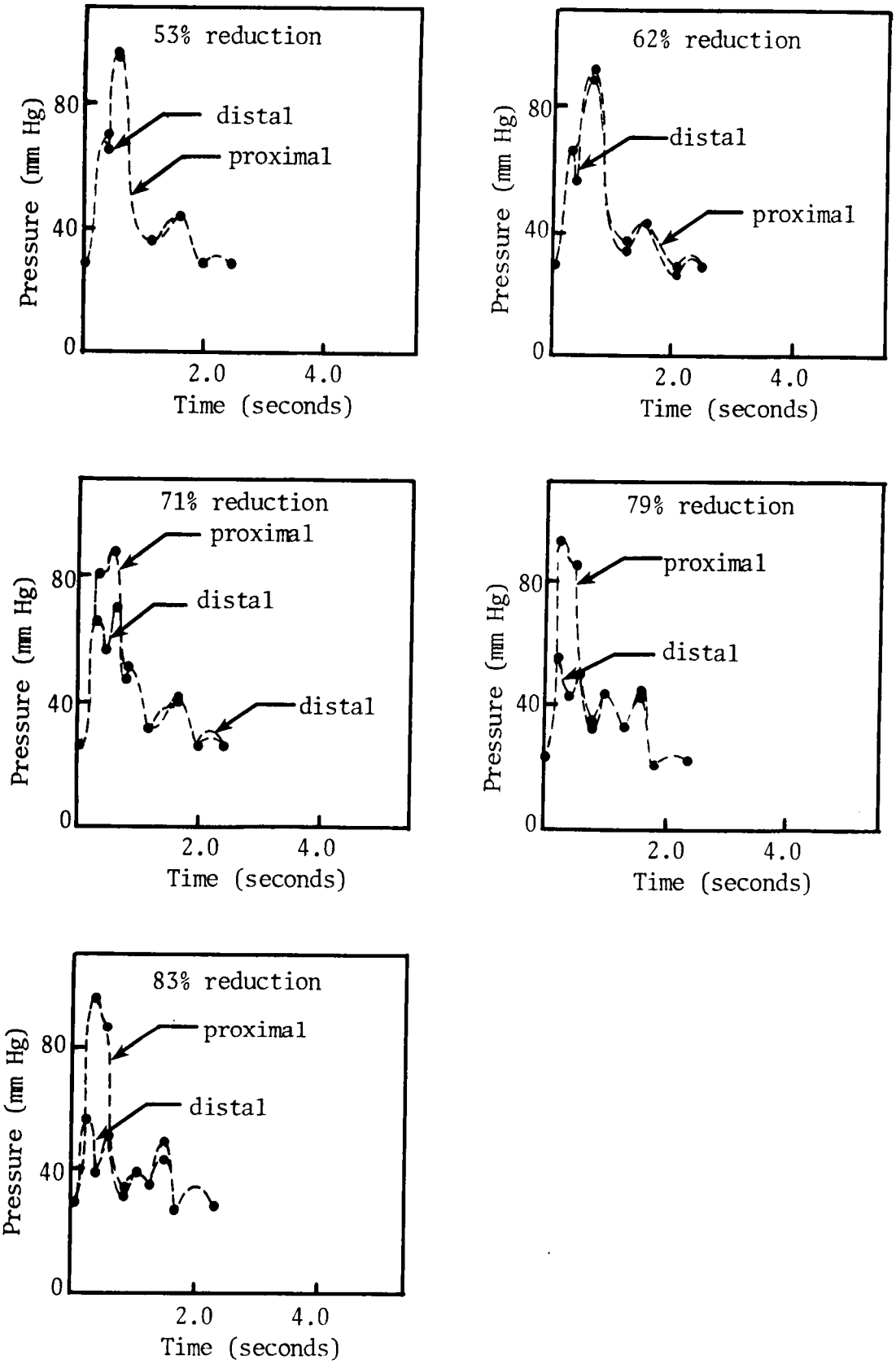


Figure 31. Pressure Curves for Various Constrictions in Model Z-7

region, no detectable variations occurred. Consequently, these pressure profiles are quite representative of the pressures in the entire region. Examination of each profile reveals that no major pressure drop existed until the vessel was restricted to at least 71%, at which time the systolic peak was seen to decrease appreciably. In the 53% reduced profile a slight drop is first observed in the systolic portion of the distal profile. This drop continues to grow with each constriction until finally at 83% the systolic peak is nearly removed. During this portion of the test, there was no noticeable pre- or poststenotic dilatation in the model.

As higher than normal frequencies appear to enhance the development of poststenotic dilatation rather than prestenotic dilatation, it was then decided to vary the frequency of the pump for the 79% constriction. All other variables were held at normal modeled physiological conditions, and the pressure profiles were determined at 1 cm intervals. Figure 32 shows the results of pressure profiles 6 cm from the stenosis throat under frequencies of 1.0, 1.56, 1.96, 2.36 and 2.76 times the normal rate. As with the previous experiments no major change in pressure occurred within a given region; thus these profiles are representative of the entire region. As can be seen the relative pressure drop that exists at normal conditions is also present at 1.56 and 1.96 times normal conditions. However, once the frequency is increased to 2.36 the

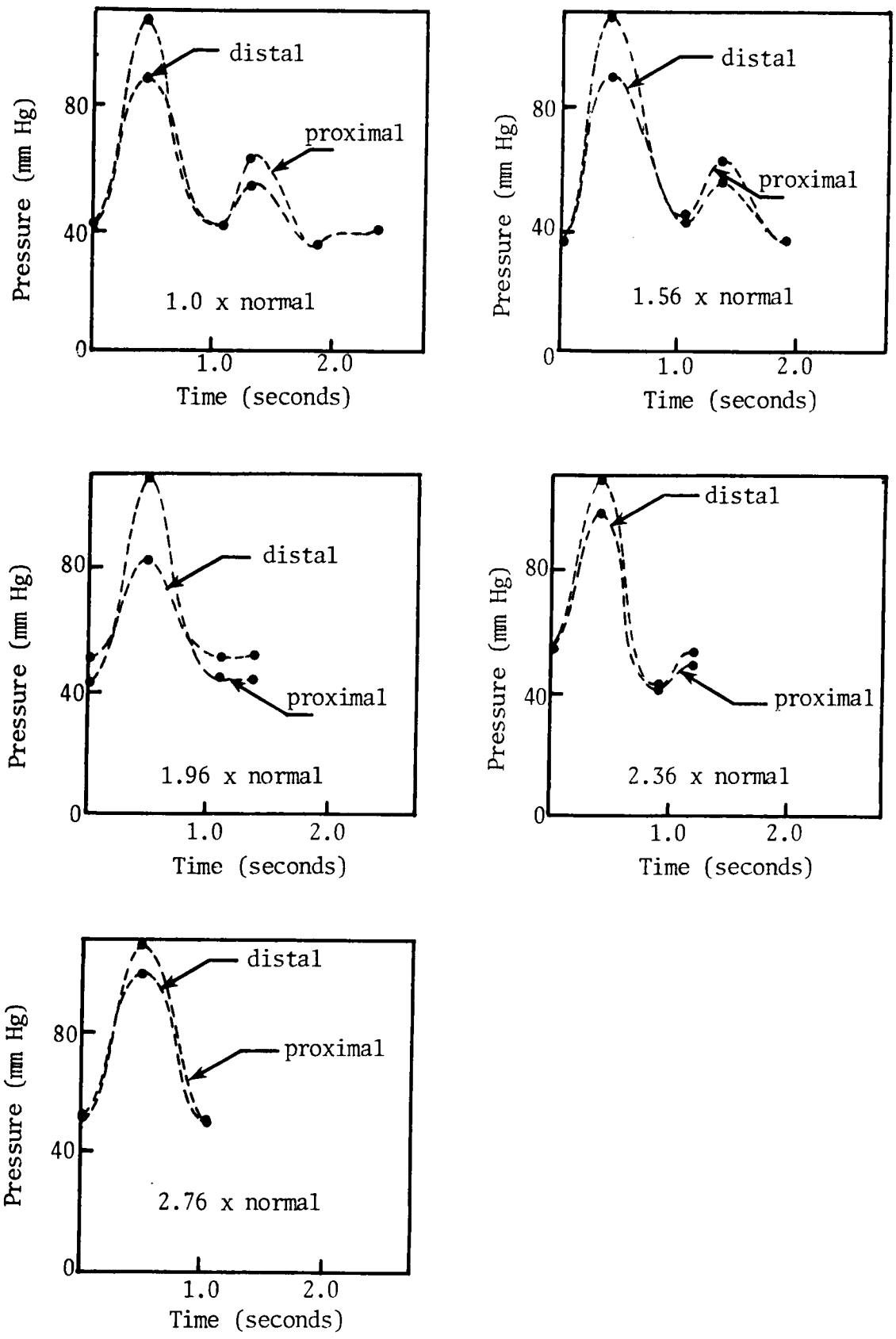


Figure 32. Pressure Curves for Various Frequencies in Model Z-7 at 79% Constriction

pressure drop appears to decrease and continues to remain decreased at 2.76. This occurrence suggests that some type of frequency dependent transition region exists where the pressure drop across the stenosis is actually decreased.

Experimental Model Z-10 was designed to compare the difference in pressure profiles between a flexible model and a rigid one. To create the rigid model effect Z-10 was prepared in the normal way, then coated with a thin layer of vaseline followed by a thick coat of clear epoxy. The pressure profiles were then obtained under normal conditions with varying frequencies. The epoxy was then carefully removed from the vessel and the same experiment was repeated. It was possible to observe that the flexible model did tend to dampen out the pressure profiles between proximal and distal regions. Unfortunately, a malfunctioning pressure transducer prevented the accurate appraisement of these pressure profiles.

## C. Pressure Inside Large Arterial Models

Over the past few years numerous studies have been conducted on rigid models of stenotic vessels with primary emphasis being placed upon the hemodynamic phenomena which occur as a fluid travels through the distal region. Intuitively, one would suggest that a rigid model is far from being an accurate model of an elastic system. However, when a vessel becomes stenotic it has been observed that the elastic properties of the wall will be altered. Such

alterations will actually cause the vessel to lose much of its elastic characteristics, particularly if the stenosis is the result of some internal disorder such as arteriosclerosis. Regardless of how realistic the rigid model studies have been, they have resulted in the development of several theories as well as some empirical equations which approximate *in vivo* stenotic conditions. However, the need for comparison of these theories and equations with flexible models is great. As of this date very little experimental work has been done on applying rigid model experimental procedures to flexible ones. This is primarily the result of not having a good clear elastic model of a stenotic vessel.

The models developed for this research project were not actually clear but they were opaque enough so that dye injection studies could be performed. With the existence of a pressure catheter, the pressure distribution may also be determined for various flow conditions. Figures 33 and 34 show typical dimensionless pressure drops for steady flow under various Reynolds number for both the 79% and 93% constricted flexible models (models Z-1 and Z-2, respectively). The Reynolds number, based upon average mean velocity, is equal to either 266, 900 or 5500. The pressure difference was determined by assuming the most proximal reading as the reference and subtracting it from the other values. To permit comparison with geometrically similar models, the location of the reading has been expressed as a dimensionless

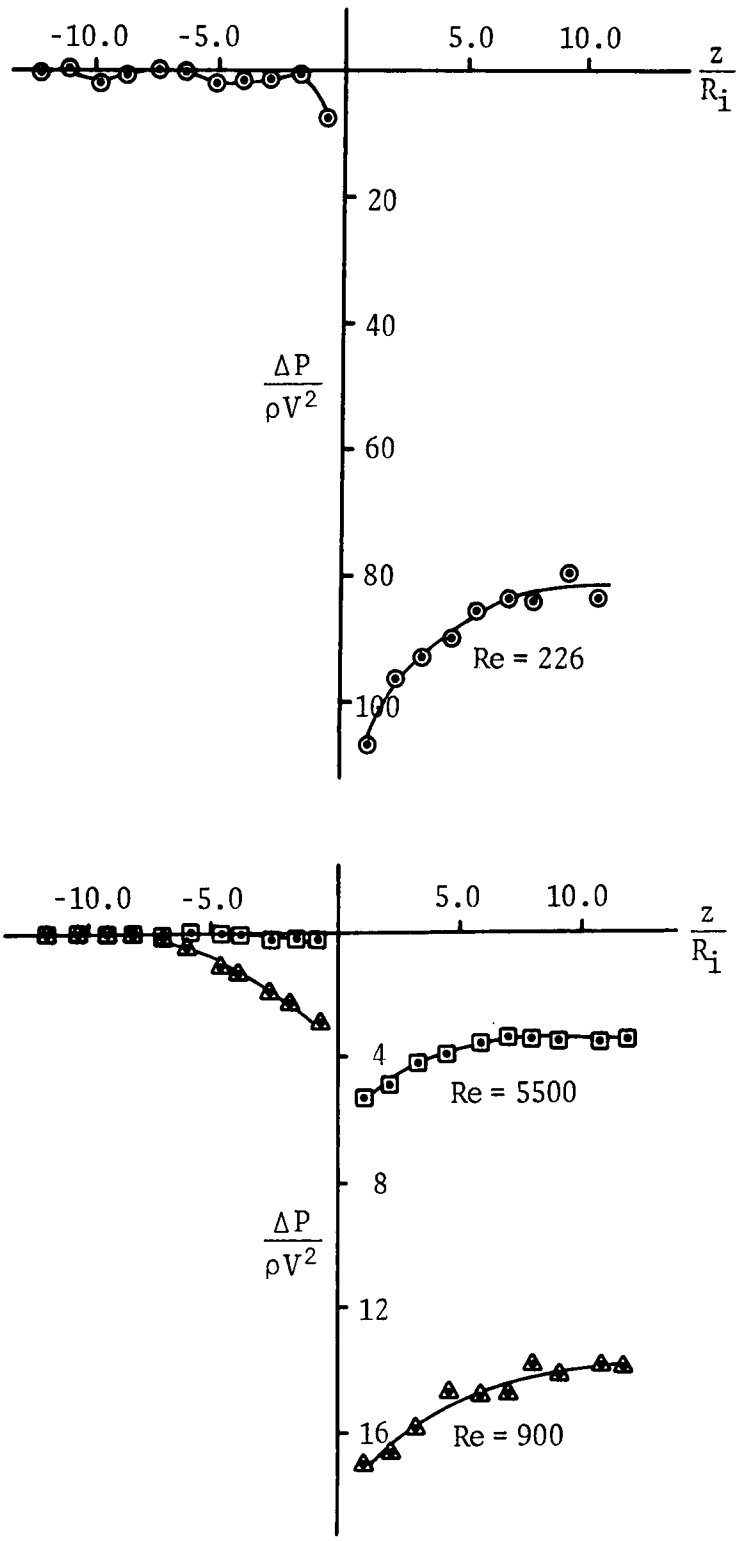


Figure 33. Dimensionless Pressure Drops for Steady Flow in a 79% Constricted Model (Z-1)

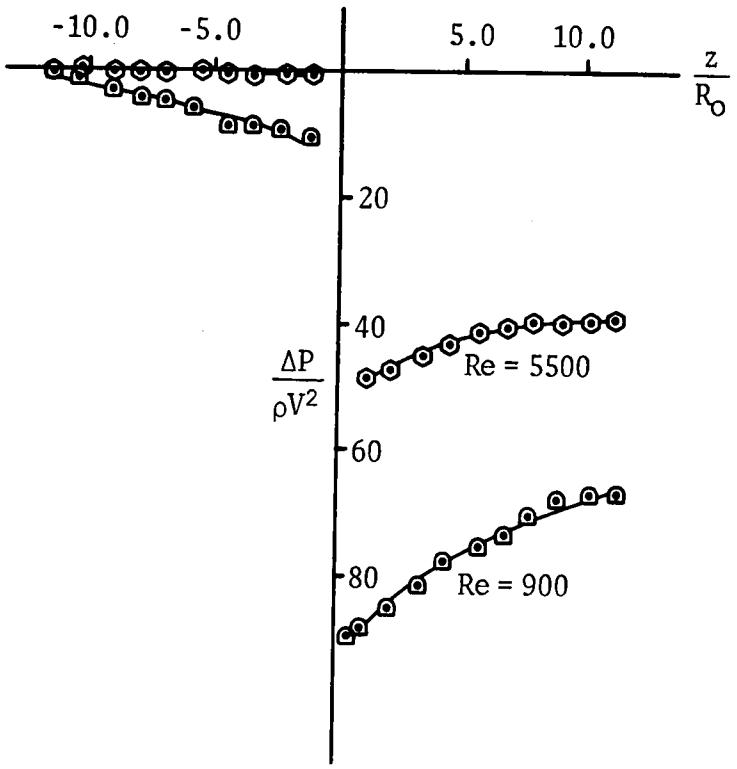


Figure 34. Dimensionless Pressure Drops for Steady Flow in a 93% Constricted Model (Z-2)

ratio. Figures 35 and 36 show the corresponding pressure profiles for models Z-3 and Z-2 respectively at various locations for pulsatile flow conditions. These readings were taken at a Reynolds number of 150 based upon average mean velocity or 750 based upon peak mean velocity. The difference in pressure drops between the 79% and 93% constricted models are quite apparent from these profiles. Also, it appears that the pressure did not vary significantly along the length of the tube distal to the stenosis for pulsatile flow conditions.

It was the intent of the latter portion of this study to examine the flexible model under both steady state and pulsatile flow conditions, thereby providing the necessary information to expand some of the equations for rigid models to include elasticity effects. The necessary experimental work was conducted, and some equations were developed similar to those of Young and Tsai (1973) and Clark (1976) to describe pressure drops for a steady flow condition. Unfortunately, time limitation has necessitated the omission of formal presentation of data at this time. With the hope that further studies will be conducted with these models, some of the experimental results for steady flow have been included in Appendix E.

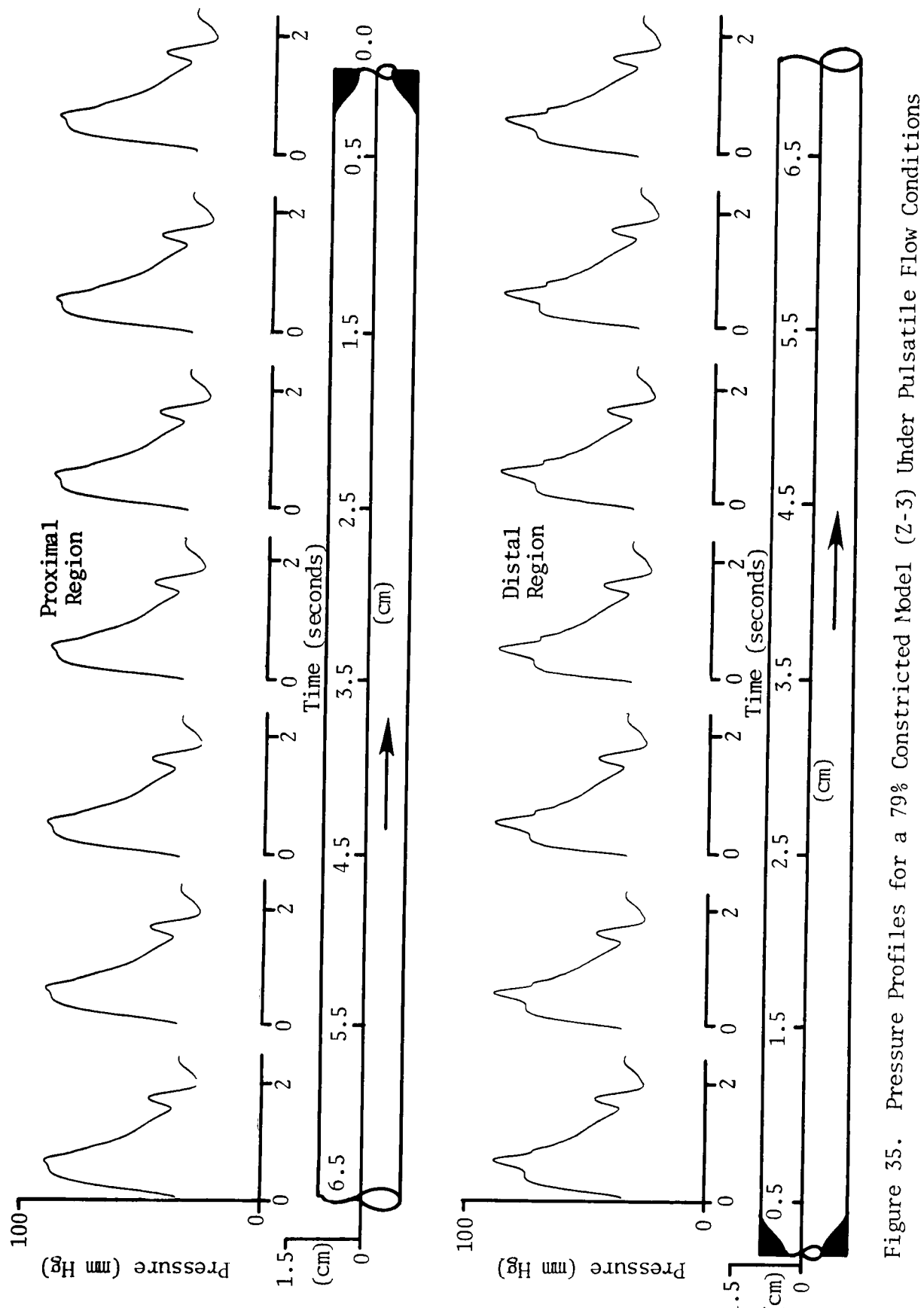


Figure 35. Pressure Profiles for a 79% Constricted Model (Z-3) Under Pulsatile Flow Conditions

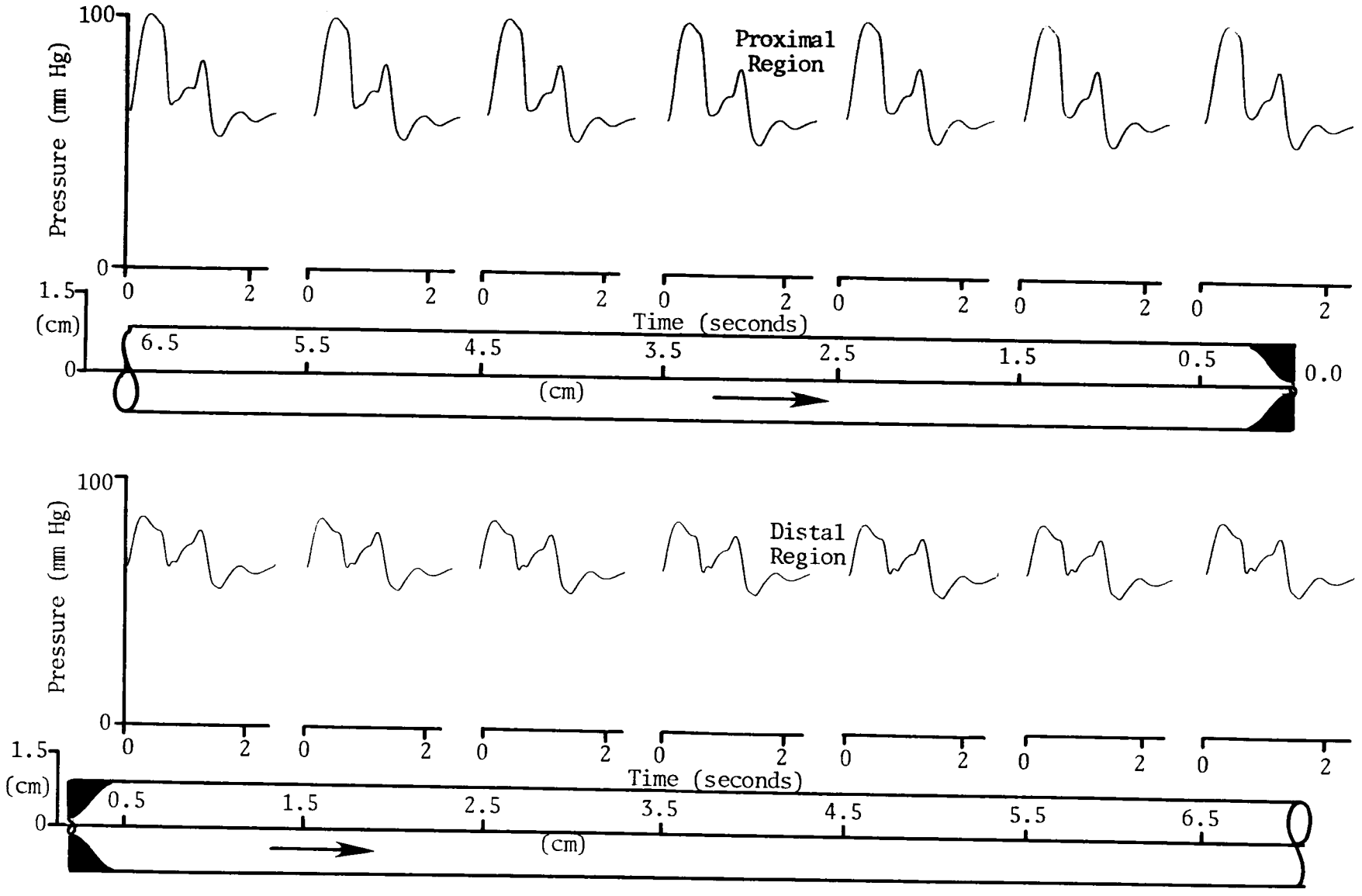


Figure 36. Pressure Profiles for a 93% Constricted Model (Z-2) Under Pulsatile Flow Conditions

# CHAPTER VII

## CONCLUSIONS AND RECOMMENDATIONS

### A. Conclusions

(1) Under normal modeled physiological conditions, poststenotic dilatation did not occur in any of the models. This suggests that the phenomenon of poststenotic dilatation may be influenced not only by mechanical forces but also by biological effects.

(2) Abnormally high velocities had little effect on the region in which the dilatation developed for the conditions studied. However, abnormally high frequencies resulted in poststenotic dilatation.

(3) It appears that the degree of constriction as well as the material of the stenosis affect the dilatation obtained. Consequently, it would be of interest to compare dilatations formed from intravascular lesions with those produced by extravascular means.

(4) Prestenotic dilatation may be related to a wave reflection, especially when the stenosis is rigid. The location of the stenosis did not affect the location of the dilatation with respect to the stenosis.

(5) The method of vessel support can affect the location of the dilatation.

(6) High variations in pressure caused dilatations to form faster.

(7) Roach (1972) pointed out that the femoral artery would dilate in 10 hours after it was ligated but would reach a steady state size after 30 days. The short time necessary for rupture to occur in these models reflects some of the dissimilarities between these models and actual arteries. This dissimilarity may be partly the result of the inability of the model to rebuild itself; in addition, the models were tested in ranges close to their yield point.

(8) The modeled vessel wall expanded in both the distal and proximal region. This weakening and bulging helped to damp out the pulsatile wave shape.

(9) No localized high pressure region was detected in any of the models, although pressures were not measured exactly adjacent to the wall.

(10) The poststenotic dilatations that did develop in this study changed their size considerably between systole and diastole.

(11) The existence of a frequency dependent pressure drop transition region appears to exist in sufficiently constricted vessels.

(12) Ligation made with sutures created severe folds and buckles on the inside wall of the models.

(13) The comparison of model variables, dimensional analysis, and the resulting mock circulatory system provide a method for obtaining data concerning the hemodynamic behavior associated with stenotic vessels. Furthermore, the method by which the models were constructed provides a means by which future flexible studies might be conducted.

B. Recommendations

(1) Any future determinations of pressure drops should be done with a differential pressure transducer. If the existing transducers are utilized, care should be taken that accurate dynamic response is assured, i.e., it may be frequency dependent.

(2) Leakage problems with the piston pump should be alleviated.

(3) The elastic properties of the models should be tested under dynamic conditions. Also, the possibility of improving the model with an additional coat of a different material should be investigated.

(4) Determine the exact influence of frequency on dilatation location.

(5) The difference between rigid and flexible models should be considered. This could be accomplished by using epoxy on the flexible models.

(6) Further dye injection studies with these models could give some indication of local flow conditions. Attempts should be made to determine the separation region and how it is affected by poststenotic dilatation.

(7) Study the effects of a rigid stenosis *in vivo* and try to determine if wave reflection does exist.

(8) Conduct an investigation of fluid flow behavior with different stenosis length ratios as well as different degrees of constriction.

(9) Conduct more experiments of a similar nature to this study so that by using dimensional analysis an equation can be developed which would predict the type of dilatation which would occur under various flow conditions.

(10) Conduct a theoretical elastohydrodynamic analysis of the stenosis problem.

(11) Relate model dilatation to actual stenotic vessels in patients by using radiograms.

# LIST OF REFERENCES

# LIST OF REFERENCES

Aars, H. Experimental Post-Stenotic Dilatation of the Ascending Aorta in Rabbits, Acta Physiology Scandinavia, 59, supp. 213, 5, 1963.

Albritton, E. C. Standard Values in Blood, Saunders, Philadelphia, 1952.

Attinger, F. M. Two-Dimensional In-Vitro Studies of Femoral Arterial Wall of the Dog, Circulation Research, 22:829-840, 1968.

Bergel, D. H. The Visco-Elastic Properties of the Arterial Wall, Ph.D. Thesis, University of London, 1960.

Bergel, D. H. The Static Elastic Properties of the Arterial Wall, Journal of Physiology, 156:445-457, 1961a.

Bergel, D. H. The Dynamic Elastic Properties of the Arterial Wall, Journal of Physiology, 156:458-469, 1961b.

Bergel, D. H. Stress-Strain Properties of Blood Vessels, Laboratory Practice, 15:77-81, 1966.

Bergel, D. H. The Properties of Blood Vessels, in Biomechanics, Its Foundations and Objectives, Y. C. Fung (Ed.), Prentice Hall, Inc., New Jersey, 1972.

Bugliarello, G., Kapur, C. and Itsiao, G. The Profile Viscosity and Other Characteristics of Blood Flow in a Non-Uniform Shear Field, Proc. Fourth Int. Congr. on Rheol. 4, Symp. on Biorheol., A. L. Copley (Ed.), Interscience, New York, pp. 351-370, 1965.

Burns, D. L. A General Theory of the Causes of Murmurs in the Cardiovascular System, American Journal of Medicine, 27:360-373, 1959.

Burns, D. L., Connolly, J. E., Holman, E. and Stofer, R. C. Experimental Observations on Post-Stenotic Dilatations, Journal of Thoracic and Cardiovascular Surgery, 38:662-669, 1959.

Burton, A. C. Relation of Structure to Function of the Tissues of the Walls of Blood Vessels, Physiology Review, 34:619-642, 1954.

Burton, A. C. Physiology and Biophysics of the Circulation, Year Book Medical Publishers, Inc., Chicago, 1972.

Clark, C. The Fluid Mechanics of Aortic Stenosis, Part I and II, Journal of Biomechanics, Vol. 9, pp. 521-528; pp. 567-573.

Cliff, S. B. Personal Communication, 1976.

Cokelet, G. R. The Rheology of Human Blood, in Biomechanics, Its Foundations and Objectives, Y. C. Fung (Ed.), Prentice Hall, Inc., New Jersey, 1972.

Daly, B. J. A Numerical Study of Pulsatile Flow through Stenosed Canine Femoral Arteries, Journal of Biomechanics, 9:465-475, 1976.

De Vries, H. and van den Berg, J. On the Origin of Post-stenotic Dilatation, Cardiologia, 33:195-211, 1958.

Ditter, D. S. Blood and Other Body Fluids, Federation of American Society for Experimental Biology, Washington, D.C., 1961.

Etkin, B., Korbacher, G. K. and Keefe, R. T. Acoustic Radiation from a Stationary Cylinder in a Fluid Stream (Aeolian Tones), Journal of the Acoustical Society of America, 29:30, 1957.

Forrester, J. H. and Young, D. F. Flow Through a Converging-Diverging Tube and Its Implications in Occlusive Vascular Disease - Part I and II, Journal of Biomechanics, Vol. 3, pp. 297-306; 307-316, 1970.

Fry, D. L. Certain Histological and Chemical Responses of the Vascular Interface to Acutely Induced Mechanical Stress in the Aorta of Dog, Circulation Research, 24:93-108, 1969.

Gosling, R. G. and King, D. H. Continuous Wave Ultrasound as an Alternative and Complement to X-Rays in Vascular Examination, in cardiovascular Applications of Ultrasound, R. S. Reneman (Ed.), North-Holland Publishing Co., New York, 1974.

Gow, B. S. and Taylor, M. G. Measurement of Viscoelastic Properties of Arteries in the Living Dog, Circulation Research, 23:111-122, 1968.

Halsted, W. S. An Experimental Study of Circumscribed Dilatations of an Artery Immediately Distal to a Partially Occluding Band, and Its Bearing on the Dilatation of the Subclavian Artery Observed in Certain Cases of Cervical Rib, The Journal of Experimental Medicine, 24:271-289, 1916.

Halsted, W. S. Cylindrical Dilatation of the Common Carotid Artery Following Partial Occlusion of the Innominate and Ligation of the Subclavian, Surgery, Gynecology and Obstetrics, 27:547-554, 1918.

Hardin, C. A. Vertebral Artery Insufficiency Produced by Cervical Osteoarthritic Spurs, Arch. Surg., 90:629, 1965.

Harvey, W. Exercitatio Anatomica de Motu Cordis et Sanguinis in Animalibus (Trans. Franklin, K. J., 1957), Wm. Blackwell and Sons, Ltd., Oxford, 1628.

Harvey, E. N. Bubble Formation in Liquids, Medical Physics, Vol. 2, edited by O. Glasser, Chicago, Year Book Publication, 137-150, 1950.

Holman, E. The Obscure Physiology of Poststenotic Dilatation: Its Relation to the Development of Aneurysms, Journal of Thoracic and Cardiovascular Surgery, 28:109-133, 1954a.

Holman, E. On the Circumscribed Dilatation of an Artery Immediately Distal to a Partially Occluding Band. Poststenotic Dilatation, Surgery, 36:3-24, 1954b.

Holman, E. The Development of Arterial Aneurysms, Surgery, Gynecology and Obstetrics, 100:599-611, 1955.

Holman, E. and Peniston, W. Hydrodynamic Factors in the Production of Aneurysms, American Journal of Surgery, 90:200-209, 1955.

Hugh, A. E. and Fox, J. A. Circulatory Cavitation, "Bubbles in the Blood," The Lancet, October 1963, pp. 717-718.

Hutchison, K. J. Effect of Variation of Transmural Pressure on the Frequency Response of Isolated Segments of Canine Carotid Arteries, Circulation Research, 35:742-751, 1974.

Kirkeeide, R. L., Young, D. F. and Cholvin, N. R. Wall Vibration Induced by Flow through Simulated Stenoses in Models and Arteries, ERI Project 1180-S, Engineering Research Institute, Iowa State University, September 1975.

Kline, J. L., Gimenez, J. L. and Maloney, R. J. Post-Stenotic Vascular Dilatation; Confirmation of an Old Hypothesis by a New Method, Journal of Thoracic and Cardiovascular Surgery, 44:738-748, 1962.

Kozman, T. A. and Forrester, J. H. Flow in a Constricted Tube at a Low Reynolds Number, 9th Annual Rocky Mountain Bioengineering Symposium and 10th Annual International ISA Biomedical Sciences Instrumentation Symposium, May 1-3, 1972, University of Nebraska Medical Center, Omaha, Nebraska.

Lambert, R. and Henry, S. Characteristics of a Biotronix BLT-610 Electromagnetic Flowmeter, Unpublished Biofluids Mechanics Report, The University of Tennessee/Knoxville, March 1975.

Laubry, C. M. A Propos des Dilatations Congenitales de 1'Atere Pulmonaire, Arch. Malcoeur, 36:62, 1943.

Lawton, R. W. The Thermoelastic Behavior of Isolated Aortic Strips of the Dog, Circulation Research, 2:344-353, 1954.

Lee, J. S. and Fung, Y. C. Flow in Locally Constricted Tubes at Low Reynolds Numbers, Journal of Applied Mechanics, 37:9-15, 1970.

Love, A. E. A Treatise on the Mathematical Theory of Elasticity, Dover Publications, Inc., New York, 1927.

Maltry, J. M. and Forrester, J. H. A Method for the Construction of Rubber Tubes with Various Geometries to Simulate Blood Vessels, Proceedings of the 29th ACEMB, September 20-24, 1975, New Orleans, Louisiana, p. 409.

Matunobu, Y. and Arakawa, M. Model Experiments on the Poststenotic Dilatation in Blood Vessels, Biorheology, 2:457-464, 1974.

McDonald, D. A. Blood Flow in Arteries, Monograph of the Physiology Society of London, edited by Edward Arnold, Williams and Wilkin, Baltimore, 1960.

Merrill, E. W., Cokelet, G. C., Britten, A. and Wells, R. E. Non-Newtonian Rheology of Human Blood - Effect of Fibrinogen Deduced by "Subtraction," Circulation Research, 13:48-55, 1963.

Morton, M. Rubber Technology, Van Nostrand Reinhold Co., New York, 1973.

Patel, D. J. The Rheology of Large Blood Vessels, in Cardiovascular Fluid Dynamics, D. H. Bergel (Ed.), Vol. 2, Academic Press, New York, 1972.

Peterson, L. H., Roderick, E. J. and Parnell, J. Mechanical Properties of Arteries in Vivo, Circulation Research, 8:622-639, 1960.

Popov, E. P. Introduction to Mechanics of Solids, Prentice Hall, Inc., New Jersey, 1968.

Roach, M. R. and Burton, A. C. The Reason for the Shape of the Distensibility Curves of Arteries, Canadian Journal of Biochemical Physiology, 35:681-690, 1957.

Roach, M. R. An Experimental Study of the Production and Time Occurrence of Poststenotic Dilatation in the Femoral and Carotid Arteries of Adult Dogs, Circulation Research, 13:537-551, 1963.

Roach, M. R. Poststenotic Dilatation in Arteries, Cardiovascular Fluid Dynamics, Vol. 2, edited by D. H. Bergel, Academic Press, New York, 1972.

Rodbard, S. Dynamics of Blood Flow in Stenotic Vascular Lesions, American Heart Journal, 72:698-704, 1966.

Rodbard, S., Ikeda, K. and Montes, M. An Analysis of Mechanisms of Post Stenotic Dilatation: Angiology, The Journal of Vascular Diseases, 18:349-367, 1967.

Rodicsek, F., Sanger, P. W., Taylor, F. H., Magistro, R. and Egidio, F. Pathogenesis and Significance of Post-Stenotic Dilatation in Great Vessels, Annals of Surgery, 147:835-844, 1958.

Spain, D. M. Atherosclerosis, Scientific American, pp. 49-56, August 1966.

Streeter, V. L. Fluid Mechanics, Fifth Edition, McGraw-Hill Book Company, New York, 1971.

Timoshenko, S. P. and Goodier, J. N. Theory of Elasticity, McGraw Hill Book Company, New York, 1970.

Van Buchem, F. S. P. Dilatation of the Pulmonary Artery in Pulmonary Stenosis, Circulation, 13:719-724, 1956.

Wieting, D. W. Dynamic Flow Characteristics of Heart Valves, Unpublished Doctoral Dissertation, University of Texas at Austin, May 1969.

Womersley, J. R. Method for the Calculation of Velocity, Rate of Flow and Viscous Drag in Arteries When the Pressure Gradient is Known, Journal of Physiology, 127: 553-563, 1955.

Young, D. F. and Tsai, F. Y. Flow Characteristics in Models of Arterial Stenosis; Parts I and II, Journal of Biomechanics, Vol. 6, pp. 395-409; pp. 547-559, 1973.

# APPENDICES

# APPENDIX A

## METHOD OF MAKING ARTERIAL MODELS

Most of the past work performed with flexible arterial models was limited to using straight extruded tubes which either had been banded by some external means or plugged with a rigid constriction. For the present study, it seemed desirable to make a one-piece model of the same type of material, thus allowing continuity between the stenosis and the tube and homogeneity between material in the constricted portion and the wall of the straight tube.

The initial approach to the problem was to design a two-piece mold in which a silicone rubber or latex could be formed. The biggest problem encountered here was the material. Because latex must be air-cured, any possibility of an enclosed mold was eliminated. Different catalysts, such as aluminum potassium sulfite, were utilized to help promote drying of the latex. Although some success was obtained in this area, the catalyst changed the texture of the finished rubber product. Therefore, it was not usable. The problem with silicone rubber was the lack of similarity between blood vessels and the finished silicone rubber product. The lack of similarity existed mainly in the elasticity of the finished model.

The second type of approach taken to the problem was to utilize wax mandrels (Maltry and Forrester, 1975). The wax selected was a fully refined paraffin with a relatively

high penetration factor of 14 for its low melting point of 61°C. Twenty inch-long tubes were precoated with a natural mold releasant to help promote releasing of the wax once it had hardened. The melted wax was then poured into the tubes. Once the wax had hardened the mandrels were eased out of the metal tubes and then mounted on a lathe with both ends supported. The appropriate geometry was then cut into the wax mandrels by utilizing a specially prepared steel form tool at a speed of approximately 400 rpm. The wax mandrels were then mounted on a slowly revolving motor (3 rpm) with their longitudinal axis horizontal. They were sprayed with the same polyethylene mold releasant which was used on the metal tubes to encourage the release of the wax from the finished rubber product. As the mandrel rotated, it was sprayed with a latex solution which had been diluted (1 part water to 1 part latex) to permit utilization of the standard spray gun at pressures of 35 psi. The latex which was used in this experiment was obtained from Ward's Scientific Products in Rochester, New York. The mandrel was sprayed evenly for one revolution as shown in Figure 37 and then allowed to dry for approximately 3 minutes. Each spray accumulated approximately .005 inch of rubber on the mandrel. This procedure was repeated until the desired wall thickness was obtained. The wall thickness decreased by approximately 70% after drying. After the appropriate wall thickness was obtained, the coated mandrels were allowed to rotate for 24 hours to insure an even wall thickness. They

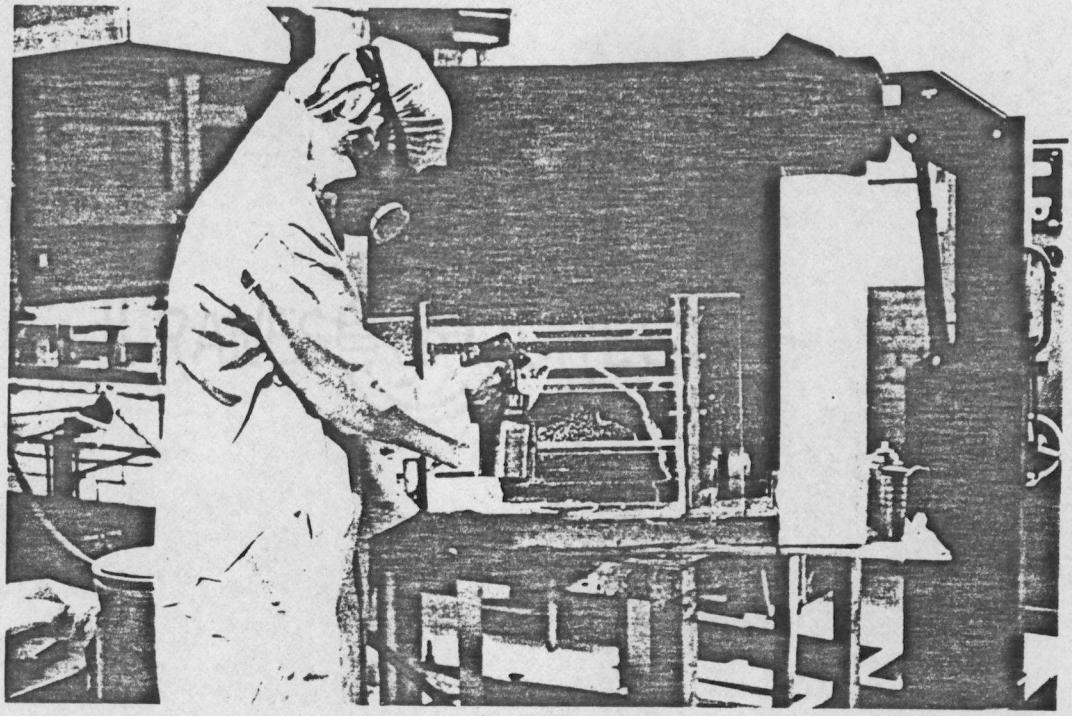

Figure 37. Wax Mandrel Being Sprayed With Latex Solution

were then placed in an air dry oven at 32°C for 48 hours. After the wax had fully cured, the wax core was removed by placing the rubber coated mandrel in 70° water for 3 minutes, thus melting the wax and leaving the rubber model with a fixed inside diameter and wall thickness. The first generation model using the wax method had a variation in wall thickness of ±6%. Although this method shows a fair amount of reliability when working with large 1 inch mandrels, problems were encountered when considering smaller diameter tubes. In the smaller diameter tubes, the latex around the wax served as an insulator, keeping the wax from melting out as rapidly as it had in the 1 inch mandrels. Attempts to drill a hole through the longitudinal axis of the wax mandrels to facilitate removal of the wax failed.

It was thus necessary to raise the temperature of the water to get the wax out, and a point was reached which caused severe damage to the latex material. Therefore, an alternative approach to the problem was felt to be necessary.

The third approach can be classified as the "slip casting method." In this procedure, it was first necessary to construct a solid Plexiglas model as shown in Figure 38. A steel rod was placed in the middle of the Plexiglas rod to provide reinforcement at the constriction. In the earlier models, there was a problem with breakage occurring at this point because of the weakness resulting from the rotation on the lathe. After the stenosis had been cut, the Plexiglas was polished using a standard polishing compound.

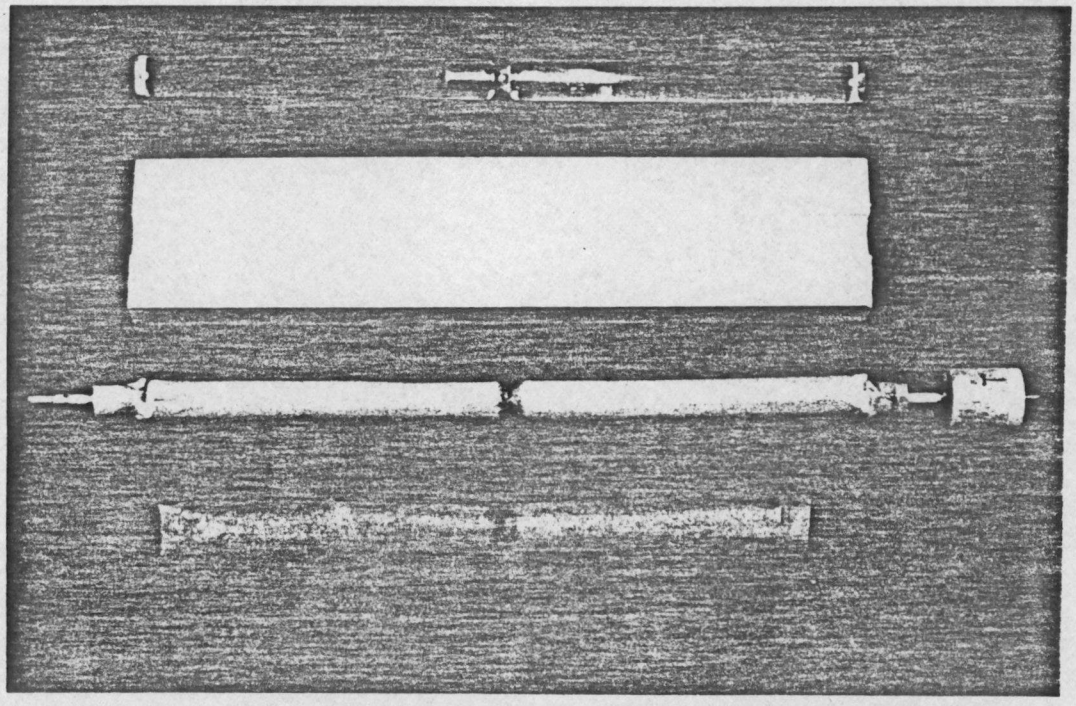

Figure 38. From Top to Bottom: Plexiglas Model, Plaster Mold, Mandrel Shell, and Resulting Latex Model

The next step was to make a plaster mold out of pottery plaster, because of its hard texture. The plaster was poured into a Plexiglas tray. The Plexiglas stenosis was then sprayed with a silicone mold releasant and placed into the tray containing the plaster. This was allowed to sit overnight, whereupon the Plexiglas rod was removed from the plaster. The plaster was then mounted in a mill end and cut down to its centerline. Measuring was done periodically with a dowel gauge to insure that the centerline of the mold had been reached. Once the mold had been finished, the Plexiglas rod was placed into one-half of the finished mold and plaster was poured on top of it. This was allowed to sit overnight. The finished product was a two-part exterior plaster mold of a stenosis.

The next step was to plug one end of the mold and pour slip cast into it. Slip cast is the standard type of casting which is used in many ceramic and hobby stores. The slip cast was allowed to remain in the mold for 10 minutes and then the excess was poured out. Slip cast dries from the outside in, thus leaving a shell on the inside of the mold. In the first experiments, cracking of the shell at the center of constriction occurred; therefore, we started inserting metal rods which had wooden dowels on either end inside the mold while the slip casting was drying. This provided support when removing the shell from the mold. The slip cast was allowed to dry for approximately two hours, whereupon it was removed from the exterior mold. After

sitting overnight, the mandrel shells (now called greenware) were sanded with fine sandpaper, whereupon the wooden ends were glued into place to provide additional support during the spraying procedure.

The greenware was then sprayed with approximately 8 coats of a plastic coating to provide water-proofing. They were then mounted on a 3 rpm motor and allowed to rotate, where they were sprayed with silicone mold releasant to prevent the plastic coating from adhering to the latex. Then over the silicone releasant, a Teflon spray was applied which permitted good attachment of the latex to the mandrel. As the mandrels rotated, they were sprayed with a latex solution -- the same as used in the wax procedure except not diluted. The desired thickness was obtained, and then the mandrels were removed from the motor. The drying time was experimented with and we found more success with allowing the mandrels to be placed in an air drying oven at 95°C for 1-2/3 hours. At the end of this period, the greenware was removed by breaking it out, thus leaving the finished rubber tube as shown in Figure 38.

Once the greenware was removed, the tube was washed out with lukewarm water to insure that all the pieces had been dissolved away. The tubes were then set aside for further experiments. The wall thickness was initially obtained by utilizing calipers; after the experiments were over, they were re-checked by cutting the vessel in half and comparing the values obtained with the initial ones.

Unlike the wax method, it was not necessary to expose the rubber to high temperatures when removing the mandrel. However, a disadvantage with this procedure is the shrinkage of the greenware as it dries, which may approximate 10-15%. Also, it was found impossible to make models smaller than one-fourth of an inch in diameter with this method.

To make the smaller models it was necessary to substitute a 3/16 inch metal rod for the greenware mandrel in the above process. The rod was coated with a thin layer of Vaseline followed by a Teflon spray. Next the rod was sprayed with the latex solution and allowed to dry in the same manner as above. Once the latex was cured it was removed by very carefully sliding it off the rod. A specially machined Plexiglas stenosis was inserted into the vessel and secured by a suture around the outside of the vessel.

# APPENDIX B

## CAM PROFILES

Cam profiles were obtained for the small mock circulatory system by a trial and error method. Problems resulting from wave reflection and capacitance of the elastic system required the construction of 18 different cams. Cams one, two and three were constructed out of brass, while the remaining fifteen were made from Plexiglas. Figures 39 and 40 show the basic shape (reduced by 59%) of the most frequently used cams. All cams rotated clockwise around the center.

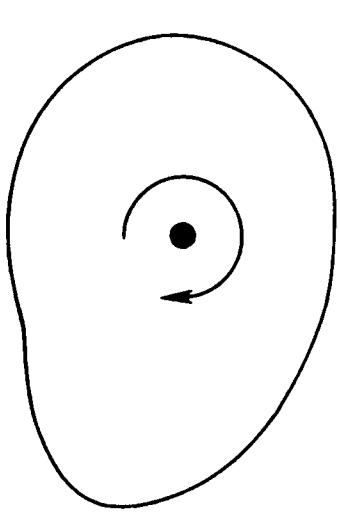

Cam #1

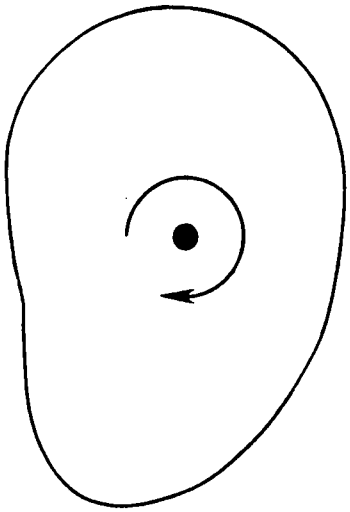

Cam #2

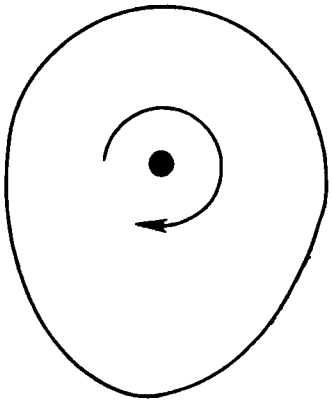

Cam #5

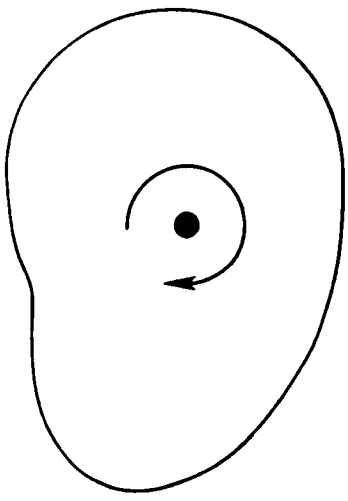

Cam #11

Figure 39. Cam Profiles for Cam Numbers 1, 2, 5 and 11

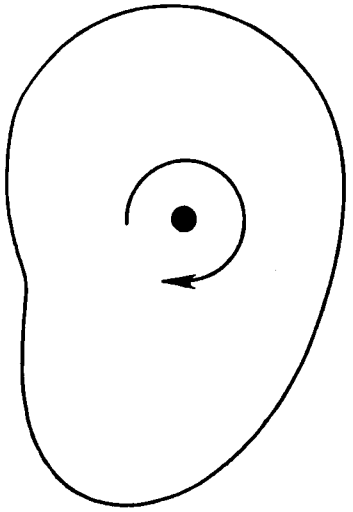

Cam #7

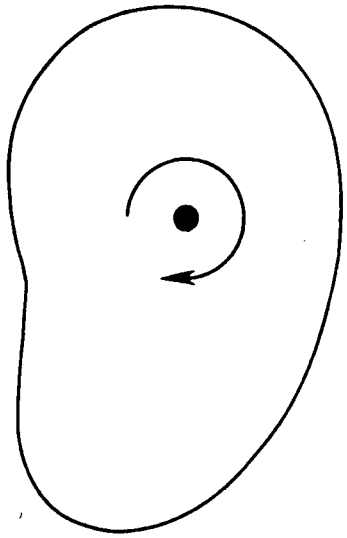

Cam #12

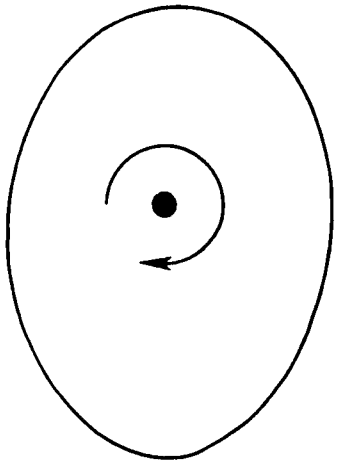

Cam #16

Figure 40. Cam Profiles for Cam Numbers 7, 12 and 16

# APPENDIX C

## DESIGN OF CATHETER

The pressure profiles for the large arterial models were obtained by utilizing a specially designed pressure catheter, Figure 41. It consisted of a 28 cm long probe (A) made from 0.73 mm outside diameter stainless steel tubing with a single side hole perpendicular to the flow (B) 5 mm from the end, which had been closed off with epoxy. This probe was attached to a 3.0 cm diameter, 42 cm long piece of copper tubing (D). As the flow passed through the copper tube it was possible to slide the stainless steel collar (C) back and forth, thus permitting relocation of the probe inside the arterial model from 0 to 11 cm beyond the end of the copper tubing. This range has been shown in the arterial model (not to scale) located below the catheter, Figure 41. A metric scale located below the collar permitted location of the probe within the model. The external end of the probe (E) was constructed such that a three way stopcock might be attached.

To obtain a theoretical estimate of the degree of distortion in the recorded pressure profiles created by this pressure catheter, calculations were performed according to a method described by McDonald (1960). By considering the bulk modulus of the fluid as well as the total volume of fluid in the catheter system, it was possible to calculate

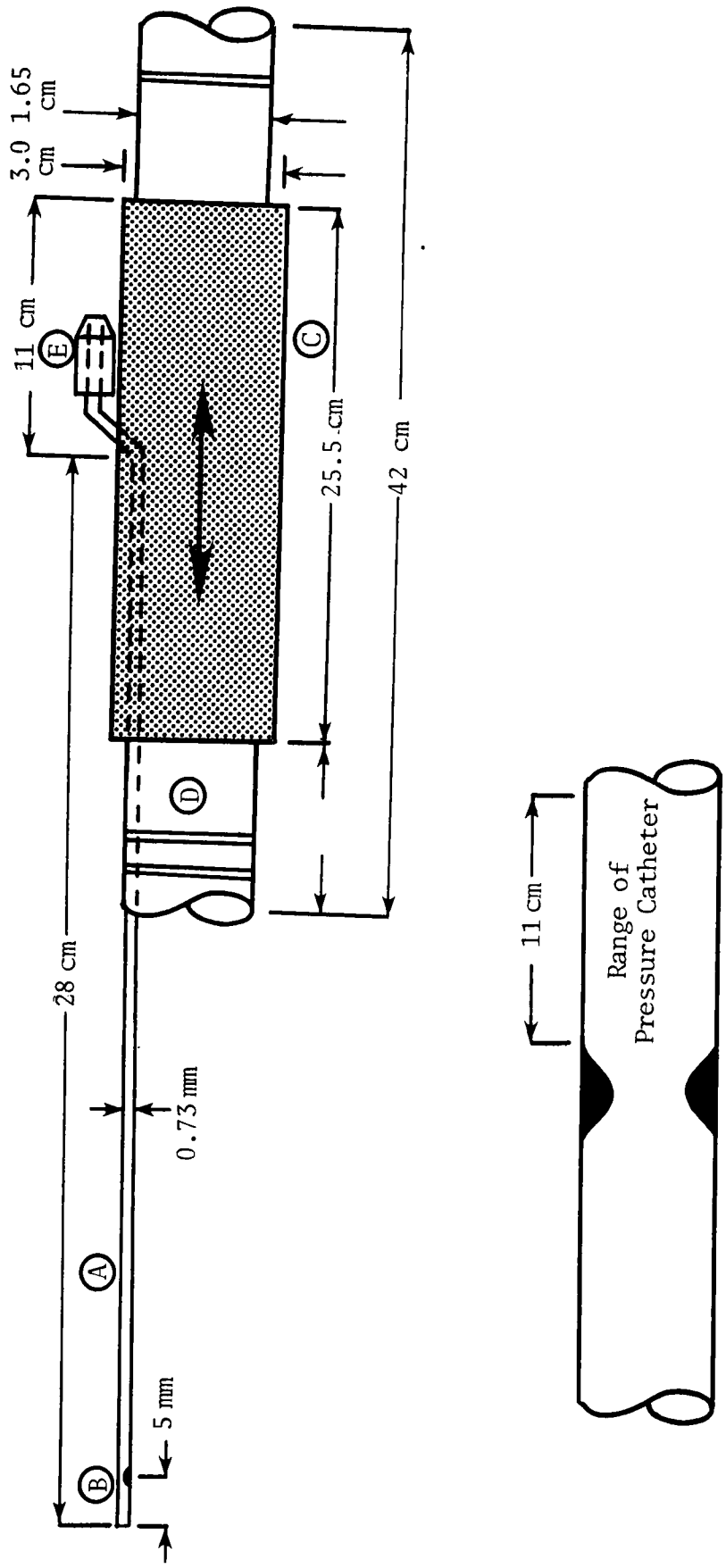


Figure 41. Dimensions of Pressure Catheter for *in vitro* Model Study

the volume elasticity of the system as 95,635 $g/(mm^4 \cdot sec^2)$. The total kinetic mass of the system was determined as 0.31 $g/(mm^4)$ by considering the length and internal radius of the catheter as well as the density of the liquid. By taking the square root of the ratio of volume elasticity to kinetic mass it was possible to determine the natural undamped frequency of the system as 556 rad/sec. To determine the system damping it was first necessary to determine the total resistance the fluid experiences as it attempts to move through the catheter system. By assuming Poiseuille flow this value was calculated as 49 $g/(mm^4 \cdot sec)$. The system damping was defined as one-half the ratio of the Poiseuille resistance to kinetic mass of the system; hence a calculated value of 79 rad/sec was obtained. The results of these calculations reveal that the natural undamped frequency is much greater than the system damping ($556 >> 79$ rad/sec), which indicates that this is an under-damped system.

By further considering the fundamental driving frequency of the mock circulatory system, it was possible to determine the recorded amplitude to be 1.007 times greater than the actual value as well as possess a phase angle of 2.3°. This theoretical analysis is dependent upon the elasticity volume characteristic of the system; consequently any air bubbles trapped in the system will obviously change these results significantly.

# APPENDIX D

## PROGRAMS AND DATA FOR MATERIAL ANALYSIS

```
C                                                                       0001
C                                                                       0002
C     BIOMEDICAL ENGINEERING PROGRAM BY JOHN MALTRY                     0003
C                                                                       0004
C     THIS ROUTINE GIVES CIRCUMFERENTIAL STRESS AND STRAIN AND          0005
C     INCREMENTAL ELASTIC MODULUS FOR A HOMOGENEOUS,ISOTROPIC,CONSTANT  0006
C     LENGTH VESSEL.                                                    0007
C                                                                       0008
C                                                                       0009
C    ***************************************************************  0010
C    * N = NUMBER OF DATA POINTS                                     *  0011
C    * RO = INITIAL OUTSIDE RADIUS   (CM)                            *  0012
C    * RI= INITIAL INSIDE RADIUS    (CM)                             *  0014
C    * THICK = WALL THICKNESS  (CM)                                  *  0015
C    * POISON = POISSON RATIO (DIMENSIONALESS)                       *  0016
C    * PPES = PRESSURE  INSIDE OF VESSEL  (MM OF HG)                 *  0017
C    * RIN = NEW INSIDE RADIUS  (CM)                                 *  0018
C    * ROUT = NEW OUTSIDE RADIUS  (CM)                               *  0019
C    * STRAIN = CIRCUMFERENTIAL STRAIN (CM/CM)                       *  0020
C    * STRESS = CIRCUMFERENTIAL STRESS (DYNES/CM**2)                 *  0021
C    * EIN = INCREMENTAL ELASTIC MODULI                              *  0022
C    * EINCP = INCREMENTAL PRESSURE-STRAIN MODULI                    *  0023
C    * EINCT = INCREMENTAL MODULI BASED UPON THIN-WALLED THEORY      *  0024
C    ***************************************************************  0025
C                                                                       0026
      DIMENSION ROUT(100),RIN(100),PRES(100),EINC(100),EINCP(100),EINCT(0027
     *100),STRESS(100),STRAIN(100),THICK(100),SAMPLE(40)               0028
      DO 700 NTIMES=1,28                                               0029
      READ(5,5) SAMPLE                                                 0030
    5 FORMAT(40A1)                                                     0031
      READ(5,15) RO,RI,POISON,N                                        0032
   15 FORMAT(3F10.5,I5)                                                0033
      WRITE(6,25) SAMPLE                                               0034
                                                                       0035
```

```
   25 FORMAT(1H1,////////,      38X,'CIRCUMFERENTIAL STRESS AND STRAIN'      0036
     *,/,41X,40A1,//)                                                       0037
      DO 100 I=1,N                                                          0038
      READ(5,35) PRES(I),ROUT(I)                                            0039
   35 FORMAT(2F10.5)                                                        0040
  100 CONTINUE                                                              0041
      A = (1.0 -POISON**2)*2.                                               0042
C     IF NO VOLUME CHANGE OCCURS IN THE WALL THEN "B" IS CONSTANT.          0043
      B= (RO**2-RI**2)                                                      0044
C     CONVERSION FACTOR FOR PRESSURE (MM OF HG TO DYNES PER CM**2)          0045
      C=1333.16                                                             0046
      WRITE(6,45)                                                           0047
   45 FORMAT(26X,'PRESSURE',2X,'ROUT', 4X,'RIN',5X,'THICK',2X,'STRAIN',5    0048
     *X,'STRESS',/,25X,'(MM OF HG)',1X,'(CM)',4X,'(CM)', 4X,'(CM)',3X,'(    0049
     *CM/CM)',1X,'(DYNES/CM**2)',//)                                        0050
C                                                                           0051
C     ***************************************************************     0052
C                                                                           0053
C     CIRCUMFERENTIAL STRESS AND STRAIN VALUES ARE CALCULATED BELOW         0054
C     BASED UPON THICK-WALLED THEORY                                        0055
C     ASSUMING THAT THE VOLUME OF THE WALL REMAINS CONSTANT THROUGHOUT      0056
C     EXPANSION THE FOLLOWING RELATION CAN BE USED TO DETERMINE THE         0057
C     INNER RADIUS AT VARYING INTRALUMINAL PRESSURE.                        0058
      DO 150 I=1,N                                                          0059
      RIN(I)=((ROUT(I)**2)-B)**0.5                                          0060
      THICK(I) = ROUT(I) - RIN(I)                                           0061
      STRAIN(I)=(ROUT(I)-ROUT(1))/ROUT(1)                                   0062
      STRESS(I)=(2.0*PRES(I) *C*RIN(I)**2)/B                                0063
      WRITE(6,55)PRES(I),ROUT(I),RIN(I),THICK(I),STRAIN(I),STRESS(I)        0064
   55 FORMAT(27X,F5.1,4X,F5.3,3X,F5.3,3X,F5.3,3X,F5.3,4X,E10.4)             0065
  150 CONTINUE                                                              0066
C                                                                           0067
C     ***************************************************************     0068
C                                                                           0069
C     EQUATION FOR YOUNG'S MODULUS OF AN ISOTROPIC TUBE, WHICH DOES NOT     0070
```

```
C      CHANGE IN LENGTH ON INFLATION, IS GIVEN BY LOVE (1927).                  0071
C      ASSUME POISSON RATIO = 0.5, THIS IS NOT STRICTLY TRUE WHEN LARGE         0072
C      STRAINS ARE CONSIDERED (BERGEL, 1960), BUT GOOD FOR ARTERIAL WALLS       0073
C      WHICH HAVE BEEN EXTENDED ISOVOLUMETRICALLY (LAWTON,1954)                 0074
C      THIS EQUATION ASSUMES ISOTROPY OF THE MATERIAL, THAT IS THAT THE         0075
C      MECHANICAL PROPERTIES ARE IDENTICAL IN ALL DIRECTIONS.                   0076
C      WITH THE ABOVE ASSUMPTIONS THE INCREMETAL MODULUS IS GIVEN BELOW.        0077
C      THIS EQUATION IS TAKEN FROM "THE STATIC ELASTIC PROPERTIES OF THE        0078
C      ARTERIAL WALL",D.H.BERGEL,J.PHYSIOL (1961),156,PP.445-457.               0079
C
C
       N=N-2                                                                    0080
       WRITE(6,65)  SAMPLE                                                      0081
    65 FORMAT(///////      ,40X,'INCREMENTAL ELASTIC MODULUS',/,40X,40A1)       0082
       WRITE(6,75)                                                              0083
    75 FORMAT(//,26X,              'PRESSURE',7X,'EINC',11X,'EINCP', 9X,'       0084
      *EINCT ' ,/,25X,'(MM OF HG)',2X,'(DYNES/CM**2)',2X,'(DYNES/CM**2)',       0085
      *2X,'(DYNES/CM**2)',//)                                                   0086
       DO 300 I = 1,N                                                           0087
       IF((RIN(I+2)-RIN(I)*B).LT.0.000001) GO TO 200                            0088
       GO TO 250                                                                0089
   200 EINC(I)=0.                                                               0090
       GO TO 300                                                                0091
   250 EINC(I)  =C*(PRES(I+2)-PRES(I))*A*ROUT(I+1)*RIN(I+1)**2/((ROUT(I+2       0092
      *)-ROUT(I))*B)                                                            0093
   300 CONTINUE                                                                 0094
C                                                                               0095
C      ************************************************************             0096
C                                                                               0097
C      THE INCREMENTAL PRESSURE-STRAIN MODULI (EINCP) IS CALCULATED BELOW       0098
C      THIS EQUATION WILL LOOK AT THREE SUCCESSIVE MEASUREMENTS OF STRAIN        0099
       DO 450 I=1,N                                                             0100
```

```
      IF((RIN(I+2)-RIN(I)*B).LT.0.000001) GO TO 350                     0101
      GO TO 400                                                         0102
  350 EINCP(I)=0.                                                       0103
      GO TO 450                                                         0104
  400 EINCP(I)=(PRES(I+2)-PRES(I))*ROUT(I+1)*C/(ROUT(I+2)-ROUT(I))      0105
  450 CONTINUE                                                          0106
C                                                                       0107
C     ****************************************************************  0108
C                                                                       0109
C     THE INCREMENTAL YOUNG'S MODULUS  (EINCT) BASED UPON THIN-WALLED   0110
C     THEORY IS CALCULATED BELOW                                        0111
      DO 600 I=1,N                                                      0112
      IF((RIN(I+2)-RIN(I)*B).LT.0.000001) GO TO 500                     0113
      GO TO 550                                                         0114
  500 EINCT(I)=0.                                                       0115
      GO TO 600                                                         0116
  550 EINCT(I) =C*(PRES(I+2)-PRES(I))*(ROUT(I+1)**2)*6.75/((ROUT(I+2)-RO 0117
     *UT(I))*ROUT(5))                                                   0118
  600 CONTINUE                                                          0119
      DO 650 I=1,N                                                      0120
      WRITE(6,85) PRES(I+1),EINC(I),EINCP(I),EINCT(I)                   0121
   85 FORMAT(27X,F5.1,7X,E9.3,6X,E9.3,6X,E9.3)                          0122
  650 CONTINUE                                                          0123
  700 CONTINUE                                                          0124
      STOP                                                              0125
      END
```

CIRCUMFERENTIAL STRESS AND STRAIN
LATEX MODEL T-13

| PRESSURE (MM OF HG) | ROUT (CM) | RIN (CM) | THICK (CM) | STRAIN (CM/CM) | STRESS (DYNES/CM**2) |
|---|---|---|---|---|---|
| 0.0 | 0.311 | 0.265 | 0.046 | 0.0 | 0.0 |
| 25.0 | 0.315 | 0.270 | 0.045 | 0.014 | 0.1829E 06 |
| 57.5 | 0.317 | 0.272 | 0.045 | 0.020 | 0.4279E 06 |
| 75.0 | 0.323 | 0.279 | 0.044 | 0.040 | 0.5880E 06 |
| 92.5 | 0.332 | 0.289 | 0.043 | 0.067 | 0.7757E 06 |
| 120.0 | 0.340 | 0.299 | 0.042 | 0.093 | 0.1074E 07 |
| 145.0 | 0.352 | 0.313 | 0.040 | 0.133 | 0.1422E 07 |
| 180.0 | 0.365 | 0.326 | 0.038 | 0.173 | 0.1926E 07 |
| 197.5 | 0.386 | 0.349 | 0.036 | 0.239 | 0.2422E 07 |

INCREMENTAL ELASTIC MODULUS
LATEX MODEL T-13

| PRESSURE (MM OF HG) | EINC (DYNES/CM**2) | EINCP (DYNES/CM**2) | EINCT (DYNES/CM**2) |
|---|---|---|---|
| 25.0 | 0.160E 08 | 0.390E 07 | 0.250E 08 |
| 57.5 | 0.108E 08 | 0.258E 07 | 0.166E 08 |
| 75.0 | 0.459E 07 | 0.104E 07 | 0.685E 07 |
| 92.5 | 0.566E 07 | 0.120E 07 | 0.809E 07 |
| 120.0 | 0.579E 07 | 0.115E 07 | 0.796E 07 |
| 145.0 | 0.627E 07 | 0.114E 07 | 0.815E 07 |
| 180.0 | 0.465E 07 | 0.772E 06 | 0.573E 07 |

CIRCUMFERENTIAL STRESS AND STRAIN
LATEX MODEL T-15

| PRESSURE (MM OF HG) | ROUT (CM) | RIN (CM) | THICK (CM) | STRAIN (CM/CM) | STRESS (DYNES/CM**2) |
|---|---|---|---|---|---|
| 0.0 | 0.286 | 0.238 | 0.048 | 0.0 | 0.0 |
| 20.0 | 0.292 | 0.245 | 0.047 | 0.021 | 0.1274E 06 |
| 40.0 | 0.299 | 0.253 | 0.046 | 0.045 | 0.2724E 06 |
| 60.0 | 0.303 | 0.258 | 0.045 | 0.059 | 0.4240E 06 |
| 80.0 | 0.311 | 0.268 | 0.043 | 0.087 | 0.6070E 06 |
| 100.0 | 0.318 | 0.276 | 0.042 | 0.112 | 0.8054E 06 |
| 120.0 | 0.326 | 0.285 | 0.041 | 0.140 | 0.1032E 07 |
| 140.0 | 0.340 | 0.301 | 0.039 | 0.189 | 0.1342E 07 |
| 160.0 | 0.354 | 0.316 | 0.038 | 0.238 | 0.1699E 07 |

INCREMENTAL ELASTIC MODULUS
LATEX MODEL T-15

| PRESSURE (MM OF HG) | EINC (DYNES/CM**2) | EINCP (DYNES/CM**2) | EINCT (DYNES/CM**2) |
|---|---|---|---|
| 20.0 | 0.429E 07 | 0.120E 07 | 0.759E 07 |
| 40.0 | 0.555E 07 | 0.145E 07 | 0.941E 07 |
| 60.0 | 0.535E 07 | 0.135E 07 | 0.885E 07 |
| 80.0 | 0.472E 07 | 0.111E 07 | 0.746E 07 |
| 100.0 | 0.512E 07 | 0.113E 07 | 0.780E 07 |
| 120.0 | 0.382E 07 | 0.790E 06 | 0.559E 07 |
| 140.0 | 0.349E 07 | 0.648E 06 | 0.478E 07 |

CIRCUMFERENTIAL STRESS AND STRAIN
LATEX MODEL T-17

| PRESSURE (MM OF HG) | ROUT (CM) | RIN (CM) | THICK (CM) | STRAIN (CM/CM) | STRESS (DYNES/CM**2) |
|---|---|---|---|---|---|
| 0.0 | 0.298 | 0.239 | 0.059 | 0.0 | 0.0 |
| 20.0 | 0.300 | 0.241 | 0.059 | 0.007 | 0.9815E 05 |
| 40.0 | 0.304 | 0.246 | 0.058 | 0.020 | 0.2044E 06 |
| 60.0 | 0.309 | 0.253 | 0.056 | 0.037 | 0.3221E 06 |
| 80.0 | 0.315 | 0.260 | 0.055 | 0.057 | 0.4547E 06 |
| 100.0 | 0.322 | 0.268 | 0.054 | 0.081 | 0.6059E 06 |
| 120.0 | 0.328 | 0.276 | 0.052 | 0.101 | 0.7660E 06 |
| 140.0 | 0.335 | 0.284 | 0.051 | 0.124 | 0.9485E 06 |
| 160.0 | 0.342 | 0.292 | 0.050 | 0.148 | 0.1149E 07 |

INCREMENTAL ELASTIC MODULUS
LATEX MODEL T-17

| PRESSURE (MM OF HG) | SINC (DYNES/CM**2) | EINCP (DYNES/CM**2) | EINCT (DYNES/CM**2) |
|---|---|---|---|
| 20.0 | 0.736E 07 | 0.267E 07 | 0.171E 08 |
| 40.0 | 0.518E 07 | 0.180E 07 | 0.117E 08 |
| 60.0 | 0.452E 07 | 0.150E 07 | 0.992E 07 |
| 80.0 | 0.413E 07 | 0.129E 07 | 0.872E 07 |
| 100.0 | 0.450E 07 | 0.132E 07 | 0.911E 07 |
| 120.0 | 0.483E 07 | 0.135E 07 | 0.946E 07 |
| 140.0 | 0.487E 07 | 0.128E 07 | 0.916E 07 |

CIRCUMFERENTIAL STRESS AND STRAIN
LATEX MODEL T-17 (DISTAL)

**(AFTER EXPERIMENT)**

| PRESSURE (MM OF HG) | ROUT (CM) | RIN (CM) | THICK (CM) | STRAIN (CM/CM) | STRESS (DYNES/CM**2) |
|---|---|---|---|---|---|
| 0.0 | 0.326 | 0.267 | 0.059 | 0.0 | 0.0 |
| 20.0 | 0.335 | 0.278 | 0.057 | 0.028 | 0.1177E 06 |
| 40.0 | 0.342 | 0.286 | 0.056 | 0.049 | 0.2499E 06 |
| 60.0 | 0.353 | 0.299 | 0.054 | 0.083 | 0.4098E 06 |
| 80.0 | 0.363 | 0.311 | 0.052 | 0.113 | 0.5901E 06 |
| 100.0 | 0.382 | 0.333 | 0.049 | 0.172 | 0.8454E 06 |
| 120.0 | 0.413 | 0.368 | 0.045 | 0.267 | 0.1240E 07 |

INCREMENTAL ELASTIC MODULUS
LATEX MODEL T-17 (DISTAL)

**(AFTER EXPERIMENT)**

| PRESSURE (MM OF HG) | EINC (DYNES/CM**2) | EINCP (DYNES/CM**2) | EINCT (DYNES/CM**2) |
|---|---|---|---|
| 20.0 | 0.370E 07 | 0.112E 07 | 0.696E 07 |
| 40.0 | 0.356E 07 | 0.101E 07 | 0.644E 07 |
| 60.0 | 0.344E 07 | 0.896E 06 | 0.588E 07 |
| 80.0 | 0.277E 07 | 0.667E 06 | 0.451E 07 |
| 100.0 | 0.194E 07 | 0.407E 06 | 0.289E 07 |

CIRCUMFERENTIAL STRESS AND STRAIN
LATEX MODEL T-17 (PROXIMAL)
(AFTER EXPERIMENT)

| PRESSURE (MM OF HG) | ROUT (CM) | RIN (CM) | THICK (CM) | STRAIN (CM/CM) | STRESS (DYNES/CM**2) |
|---|---|---|---|---|---|
| 0.0 | 0.326 | 0.267 | 0.059 | 0.0 | 0.0 |
| 20.0 | 0.336 | 0.279 | 0.057 | 0.031 | 0.1187E 06 |
| 40.0 | 0.344 | 0.289 | 0.055 | 0.055 | 0.2541E 06 |
| 60.0 | 0.357 | 0.304 | 0.053 | 0.095 | 0.4228E 06 |
| 80.0 | 0.370 | 0.319 | 0.051 | 0.135 | 0.6213E 06 |
| 100.0 | 0.396 | 0.349 | 0.047 | 0.215 | 0.9284E 06 |
| 120.0 | 0.421 | 0.377 | 0.044 | 0.291 | 0.1301E 07 |

INCREMENTAL ELASTIC MODULUS
LATEX MODEL T-17 (PROXIMAL)
(AFTER EXPERIMENT)

| PRESSURE (MM OF HG) | EINC (DYNES/CM**2) | EINCR (DYNES/CM**2) | EINCT (DYNES/CM**2) |
|---|---|---|---|
| 20.0 | 0.332E 07 | 0.995E 06 | 0.610E 07 |
| 40.0 | 0.312E 07 | 0.374E 06 | 0.548E 07 |
| 60.0 | 0.290E 07 | 0.732E 06 | 0.477E 07 |
| 80.0 | 0.221E 07 | 0.506E 06 | 0.341E 07 |
| 100.0 | 0.216E 07 | 0.414E 06 | 0.299E 07 |

CIRCUMFERENTIAL STRESS AND STRAIN
LATEX MODEL T-18

| PRESSURE (MM OF HG) | ROUT (CM) | RIN (CM) | THICK (CM) | STRAIN (CM/CM) | STRESS (DYNES/CM**2) |
|---|---|---|---|---|---|
| 0.0 | 0.300 | 0.238 | 0.062 | 0.0 | 0.0 |
| 20.0 | 0.306 | 0.246 | 0.060 | 0.020 | 0.9637E 05 |
| 40.0 | 0.309 | 0.249 | 0.060 | 0.030 | 0.1986E 06 |
| 60.0 | 0.313 | 0.254 | 0.059 | 0.043 | 0.3099E 06 |
| 80.0 | 0.318 | 0.260 | 0.058 | 0.060 | 0.4334E 06 |
| 100.0 | 0.322 | 0.265 | 0.057 | 0.073 | 0.5622E 06 |
| 120.0 | 0.329 | 0.274 | 0.055 | 0.097 | 0.7183E 06 |
| 140.0 | 0.333 | 0.278 | 0.055 | 0.110 | 0.8677E 06 |
| 160.0 | 0.337 | 0.283 | 0.054 | 0.123 | 0.1026E 07 |
| 180.0 | 0.342 | 0.289 | 0.053 | 0.140 | 0.1203E 07 |

INCREMENTAL ELASTIC MODULUS
LATEX MODEL T-18

| PRESSURE (MM OF HG) | EINC (DYNES/CM**2) | EINCP (DYNES/CM**2) | EINCT (DYNES/CM**2) |
|---|---|---|---|
| 20.0 | 0.491E 07 | 0.181E 07 | 0.118E 08 |
| 40.0 | 0.658E 07 | 0.235E 07 | 0.154E 08 |
| 60.0 | 0.539E 07 | 0.185E 07 | 0.123E 08 |
| 80.0 | 0.574E 07 | 0.188E 07 | 0.127E 08 |
| 100.0 | 0.494E 07 | 0.156E 07 | 0.107E 08 |
| 120.0 | 0.537E 07 | 0.159E 07 | 0.111E 08 |
| 140.0 | 0.774E 07 | 0.222E 07 | 0.157E 08 |
| 160.0 | 0.720E 07 | 0.200E 07 | 0.143E 08 |

CIRCUMFERENTIAL STRESS AND STRAIN
LATEX MODEL T-19

| PRESSURE (MM OF HG) | ROUT (CM) | RIN (CM) | THICK (CM) | STRAIN (CM/CM) | STRESS (DYNES/CM**2) |
|---|---|---|---|---|---|
| 0.0 | 0.300 | 0.238 | 0.062 | 0.0 | 0.0 |
| 20.0 | 0.304 | 0.243 | 0.061 | 0.013 | 0.9442E 05 |
| 40.0 | 0.308 | 0.248 | 0.060 | 0.027 | 0.1967E 06 |
| 60.0 | 0.313 | 0.254 | 0.059 | 0.043 | 0.3099E 06 |
| 80.0 | 0.319 | 0.262 | 0.057 | 0.063 | 0.4374E 06 |
| 100.0 | 0.325 | 0.269 | 0.056 | 0.083 | 0.5777E 06 |
| 120.0 | 0.329 | 0.274 | 0.055 | 0.097 | 0.7183E 06 |
| 140.0 | 0.331 | 0.276 | 0.055 | 0.103 | 0.8528E 06 |
| 160.0 | 0.336 | 0.282 | 0.054 | 0.120 | 0.1017E 07 |

INCREMENTAL ELASTIC MODULUS
LATEX MODEL T-19

| PRESSURE (MM OF HG) | EINC (DYNES/CM**2) | EINCP (DYNES/CM**2) | EINCT (DYNES/CM**2) |
|---|---|---|---|
| 20.0 | 0.538E 07 | 0.203E 07 | 0.130E 08 |
| 40.0 | 0.505E 07 | 0.182E 07 | 0.119E 08 |
| 60.0 | 0.441E 07 | 0.152E 07 | 0.100E 08 |
| 80.0 | 0.436E 07 | 0.142E 07 | 0.957E 07 |
| 100.0 | 0.563E 07 | 0.173E 07 | 0.119E 08 |
| 120.0 | 0.985E 07 | 0.292E 07 | 0.204E 08 |
| 140.0 | 0.864E 07 | 0.252E 07 | 0.177E 08 |

CIRCUMFERENTIAL STRESS AND STRAIN
LATEX MODEL T-20

| PRESSURE (MM OF HG) | ROUT (CM) | RIN (CM) | THICK (CM) | STRAIN (CM/CM) | STRESS (DYNES/CM**2) |
|---|---|---|---|---|---|
| 0.0 | 0.301 | 0.238 | 0.063 | 0.0 | 0.0 |
| 20.0 | 0.307 | 0.246 | 0.061 | 0.020 | 0.9468E 05 |
| 40.0 | 0.310 | 0.249 | 0.061 | 0.030 | 0.1952E 06 |
| 60.0 | 0.314 | 0.254 | 0.060 | 0.043 | 0.3045E 06 |
| 80.0 | 0.319 | 0.260 | 0.059 | 0.060 | 0.4259E 06 |
| 100.0 | 0.325 | 0.268 | 0.057 | 0.080 | 0.5627E 06 |
| 120.0 | 0.331 | 0.275 | 0.056 | 0.100 | 0.7124E 06 |
| 140.0 | 0.338 | 0.283 | 0.055 | 0.123 | 0.8826E 06 |
| 160.0 | 0.345 | 0.292 | 0.053 | 0.146 | 0.1062E 07 |

INCREMENTAL ELASTIC MODULUS
LATEX MODEL T-20

| PRESSURE (MM OF HG) | EINC (DYNES/CM**2) | EINCP (DYNES/CM**2) | EINCT (DYNES/CM**2) |
|---|---|---|---|
| 20.0 | 0.484E 07 | 0.182E 07 | 0.118E 08 |
| 40.0 | 0.648E 07 | 0.236E 07 | 0.155E 08 |
| 60.0 | 0.531E 07 | 0.186E 07 | 0.124E 08 |
| 80.0 | 0.463E 07 | 0.155E 07 | 0.104E 08 |
| 100.0 | 0.457E 07 | 0.144E 07 | 0.993E 07 |
| 120.0 | 0.453E 07 | 0.136E 07 | 0.951E 07 |
| 140.0 | 0.457E 07 | 0.129E 07 | 0.921E 07 |

CIRCUMFERENTIAL STRESS AND STRAIN
LATEX MODEL T-21

| PRESSURE (MM OF HG) | ROUT (CM) | RIN (CM) | THICK (CM) | STRAIN (CM/CM) | STRESS (DYNES/CM**2) |
|---|---|---|---|---|---|
| 0.0 | 0.296 | 0.239 | 0.057 | 0.0 | 0.0 |
| 20.0 | 0.298 | 0.241 | 0.057 | 0.007 | 0.1029E 06 |
| 40.0 | 0.302 | 0.246 | 0.056 | 0.020 | 0.2123E 06 |
| 60.0 | 0.306 | 0.251 | 0.055 | 0.034 | 0.3312E 06 |
| 80.0 | 0.310 | 0.256 | 0.054 | 0.047 | 0.4589E 06 |
| 100.0 | 0.318 | 0.266 | 0.052 | 0.074 | 0.6175E 06 |
| 120.0 | 0.326 | 0.275 | 0.051 | 0.101 | 0.7951E 06 |
| 140.0 | 0.334 | 0.285 | 0.049 | 0.128 | 0.9923E 06 |
| 160.0 | 0.343 | 0.295 | 0.048 | 0.159 | 0.1219E 07 |

INCREMENTAL ELASTIC MODULUS
LATEX MODEL T-21

| PRESSURE (MM OF HG) | EINC (DYNES/CM**2) | EINCP (DYNES/CM**2) | EINCT (DYNES/CM**2) |
|---|---|---|---|
| 20.0 | 0.760E 07 | 0.265E 07 | 0.172E 08 |
| 40.0 | 0.601E 07 | 0.201E 07 | 0.132E 08 |
| 60.0 | 0.634E 07 | 0.204E 07 | 0.136E 08 |
| 80.0 | 0.445E 07 | 0.138E 07 | 0.930E 07 |
| 100.0 | 0.368E 07 | 0.106E 07 | 0.734E 07 |
| 120.0 | 0.405E 07 | 0.109E 07 | 0.771E 07 |
| 140.0 | 0.418E 07 | 0.105E 07 | 0.762E 07 |

CIRCUMFERENTIAL STRESS AND STRAIN
LATEX MODEL T-28

| PRESSURE (MM OF HG) | ROUT (CM) | RIN (CM) | THICK (CM) | STRAIN (CM/CM) | STRESS (DYNES/CM**2) |
|---|---|---|---|---|---|
| 0.0 | 0.301 | 0.238 | 0.063 | 0.0 | 0.0 |
| 20.0 | 0.305 | 0.243 | 0.062 | 0.013 | 0.9276E 05 |
| 40.0 | 0.309 | 0.248 | 0.061 | 0.027 | 0.1932E 06 |
| 60.0 | 0.315 | 0.255 | 0.060 | 0.047 | 0.3075E 06 |
| 80.0 | 0.319 | 0.260 | 0.059 | 0.060 | 0.4259E 06 |
| 100.0 | 0.327 | 0.270 | 0.057 | 0.086 | 0.5730E 06 |
| 120.0 | 0.330 | 0.274 | 0.056 | 0.096 | 0.7061E 06 |
| 140.0 | 0.332 | 0.276 | 0.056 | 0.103 | 0.8384E 06 |
| 160.0 | 0.335 | 0.280 | 0.055 | 0.113 | 0.9833E 06 |

INCREMENTAL ELASTIC MODULUS
LATEX MODEL T-28

| PRESSURE (MM OF HG) | EINC (DYNES/CM**2) | EINCP (DYNES/CM**2) | EINCT (DYNES/CM**2) |
|---|---|---|---|
| 20.0 | 0.530E 07 | 0.203E 07 | 0.131E 08 |
| 40.0 | 0.448E 07 | 0.165E 07 | 0.108E 08 |
| 60.0 | 0.484E 07 | 0.168E 07 | 0.112E 08 |
| 80.0 | 0.425E 07 | 0.142E 07 | 0.957E 07 |
| 100.0 | 0.511E 07 | 0.159E 07 | 0.110E 08 |
| 120.0 | 0.117E 08 | 0.352E 07 | 0.246E 08 |
| 140.0 | 0.119E 08 | 0.354E 07 | 0.249E 08 |

CIRCUMFERENTIAL STRESS AND STRAIN
LATEX MODEL Z-0

| PRESSURE (MM OF HG) | ROUT (CM) | RIN (CM) | THICK (CM) | STRAIN (CM/CM) | STRESS (DYNES/CM**2) |
|---|---|---|---|---|---|
| 0.0 | 0.940 | 0.851 | 0.089 | 0.0 | 0.0 |
| 20.0 | 0.951 | 0.863 | 0.088 | 0.012 | 0.2492E 06 |
| 40.0 | 0.999 | 0.916 | 0.083 | 0.063 | 0.5611E 06 |
| 60.0 | 1.070 | 0.993 | 0.077 | 0.138 | 0.9891E 06 |
| 80.0 | 1.120 | 1.046 | 0.074 | 0.191 | 0.1465E 07 |
| 100.0 | 1.280 | 1.216 | 0.064 | 0.362 | 0.2474E 07 |

INCREMENTAL ELASTIC MODULUS
LATEX MODEL Z-0

| PRESSURE (MM OF HG) | EINC (DYNES/CM**2) | EINCP (DYNES/CM**2) | EINCT (DYNES/CM**2) |
|---|---|---|---|
| 20.0 | 0.603E 07 | 0.860E 06 | 0.493E 07 |
| 40.0 | 0.353E 07 | 0.448E 06 | 0.270E 07 |
| 60.0 | 0.437E 07 | 0.472E 06 | 0.304E 07 |
| 80.0 | 0.293E 07 | 0.284E 06 | 0.192E 07 |

CIRCUMFERENTIAL STRESS AND STRAIN
LATEX MODEL Z-1

| PRESSURE (MM OF HG) | ROUT (CM) | RIN (CM) | THICK (CM) | STRAIN (CM/CM) | STRESS (DYNES/CM**2) |
|---|---|---|---|---|---|
| 0.0 | 0.971 | 0.844 | 0.127 | 0.0 | 0.0 |
| 20.0 | 0.987 | 0.862 | 0.125 | 0.016 | 0.1720E 06 |
| 40.0 | 1.003 | 0.881 | 0.122 | 0.033 | 0.3588E 06 |
| 60.0 | 1.042 | 0.925 | 0.117 | 0.073 | 0.5936E 06 |
| 80.0 | 1.082 | 0.970 | 0.112 | 0.114 | 0.8701E 06 |
| 100.0 | 1.138 | 1.032 | 0.106 | 0.172 | 0.1231E 07 |
| 120.0 | 1.225 | 1.127 | 0.098 | 0.262 | 0.1763E 07 |

INCREMENTAL ELASTIC MODULUS
LATEX MODEL Z-1

| PRESSURE (MM OF HG) | EINC (DYNES/CM**2) | EINCR (DYNES/CM**2) | EINCT (DYNES/CM**2) |
|---|---|---|---|
| 20.0 | 0.796E 07 | 0.164E 07 | 0.101E 08 |
| 40.0 | 0.491E 07 | 0.972E 06 | 0.608E 07 |
| 60.0 | 0.391E 07 | 0.703E 06 | 0.457E 07 |
| 80.0 | 0.368E 07 | 0.601E 06 | 0.406E 07 |
| 100.0 | 0.294E 07 | 0.424E 06 | 0.301E 07 |

CIRCUMFERENTIAL STRESS AND STRAIN
LATEX MODEL Z-2

| PRESSURE (MM OF HG) | ROUT (CM) | RIN (CM) | THICK (CM) | STRAIN (CM/CM) | STRESS (DYNES/CM**2) |
|---|---|---|---|---|---|
| 0.0 | 0.955 | 0.848 | 0.107 | 0.0 | 0.0 |
| 20.0 | 0.963 | 0.857 | 0.106 | 0.008 | 0.2030E 06 |
| 40.0 | 0.979 | 0.875 | 0.104 | 0.025 | 0.4232E 06 |
| 60.0 | 1.019 | 0.919 | 0.100 | 0.067 | 0.7011E 06 |
| 80.0 | 1.090 | 0.998 | 0.092 | 0.141 | 0.1100E 07 |
| 100.0 | 1.194 | 1.110 | 0.084 | 0.250 | 0.1704E 07 |

INCREMENTAL ELASTIC MODULUS
LATEX MODEL Z-2

| PRESSURE (MM OF HG) | EINC (DYNES/CM**2) | EINCP (DYNES/CM**2) | EINCT (DYNES/CM**2) |
|---|---|---|---|
| 20.0 | 0.122E 08 | 0.214E 07 | 0.128E 08 |
| 40.0 | 0.555E 07 | 0.932E 06 | 0.565E 07 |
| 60.0 | 0.322E 07 | 0.490E 06 | 0.309E 07 |
| 80.0 | 0.257E 07 | 0.332E 06 | 0.224E 07 |

CIRCUMFERENTIAL STRESS AND STRAIN
LATEX MODEL Z-3

| PRESSURE (MM OF HG) | ROUT (CM) | RIN (CM) | THICK (CM) | STRAIN (CM/CM) | STRESS (DYNES/CM**2) |
|---|---|---|---|---|---|
| 0.0 | 0.947 | 0.848 | 0.099 | 0.0 | 0.0 |
| 20.0 | 0.963 | 0.866 | 0.097 | 0.017 | 0.2250E 06 |
| 40.0 | 0.974 | 0.878 | 0.096 | 0.029 | 0.4627E 06 |
| 60.0 | 1.003 | 0.910 | 0.093 | 0.059 | 0.7457E 06 |
| 80.0 | 1.090 | 1.005 | 0.085 | 0.151 | 0.1213E 07 |
| 100.0 | 1.178 | 1.100 | 0.078 | 0.244 | 0.1815E 07 |

INCREMENTAL ELASTIC MODULUS
LATEX MODEL Z-3

| PRESSURE (MM OF HG) | EINC (DYNES/CM**2) | EINCP (DYNES/CM**2) | EINCT (DYNES/CM**2) |
|---|---|---|---|
| 20.0 | 0.1205 08 | 0.190E 07 | 0.113E 08 |
| 40.0 | 0.845E 07 | 0.130E 07 | 0.783E 07 |
| 60.0 | 0.322E 07 | 0.461E 06 | 0.286E 07 |
| 80.0 | 0.283E 07 | 0.332E 06 | 0.224E 07 |

CIRCUMFERENTIAL STRESS AND STRAIN
LATEX MODEL Z-4

| PRESSURE (MM OF HG) | ROUT (CM) | RIN (CM) | THICK (CM) | STRAIN (CM/CM) | STRESS (DYNES/CM**2) |
|---|---|---|---|---|---|
| 0.0 | 0.945 | 0.845 | 0.100 | 0.0 | 0.0 |
| 20.0 | 0.966 | 0.868 | 0.098 | 0.022 | 0.2247E 06 |
| 40.0 | 0.980 | 0.884 | 0.096 | 0.037 | 0.4656E 06 |
| 60.0 | 1.000 | 0.906 | 0.094 | 0.058 | 0.7338E 06 |
| 80.0 | 1.100 | 1.015 | 0.085 | 0.164 | 0.1229E 07 |
| 100.0 | 1.180 | 1.102 | 0.078 | 0.249 | 0.1807E 07 |

INCREMENTAL ELASTIC MODULUS
LATEX MODEL Z-4

| PRESSURE (MM OF HG) | EINC (DYNES/CM**2) | EINCR (DYNES/CM**2) | EINCT (DYNES/CM**2) |
|---|---|---|---|
| 20.0 | 0.930E 07 | 0.147E 07 | 0.872E 07 |
| 40.0 | 0.101E 08 | 0.154E 07 | 0.924E 07 |
| 60.0 | 0.306E 07 | 0.444E 06 | 0.273E 07 |
| 80.0 | 0.282E 07 | 0.326E 06 | 0.220E 07 |

CIRCUMFERENTIAL STRESS AND STRAIN
LATEX MODEL Z-7

| PRESSURE (MM OF HG) | ROUT (CM) | RIN (CM) | THICK (CM) | STRAIN (CM/CM) | STRESS (DYNES/CM**2) |
|---|---|---|---|---|---|
| 0.0 | 0.970 | 0.850 | 0.120 | 0.0 | 0.0 |
| 20.0 | 0.985 | 0.867 | 0.118 | 0.015 | 0.1836E 06 |
| 40.0 | 0.999 | 0.883 | 0.116 | 0.030 | 0.3807E 06 |
| 60.0 | 1.052 | 0.942 | 0.110 | 0.085 | 0.6507E 06 |
| 80.0 | 1.090 | 0.985 | 0.105 | 0.124 | 0.9471E 06 |
| 100.0 | 1.140 | 1.040 | 0.100 | 0.175 | 0.1320E 07 |

INCREMENTAL ELASTIC MODULUS
LATEX MODEL Z-7

| PRESSURE (MM OF HG) | EINC (DYNES/CM**2) | EINCP (DYNES/CM**2) | EINCT (DYNES/CM**2) |
|---|---|---|---|
| 20.0 | 0.935E 07 | 0.181E 07 | 0.110E 08 |
| 40.0 | 0.426E 07 | 0.795E 06 | 0.492E 07 |
| 60.0 | 0.376E 07 | 0.616E 06 | 0.402E 07 |
| 80.0 | 0.440E 07 | 0.661E 06 | 0.446E 07 |

CIRCUMFERENTIAL STRESS AND STRAIN
LATEX MODEL Z-8

| PRESSURE (MM OF HG) | ROUT (CM) | RIN (CM) | THICK (CM) | STRAIN (CM/CM) | STRESS (DYNES/CM**2) |
|---|---|---|---|---|---|
| 0.0 | 0.960 | 0.833 | 0.127 | 0.0 | 0.0 |
| 20.0 | 0.976 | 0.851 | 0.125 | 0.017 | 0.1698E 06 |
| 40.0 | 0.988 | 0.865 | 0.123 | 0.029 | 0.3505E 06 |
| 60.0 | 1.020 | 0.901 | 0.119 | 0.062 | 0.5710E 06 |
| 80.0 | 1.060 | 0.947 | 0.113 | 0.104 | 0.8392E 06 |
| 100.0 | 1.140 | 1.035 | 0.105 | 0.187 | 0.1255E 07 |
| 120.0 | 1.226 | 1.129 | 0.097 | 0.277 | 0.1792E 07 |

INCREMENTAL ELASTIC MODULUS
LATEX MODEL Z-8

| PRESSURE (MM OF HG) | EINC (DYNES/CM**2) | EINCP (DYNES/CM**2) | EINCT (DYNES/CM**2) |
|---|---|---|---|
| 20.0 | 0.838E 07 | 0.186E 07 | 0.116E 08 |
| 40.0 | 0.590E 07 | 0.120E 07 | 0.753E 07 |
| 60.0 | 0.404E 07 | 0.755E 06 | 0.491E 07 |
| 80.0 | 0.278E 07 | 0.471E 06 | 0.318E 07 |
| 100.0 | 0.259E 07 | 0.366E 06 | 0.266E 07 |

CIRCUMFERENTIAL STRESS AND STRAIN
LATEX MODEL Z-10

| PRESSURE (MM OF HG) | ROUT (CM) | RIN (CM) | THICK (CM) | STRAIN (CM/CM) | STRESS (DYNES/CM**2) |
|---|---|---|---|---|---|
| 0.0 | 0.975 | 0.853 | 0.122 | 0.0 | 0.0 |
| 20.0 | 0.989 | 0.869 | 0.120 | 0.014 | 0.1806E 06 |
| 40.0 | 1.020 | 0.904 | 0.116 | 0.046 | 0.3909E 06 |
| 60.0 | 1.050 | 0.938 | 0.112 | 0.077 | 0.6309E 06 |
| 80.0 | 1.093 | 0.986 | 0.107 | 0.121 | 0.9293E 06 |
| 100.0 | 1.142 | 1.040 | 0.102 | 0.171 | 0.1293E 07 |

INCREMENTAL ELASTIC MODULUS
LATEX MODEL Z-10

| PRESSURE (MM OF HG) | EINC (DYNES/CM**2) | EINCP (DYNES/CM**2) | EINCT (DYNES/CM**2) |
|---|---|---|---|
| 20.0 | 0.595E 07 | 0.117E 07 | 0.716E 07 |
| 40.0 | 0.490E 07 | 0.892E 06 | 0.562E 07 |
| 60.0 | 0.454E 07 | 0.767E 06 | 0.497E 07 |
| 80.0 | 0.414E 07 | 0.634E 06 | 0.428E 07 |

CIRCUMFERENTIAL STRESS AND STRAIN
CAROTID ARTERY (HUTCHISON)

| PRESSURE (MM OF HG) | ROUT (CM) | RIN (CM) | THICK (CM) | STRAIN (CM/CM) | STRESS (DYNES/CM**2) |
|---|---|---|---|---|---|
| 5.0 | 0.163 | 0.125 | 0.038 | 0.0 | 0.1903E 05 |
| 10.0 | 0.169 | 0.133 | 0.036 | 0.037 | 0.4292E 05 |
| 20.0 | 0.179 | 0.145 | 0.034 | 0.093 | 0.1028E 06 |
| 30.0 | 0.189 | 0.157 | 0.032 | 0.160 | 0.1811E 06 |
| 40.0 | 0.213 | 0.186 | 0.027 | 0.307 | 0.3355E 06 |
| 50.0 | 0.220 | 0.194 | 0.026 | 0.350 | 0.4563E 06 |
| 60.0 | 0.227 | 0.201 | 0.026 | 0.393 | 0.5933E 06 |
| 70.0 | 0.231 | 0.206 | 0.025 | 0.417 | 0.7234E 06 |
| 80.0 | 0.235 | 0.210 | 0.025 | 0.442 | 0.8631E 06 |
| 100.0 | 0.240 | 0.216 | 0.024 | 0.472 | 0.1137E 07 |
| 120.0 | 0.244 | 0.220 | 0.024 | 0.497 | 0.1421E 07 |
| 140.0 | 0.246 | 0.223 | 0.023 | 0.509 | 0.1691E 07 |

INCREMENTAL ELASTIC MODULUS
CAROTID ARTERY (HUTCHISON)

| PRESSURE (MM OF HG) | EINC (DYNES/CM**2) | EINCP (DYNES/CM**2) | EINCT (DYNES/CM**2) |
|---|---|---|---|
| 10.0 | 0.510E 06 | 0.211E 06 | 0.113E 07 |
| 20.0 | 0.690E 06 | 0.239E 06 | 0.135E 07 |
| 30.0 | 0.503E 06 | 0.148E 06 | 0.888E 06 |
| 40.0 | 0.864E 06 | 0.183E 06 | 0.124E 07 |
| 50.0 | 0.215E 07 | 0.419E 06 | 0.292E 07 |
| 60.0 | 0.306E 07 | 0.550E 06 | 0.396E 07 |
| 70.0 | 0.448E 07 | 0.770E 06 | 0.564E 07 |
| 80.0 | 0.634E 07 | 0.104E 07 | 0.776E 07 |
| 100.0 | 0.909E 07 | 0.142E 07 | 0.108E 08 |
| 120.0 | 0.144E 08 | 0.217E 07 | 0.168E 08 |

CIRCUMFERENTIAL STRESS AND STRAIN
CAROTID ARTERY (BERGEL)

| PRESSURE (MM OF HG) | ROUT (CM) | RIN (CM) | THICK (CM) | STRAIN (CM/CM) | STRESS (DYNES/CM**2) |
|---|---|---|---|---|---|
| 0.0 | 0.145 | 0.106 | 0.039 | 0.0 | 0.0 |
| 20.0 | 0.165 | 0.132 | 0.033 | 0.138 | 0.9498E 05 |
| 40.0 | 0.184 | 0.155 | 0.029 | 0.269 | 0.2622E 06 |
| 60.0 | 0.197 | 0.170 | 0.027 | 0.359 | 0.4743E 06 |
| 80.0 | 0.202 | 0.176 | 0.026 | 0.393 | 0.6758E 06 |
| 100.0 | 0.208 | 0.183 | 0.025 | 0.434 | 0.9118E 06 |
| 120.0 | 0.210 | 0.185 | 0.025 | 0.448 | 0.1121E 07 |
| 140.0 | 0.213 | 0.189 | 0.024 | 0.469 | 0.1357E 07 |
| 160.0 | 0.216 | 0.192 | 0.024 | 0.490 | 0.1607E 07 |
| 180.0 | 0.219 | 0.195 | 0.024 | 0.510 | 0.1872E 07 |
| 200.0 | 0.221 | 0.198 | 0.023 | 0.524 | 0.2127E 07 |
| 220.0 | 0.224 | 0.201 | 0.023 | 0.545 | 0.2420E 07 |
| 240.0 | 0.227 | 0.204 | 0.023 | 0.566 | 0.2729E 07 |

INCREMENTAL ELASTIC MODULUS
CAROTID ARTERY (BERGEL)

| PRESSURE (MM OF HG) | EINC (DYNES/CM**2) | EINCP (DYNES/CM**2) | EINCT (DYNES/CM**2) |
|---|---|---|---|
| 20.0 | 0.603E 06 | 0.226E 06 | 0.124E 07 |
| 40.0 | 0.113E 07 | 0.307E 06 | 0.189E 07 |
| 60.0 | 0.260E 07 | 0.584E 06 | 0.384E 07 |
| 80.0 | 0.465E 07 | 0.979E 06 | 0.661E 07 |
| 100.0 | 0.711E 07 | 0.139E 07 | 0.964E 07 |
| 120.0 | 0.118E 08 | 0.224E 07 | 0.157E 08 |
| 140.0 | 0.103E 08 | 0.189E 07 | 0.135E 08 |
| 160.0 | 0.108E 08 | 0.192E 07 | 0.139E 08 |
| 180.0 | 0.137E 08 | 0.234E 07 | 0.171E 08 |
| 200.0 | 0.141E 08 | 0.236E 07 | 0.174E 08 |
| 220.0 | 0.123E 08 | 0.199E 07 | 0.149E 08 |

## CIRCUMFERENTIAL STRESS AND STRAIN
## LATEX TUBE FROM R.L.P.

| PRESSURE (MM OF HG) | ROUT (CM) | RIN (CM) | THICK (CM) | STRAIN (CM/CM) | STRESS (DYNES/CM**2) |
|---|---|---|---|---|---|
| 26.0 | 0.548 | 0.496 | 0.052 | 0.0 | 0.3173E 06 |
| 47.0 | 0.551 | 0.500 | 0.051 | 0.005 | 0.5813E 06 |
| 75.0 | 0.554 | 0.503 | 0.051 | 0.011 | 0.9399E 06 |
| 100.0 | 0.567 | 0.517 | 0.050 | 0.035 | 0.1325E 07 |
| 125.0 | 0.573 | 0.524 | 0.049 | 0.046 | 0.1699E 07 |
| 150.0 | 0.581 | 0.533 | 0.048 | 0.060 | 0.2107E 07 |
| 175.0 | 0.589 | 0.541 | 0.048 | 0.075 | 0.2540E 07 |
| 200.0 | 0.596 | 0.549 | 0.047 | 0.088 | 0.2995E 07 |
| 225.0 | 0.604 | 0.558 | 0.046 | 0.102 | 0.3465E 07 |
| 250.0 | 0.609 | 0.563 | 0.046 | 0.111 | 0.3925E 07 |
| 225.0 | 0.605 | 0.559 | 0.046 | 0.104 | 0.3478E 07 |
| 200.0 | 0.598 | 0.551 | 0.047 | 0.091 | 0.3008E 07 |
| 175.0 | 0.592 | 0.545 | 0.047 | 0.080 | 0.2571E 07 |
| 150.0 | 0.585 | 0.537 | 0.048 | 0.068 | 0.2142E 07 |
| 125.0 | 0.576 | 0.527 | 0.049 | 0.051 | 0.1720E 07 |
| 100.0 | 0.568 | 0.518 | 0.050 | 0.036 | 0.1331E 07 |
| 75.0 | 0.561 | 0.511 | 0.050 | 0.024 | 0.9689E 06 |
| 50.0 | 0.554 | 0.503 | 0.051 | 0.011 | 0.6266E 06 |
| 24.0 | 0.549 | 0.498 | 0.051 | 0.002 | 0.3187E 06 |

## INCREMENTAL ELASTIC MODULUS
## LATEX TUBE FROM R.L.P.

| PRESSURE (MM OF HG) | EINC (DYNES/CM**2) | EINCP (DYNES/CM**2) | EINCT (DYNES/CM**2) |
|---|---|---|---|
| 47.0 | 0.417E 08 | 0.600E 07 | 0.389E 08 |
| 75.0 | 0.172E 08 | 0.245E 07 | 0.160E 08 |
| 100.0 | 0.148E 08 | 0.199E 07 | 0.133E 08 |
| 125.0 | 0.209E 08 | 0.273E 07 | 0.184E 08 |
| 150.0 | 0.191E 08 | 0.242E 07 | 0.166E 08 |
| 175.0 | 0.214E 08 | 0.262E 07 | 0.182E 08 |
| 200.0 | 0.222E 08 | 0.265E 07 | 0.186E 08 |
| 225.0 | 0.268E 08 | 0.310E 07 | 0.220E 08 |
| 250.0 | 0.0 | 0.0 | 0.0 |
| 225.0 | 0.319E 08 | 0.367E 07 | 0.261E 08 |
| 200.0 | 0.259E 08 | 0.307E 07 | 0.216E 08 |
| 175.0 | 0.251E 08 | 0.304E 07 | 0.212E 08 |
| 150.0 | 0.196E 08 | 0.244E 07 | 0.168E 08 |
| 125.0 | 0.175E 08 | 0.226E 07 | 0.153E 08 |
| 100.0 | 0.189E 08 | 0.252E 07 | 0.169E 08 |
| 75.0 | 0.194E 08 | 0.267E 07 | 0.177E 08 |
| 50.0 | 0.213E 08 | 0.302E 07 | 0.197E 08 |

# APPENDIX E

## PROGRAM AND DATA FOR FOURIER ANALYSIS OF PRESSURE CURVES

```
C
C       THIS PROGRAM PREFORMS A FOURIER SERIES OF THE PRESSURE WAVE OF
C       THE FEMORAL ARTERY OF A CANINE.  THE DATA POINTS WERE TAKEN FROM A
C       PLOT BY D. A. MCDONALD, ' THE RELATION OF PULSATILE PRESSURE TO
C       FLOW IN ARTERIES. J. PHYSIL.(1955), 127, 533-552.
C
C       THE ARRAY 'F' IS THE SET OF DATA POINTS
C
        DIMENSION F(500),A(500),B(500),YVALUE(500),ERROR(500),FN(500) ,
       *Y(500),NF(500),HZ(500),XVALUE(500),POWER(500),FVALUE(500),YSTORE(5
       *00),IBUF(664)
        M=294
        DO 100 I=1,M
        READ(5,5) NF(I)
  100 CONTINUE
    5 FORMAT(22X,I4)
   15 FORMAT(10X,'F (',I3,') =    ',I5)
        DO 110 I= 1,M
C       THE ARRAY 'F' IS MULTIPLY BY A CONSTANT SUCH THAT THE Y-AXIS IS
C       IN MM OF HG INSTEAD OF INCHES.
  110 F(I)=((FLOAT(NF(I)-NF(1)))*83.77/100.0)+80.00
13      CONTINUE
        DO 160 K=1,26
        AN=0.0
        BN=0.0
        N = K -1
C       THE FOURIES SERIS PREFORMS 25 HARMONICS
        IF(N.EQ.0) GO TO 130
        DO 120 I=1,M
C       ARRAY 'A' AND 'B' ARE THE COEFFICIENTS OF THE FOURIES SERIS.
        AN=((2./M)* F(I) * COS((I-0.5) *N*2.*3.14159/M))+AN
  120 BN= ((2./M)* F(I) *SIN((I-.5)*N*2.*3.14159/M)) + BN
        A(N) = AN
        B(N) = BN
        WRITE(6,25) N,A(N),N,B(N)
```

```
   25 FORMAT(30X,'A (',I3,') = ',F10.4,10X,'B ( ',I3,') = ',F10.4)
      GO TO 150
  130 CONTINUE
      DO 140 I =1,M
  140 AN = F(I) + AN
      AN = AN /M
      AO= AN
      WRITE(6,35) AO
   35 FORMAT(30X,'A0 = ',F10.4)
C     THE POWER IS ACTUAL THE AMPLITUDE OF THE  WAVE SHAPE.
  150 POWER(N)=SQRT(AN**2+BN**2)
      HZ(K)=N
  160 WRITE(6,45) N,POWER(N)
   45 FORMAT(/30X,'FREQUENCY =  ',I3,' HZ',/30X,'POWER =  ',F8.4,//)
C     'K' IS THE MAX. NUMBER OF FREQUENCY WHICH MAY BE EXAMINED.
C
      K=25
C     'W' IS IN RADIANS PER MILLISECONDS.
C
      W= 2.0 *3.14159 /360.0
  170 CONTINUE
      TERROR = 0.0
      DO 220 I = 1,M
      SERIS = 0.0
      II = I-1
C     0.008222 INCHES PER MILLISECONDS ON GRAPH
C     DATA POINTS TAKEN EVERY 0.01 INCHES.
      TIME = (FLOAT(II)*0.01/0.008222)
      XVALUE(I)=TIME
      DO 180 N = 1,K
C     THE YVALUE ARE CAL. FROM THE COEFFICENTS AND COMPAIRED TO THE
C     ACTUAL VALUE.
  180 SERIS = (A(N)*COS(FLOAT(N)*W*TIME))+(B(N)*SIN(FLOAT(N)*W*TIME)) +
     * SERIS
      YVALUE(I)= SERIS + AO
```

```
      LIMIT = 3
      IF(K.NE. LIMIT) GO TO 190
      YSTORE (I) = YVALUE(I)
  190 CONTINUE
      IF (F(I).NE. 0.0) GO TO 200
      ERROR(I) = ABS(YVALUE(I) *100.)
      GO TO 210
  200 ERROR(I)= ABS((YVALUE(I)-F(I))*100.0/F(I))
  210 CONTINUE
  220 TERROR = TERROR + ERROR(I)
      TERROR = TERROR /FLOAT(M)
      WRITE(6,55) K,TERROR
   55 FORMAT(/30X,' THE TOTAL PERCENT ERROR FOR A FREQUENCY OF ',I3,' HZ
     *. IS ', F10.5,/)
      K= K-1
      IF ( K.NE. 0 ) GO TO 170
      DO 230 I=1,M
      FVALUE(I)=F(I)
230   YVALUE(I)=YSTORE(I)
      CALL PLOTS(IBUFF, 664,10.0,'JOHN MALTRY#',8INS#')
      CALL FACTOR(0.5)
      CALL PLOT(0.0,0.5,-3)
      CALL SCALE(XVALUE,4.0,294,1)
      CALL SCALE (FVALUE,4.0,294,1)
      CALL AXIS(0.0,0.0,12HMILLISECONDS,-12,4.0,0.0,XVALUE(295),XVALUE(2
     *96))
      CALL AXIS(.0,.0,8HMM OF HG,8,4.,90.,FVALUE(295),FVALUE(296))
      CALL FLINE(XVALUE,FVALUE,294,1,0,2)
      CALL SYMBOL(0.0,4.5,0.14,36HPRESSURE WAVE FOR THE FEMORAL ARTERY,
     *0.0,36)
      CALL PLOT(0.0,0.0,3)
      CALL SCALE(YVALUE,4.0,294,1)
      CALL FLINE(XVALUE,YVALUE,294,1,0,1)
      CALL SYMBOL(1.0,4.25,0.07,20HACTUAL PRESSURE WAVE,0.0,20)
      CALL SYMBOL(1.0,4.0,0.07,30HFOURIER SERIES WAVE WITH 3 HZ.,0.0,30)
      CALL PLOT(12.0,0.0,999)
```

A0 = 107.7109

FREQUENCY = 0 HZ
POWER = 107.7109

A ( 1) = -0.2301 B ( 1) = 28.9146

FREQUENCY = 1 HZ
POWER = 28.9155

A ( 2) = -24.8279 B ( 2) = 1.6884

FREQUENCY = 2 HZ
POWER = 24.8852

A ( 3) = -2.7345 B ( 3) = -7.2385

FREQUENCY = 3 HZ
POWER = 7.7378

A ( 4) = 1.0209 B ( 4) = -1.9415

FREQUENCY = 4 HZ
POWER = 2.2076

A ( 5) = 0.2577 B ( 5) = -0.0721

FREQUENCY = 5 HZ
POWER = 0.2675

A ( 6) = -0.3210 B ( 6) = 0.1237

FREQUENCY = 6 HZ
POWER = 0.3440

A ( 7) = -0.0827 B ( 7) = 0.1296

FREQUENCY = 7 HZ
POWER = 0.1538

A ( 8) = -0.0362 B ( 8) = -0.0811

FREQUENCY = 8 HZ
POWER = 0.0888

A ( 9) = 0.1463 B ( 9) = -0.0281

FREQUENCY = 9 HZ
POWER = 0.1490

A ( 10) = 0.2286 B ( 10) = 0.0119

FREQUENCY = 10 HZ
POWER = 0.2289

A ( 11) = 0.0538 B ( 11) = 0.2383

FREQUENCY = 11 HZ
POWER = 0.2443

A ( 12) = -0.1986 B ( 12) = 0.1235

FREQUENCY = 12 HZ
POWER = 0.2339

A ( 13) = -0.3043 B ( 13) = 0.0132

FREQUENCY = 13 HZ
POWER = 0.3046

A ( 14) = 0.1035 B ( 14) = -0.1838

FREQUENCY = 14 HZ
POWER = 0.2109

A ( 15) = -0.0294 B ( 15) = 0.1119

FREQUENCY = 15 HZ
POWER = 0.1157

A ( 16) = -0.0566 B ( 16) = -0.0175

FREQUENCY = 16 HZ
POWER = 0.0689

A ( 17) = 0.1069 B ( 17) = -0.1362

FREQUENCY = 17 HZ
POWER = 0.1732

A ( 18) = 0.0456 B ( 18) = 0.0398

FREQUENCY = 18 HZ
POWER = 0.0944

A ( 19) = -0.1714 B ( 19) = -0.0178

FREQUENCY = 19 HZ
POWER = 0.1723

A ( 20) = -0.0627 B ( 20) = 0.0352

FREQUENCY = 20 HZ
POWER = 0.0719

A ( 21) = -0.0420 B ( 21) = -0.0436

FREQUENCY = 21 HZ
POWER = 0.0605

A ( 22) = 0.0212 B ( 22) = 0.0067

FREQUENCY = 22 HZ
POWER = 0.0223

A ( 23) = 0.0748 B ( 23) = 0.0845

FREQUENCY = 23 HZ
POWER = 0.1129

A ( 24) = 0.0050 B ( 24) = 0.1060

FREQUENCY = 24 HZ
POWER = 0.1062

A ( 25) = -0.0279 B ( 25) = 0.0681

FREQUENCY = 25 HZ
POWER = 0.0736

THE TOTAL PERCENT ERROR FOR A FREQUENCY OF

| | | | |
|---|---|---|---|
| 25 HZ. IS | 0.75995 | 12 HZ. IS | 0.77372 |
| 24 HZ. IS | 0.76232 | 11 HZ. IS | 0.79374 |
| 23 HZ. IS | 0.76372 | 10 HZ. IS | 0.80238 |
| 22 HZ. IS | 0.76276 | 9 HZ. IS | 0.80473 |
| 21 HZ. IS | 0.76303 | 8 HZ. IS | 0.80596 |
| 20 HZ. IS | 0.76491 | 7 HZ. IS | 0.80523 |
| 19 HZ. IS | 0.75959 | 6 HZ. IS | 0.81271 |
| 18 HZ. IS | 0.76207 | 5 HZ. IS | 0.84781 |
| 17 HZ. IS | 0.76331 | 4 HZ. IS | 0.86373 |
| 16 HZ. IS | 0.76638 | 3 HZ. IS | 1.40264 |
| 15 HZ. IS | 0.76560 | 2 HZ. IS | 4.89773 |
| 14 HZ. IS | 0.77027 | 1 HZ. IS | 15.44430 |
| 13 HZ. IS | 0.78736 | | |

# APPENDIX F

## PRESSURE DATA FOR STEADY FLOW

TABLE 18

PRESSURE DROPS AT SET LOCATIONS FOR VARIOUS VOLUME FLOW RATES

| Z-1 | | | | Z-2 | | | |
|---|---|---|---|---|---|---|---|
| $P_1$ = 9.5 cm proximal<br>$P_2$ = 10 cm distal | | $P_1$ = 9.5 cm proximal<br>$P_2$ = 1.0 cm distal | | $P_1$ = 9.5 cm proximal<br>$P_2$ = 0.5 cm distal | | $P_1$ = 9.5 cm proximal<br>$P_2$ = 10.0 cm distal | |
| Q $\left(\frac{ml}{sec}\right)$ | $\Delta P$ $\left(\text{cm of } H_2O\right)$ | Q $\left(\frac{ml}{sec}\right)$ | $\Delta P$ $\left(\text{cm of } H_2O\right)$ | Q $\left(\frac{ml}{sec}\right)$ | $\Delta P$ $\left(\text{cm of } H_2O\right)$ | Q $\left(\frac{ml}{sec}\right)$ | $\Delta P$ $\left(\text{cm of } H_2O\right)$ |
| 2.89 | 0.247 | 0.77 | 0.30 | 7.62 | 0.45 | 1.95 | 0.5 |
| 5.78 | 0.217 | 1.55 | 0.33 | 9.77 | 0.90 | 3.91 | 1.1 |
| 12.14 | 0.200 | 2.16 | 0.36 | 11.77 | 1.35 | 6.84 | 1.6 |
| 15.99 | 0.260 | 2.93 | 0.42 | 13.68 | 1.75 | 9.77 | 2.6 |
| 17.53 | 0.325 | 4.64 | 0.45 | 14.66 | 2.00 | 13.68 | 3.8 |
| 20.81 | 0.408 | 5.33 | 0.49 | 16.61 | 2.55 | 16.61 | 5.1 |
| 22.15 | 0.490 | 6.18 | 0.55 | 18.57 | 3.50 | 19.54 | 6.5 |
| 23.12 | 0.534 | 8.50 | 0.71 | 21.89 | 4.75 | 24.43 | 8.5 |
| 28.90 | 0.808 | 10.43 | 0.92 | 25.41 | 6.50 | 26.38 | 9.6 |
| 32.75 | 1.004 | 12.75 | 1.05 | 29.31 | 8.70 | 31.27 | 12.4 |
| 38.14 | 1.412 | 14.30 | 1.53 | 33.22 | 11.30 | 32.25 | 13.4 |
| 44.69 | 1.802 | 17.38 | 1.84 | 36.15 | 13.70 | 34.20 | 14.2 |
| 53.94 | 2.692 | 18.54 | 2.04 | 39.08 | 16.00 | 39.08 | 17.1 |
| 59.72 | 3.327 | 53.21 | 2.97 | 50.81 | 19.00 | 44.95 | 22.9 |
| 63.57 | 3.835 | 59.52 | 1.46 | 54.72 | 23.60 | 65.47 | 41.3 |
| 65.50 | 4.089 | 62.22 | 3.89 | 60.58 | 28.90 | 71.33 | 45.6 |
| | | 68.18 | 4.78 | 63.51 | 34.00 | | |
| | | 73.95 | 5.33 | 66.44 | 40.20 | | |
| | | | | 69.38 | 47.20 | | |
| 78% reduction; $\mu$ = 1.01 C.P.<br>$\rho$ = 1.011 g/cm$^3$; $\bar{R}_i$ = 0.862 cm | | | | 90% reduction; $\mu$ = 1.01 C.P.<br>$\rho$ = 1.011 g/cm$^3$; $\bar{R}_i$ = 0.87 cm | | | |

TABLE 19

PRESSURE DROPS ALONG VESSEL FOR VARIOUS REYNOLDS NUMBERS

| Distance From Throat (cm) | $\Delta P = P_x - P_{(-10)}$ (cm of $H_2O$) | | | | | |
|---|---|---|---|---|---|---|
| | Z-1 | | | | Z-2 | |
| | Re = 266 | Re = 900 | Re = 1800 | Re = 5500 | Re = 900 | Re = 5500 |
| -10.0 | 0.000 | 0.000 | 0.000 | 0.000 | 0.000 | -- |
| - 9.0 | 0.000 | 0.003 | 0.005 | 0.041 | 0.037 | 0.000 |
| - 8.0 | 0.005 | 0.003 | -0.003 | 0.082 | 0.069 | 0.737 |
| - 7.0 | 0.003 | 0.000 | -0.003 | 0.089 | 0.108 | 0.737 |
| - 6.0 | 0.000 | 0.005 | -0.010 | 0.086 | 0.115 | 1.219 |
| - 5.0 | 0.000 | 0.015 | -0.013 | 0.074 | 0.145 | 1.473 |
| - 4.0 | 0.005 | 0.030 | -0.003 | 0.064 | 0.232 | 1.473 |
| - 3.0 | 0.003 | 0.036 | -0.003 | 0.025 | 0.252 | 1.473 |
| - 2.0 | 0.003 | 0.056 | 0.008 | 0.003 | 0.264 | 1.473 |
| - 1.0 | 0.000 | 0.061 | 0.015 | 0.066 | 0.292 | 1.219 |
| - 0.5 | 0.018 | 0.079 | 0.018 | 0.117 | -- | -- |
| 1.0 | 0.259 | 0.470 | 1.054 | 5.682 | 2.449 | 128.5 |
| 2.0 | 0.234 | 0.462 | 0.815 | 4.963 | 2.390 | 128.5 |
| 3.0 | 0.224 | 0.437 | 0.775 | 4.265 | 2.288 | 125.2 |
| 4.0 | 0.216 | 0.404 | 0.749 | 3.940 | 2.189 | 117.6 |
| 5.0 | 0.206 | 0.414 | 0.749 | 3.673 | 2.086 | 112.3 |
| 6.0 | 0.203 | 0.414 | 0.747 | 3.536 | 2.037 | 108.7 |
| 7.0 | 0.203 | 0.384 | 0.734 | 3.449 | 1.955 | 106.4 |
| 8.0 | 0.193 | 0.394 | 0.729 | 3.429 | 1.863 | 104.8 |
| 9.0 | 0.203 | 0.386 | 0.716 | 3.414 | 1.822 | 103.7 |
| 10.0 | 0.218 | 0.384 | 0.721 | 3.401 | 1.808 | 103.0 |
| | 78% reduction<br>$\mu$ = 1.01 C.P.<br>$\rho$ = 1.011 g/cm$^3$<br>$R_i$ = .862 cm | | | | 90% reduction<br>$\mu$ = 1.01 C.P.<br>$\rho$ = 1.011 g/cm$^3$<br>$R_i$ = .872 cm | |

# VITA

John Michael Maltry III was born on July 8, 1951 in Erie, Pennsylvania to Martha and John M. Maltry. He attended public schools in Georgia, Kentucky and North Carolina. In 1970 he graduated from Enka High School, where he served as student body president during his senior year.

The author attended North Carolina State University, Raleigh from 1970 to 1971, then transferred to the University of Tennessee, Knoxville where he studied Chemical Engineering until 1973. During this time he was employed as a Chemical Engineering Co-op Student by Champion Papers in Canton, North Carolina. In 1973 he transferred to the Engineering Science and Mechanics Department from which he received his Bachelor of Science degree with major concentration in Biomedical Engineering in 1975. At the completion of his undergraduate degree the author was selected by the faculty of the Department of Engineering Science and Mechanics as the first recipient of the H. L. Weissberg Award. This award is made to the outstanding senior who emulates independent and interdisciplinary academic pursuits.

In 1976 the author entered graduate school at the University of Tennessee, Knoxville in pursuit of a Master of Science Degree in Engineering Science. He was employed as a graduate teaching assistant during these years with the above department as well as a research assistant under the direction of Dr. John H. Forrester.

From 1977 to the present he has been employed as a Process Engineer with Dade Division of American Hospital Supply Corporation in Miami, Florida. His job objectives have been directed toward improvement of various biochemical processes as well as increasing financial efficiency for Dade.